

SELECTED
FEB 19 1991
B D

1b. RESTRICTIVE MARKINGS		3. DISTRIBUTION/AVAILABILITY OF REPORT Approved for public release; distribution is unlimited	
2a. SECURITY CLASSIFICATION AUTHORITY		5. MONITORING ORGANIZATION REPORT NUMBER(S) AFOSR-TR- 91 0032	
2b. DECLASSIFICATION/DOWNGRADING SCHEDULE		7a. NAME OF MONITORING ORGANIZATION AFOSR/NC	
4. PERFORMING ORGANIZATION REPORT NUMBER(S)		7b. ADDRESS (City, State, and ZIP Code) Building 410, Bolling AFB DC 20332-6448	
6a. NAME OF PERFORMING ORGANIZATION University of Dayton	6b. OFFICE SYMBOL (if applicable)	9. PROCUREMENT INSTRUMENT IDENTIFICATION NUMBER AFOSR-88-0044	
6c. ADDRESS (City, State, and ZIP Code) Dayton, OH 45469-2357		10. SOURCE OF FUNDING NUMBERS	
8a. NAME OF FUNDING/SPONSORING ORGANIZATION AFOSR	8b. OFFICE SYMBOL (if applicable) NC	PROGRAM ELEMENT NO. 61102F	TASK NO. A3
8c. ADDRESS (City, State, and ZIP Code) Building 410, Bolling AFB DC 20332-6448		PROJECT NO. 2303	WORK UNIT ACCESSION NO.
11. TITLE (Include Security Classification) (U) X-RAY DIFFRACTION STUDIES OF THE STRUCTURE OF ORDERED POLYMERS AND RELATED ELECTRO-ACTIVE MATERIALS			
12. PERSONAL AUTHOR(S) Albert V. Fratini			
13a. TYPE OF REPORT Final Report	13b. TIME COVERED FROM 11-01-87 TO 11-30-90	14. DATE OF REPORT (Year, Month, Day) December 31, 1990	15. PAGE COUNT 85
16. SUPPLEMENTARY NOTATION			
17. COSATI CODES		18. SUBJECT TERMS (Continue on reverse if necessary and identify by block number)	
FIELD	GROUP	SUB-GROUP	
		Polyphenyls, polyparaphenylene oligomers, Electro-active Materials, molten salt precursor, quasi-particles, rigid-rod polymers, hyperpolarizabilities, crystal structure	
19. ABSTRACT (Continue on reverse if necessary and identify by block number)			
<p>The structures of poly(p-phenylenebenzobisthiazole) (PBZT) and poly(p-phenylenebenzobisoxazole) (PBO) fibers have been determined by fiber diffraction techniques (see Reprint 4 for details). D-spacings were obtained from equatorial and meridional scans recorded on a four-circle diffractometer. Intensity data were derived from x-ray rotation patterns taken on Weissenberg and vacuum cylindrical cameras. Unit cells were found to be monoclinic and non-primitive, each containing two chains per cell. The conformational torsion angle between the bisthiazole and phenylene units and the orientation of chains within the unit cells were obtained from a 'linked-atom least-squares' (LALS) refinement procedure. A packing model has been proposed for each fiber in which two independent molecular chains are displaced longitudinally by discrete rather than random increments. Primitive unit cells (Z = 1), besides requiring</p>			
20. DISTRIBUTION/AVAILABILITY OF ABSTRACT <input type="checkbox"/> UNCLASSIFIED/UNLIMITED <input type="checkbox"/> SAME AS RPT. <input type="checkbox"/> DTIC USERS		21. ABSTRACT SECURITY CLASSIFICATION UNCLASSIFIED	
22a. NAME OF RESPONSIBLE INDIVIDUAL Lt Col L P Davis		22b. TELEPHONE (Include Area Code) (202) 7674963	22c. OFFICE SYMBOL AFOSR/NC

perfect axial registry of molecular chains, suffered from the occurrence of short intermolecular contacts and were rejected from further consideration.

In another phase of the research on polyparaphenylene oligomers, variable temperature crystal data for the unsubstituted p-quinquephenyl (PQP), p-sexiphenyl (PSP), p-septiphenyl (PSeptiP), as well as the substituted 2²,4⁵-diphenyl-p-quinquephenyl (DPQP), 2²,6⁵-diphenyl-p-septiphenyl (DPSP), and 1,2,4-triphenylbenzene (TPB) oligomers are reported. The unsubstituted oligomers exhibit a solid state transition when cooled from room temperature to 110K, as indicated by a change in crystallographic space group. No transition is observed for the substituted oligomers other than the usual contraction of the unit cell. The transition observed for the unsubstituted oligomers is interpreted in terms of a conformational change from an "average" planar structure to a static non-planar one. Comparisons of the room and low temperature crystal data are presented.

The crystal structure analysis of the molten salt precursor, 1-methyl-3-ethylimidazolium chloride (MEICl), was completed as part of an investigation of the ion-ion interactions in room temperature melts, where mole fraction N of AlCl₃ is less than 0.5. Hygroscopic crystals of MEICl were grown in acetonitrile and sealed under helium gas in a capillary tube. The MEI⁺ ions cluster in four distinct layers perpendicular to the c-axis. Similarly, the arrangement of Cl⁻ ions is a layered one. Each Cl⁻ ion interacts with three MEI⁺ ions and each MEI⁺ ion is associated with three nearest Cl ions. Cl⁻ ions are situated in reasonable hydrogen-bonded positions rather than at random, suggesting this interaction to be a weak hydrogen bond. Evidence for hydrogen bonding of Cl⁻ ions at the three ring C-H bonds in basic MEICl/AlCl₃ melts is presented.

In the area of research on electro-active materials, the effect of alkyl substitution on the amino group and the placement of bulky groups on the aromatic ring in nitroaniline derivatives have been investigated through a determination of the crystal structures of 2-[2-(N,N-dimethylamino)-5-nitrophenyl]benzothiazole, 2-[2-(N-methylamino)-5-nitrophenyl]benzothiazole, 2-[2-(N,N-diethylamino)-5-nitrophenyl]benzothiazole, and 2-(trimethylsilylethynyl)-4-nitro-N,N-dimethylaniline. In all four compounds, the alkyl groups attached to the amino nitrogen atom prevent the formation of intermolecular (N)-H...O hydrogen bonds between amino and nitro groups. Instead, the molecules exhibit (C)-H...O intermolecular interactions between the nitro group and hydrogen atoms of the aromatic ring and alkyl groups. Two distinct types of packing, herringbone patterns and planar stacks, are observed with the closest interactions associated with the planar stacking of molecules.

In the area of computational chemistry, semiempirical AM1 calculations have been performed for the second hyperpolarizabilities, $\chi^{(2)}$, of poly-p-phenylene and polythiophene oligomers. Calculated values are compared with experimental degenerate four wave mixing results and static field estimates from these experimental results. The relative calculated values agree well with experimental values when the latter are corrected for dispersion effects. Another area is the study of the electronic structure and statistical properties of quasi-particles in polymeric materials. Solitons, antisolitons, polarons, and bipolarons are known to play a role in the conduction of electric current in these polymeric materials. Pristine and doped polyacetylenes have been used initially to study the geometrical and electronic distortions in oligomers and infinite polymers. The computational approach has been based on the semiempirical self-consistent LCAO-MO theory at the AM1 level of approximation for finite systems and the corresponding LCAO-CO theory in the tight binding approximation for infinite systems.

X-RAY DIFFRACTION STUDIES OF THE STRUCTURE OF
ORDERED POLYMERS AND RELATED ELECTRO-ACTIVE MATERIALS

Albert V. Fratini
Department of Chemistry
University of Dayton
Dayton, Ohio 45469

Final Technical Report, November 1, 1987 - October 31, 1990

Grant AFOSR-88-0044

Air Force Office of Scientific Research

December, 1990

Approved for public release;
distribution unlimited.

I. SUMMARY

The structures of poly(p-phenylenebenzobisthiazole) (PBZT) and poly(p-phenylenebenzobisoxazole) (PBO) fibers have been determined by fiber diffraction techniques (see Reprint 4 for details). D-spacings were obtained from equatorial and meridional scans recorded on a four-circle diffractometer. Intensity data were derived from x-ray rotation patterns taken on Weissenberg and vacuum cylindrical cameras. Unit cells were found to be monoclinic and non-primitive, each containing two chains per cell. The conformational torsion angle between the bisthiazole and phenylene units and the orientation of chains within the unit cells were obtained from a 'linked-atom least-squares' (LALS) refinement procedure. A packing model has been proposed for each fiber in which two independent molecular chains are displaced longitudinally by discrete rather than random increments. Primitive unit cells ($Z = 1$), besides requiring perfect axial registry of molecular chains, suffered from the occurrence of short intermolecular contacts and were rejected from further consideration.

In another phase of the research on polyparaphenylene oligomers, variable temperature crystal data for the unsubstituted p-quinquephenyl (PQP), p-sexiphenyl (PSP), p-septiphenyl (PSeptiP), as well as the substituted $2^2,4^5$ -diphenyl-p-quinquephenyl (DPQP), $2^2,6^5$ -diphenyl-p-septiphenyl (DPSP), and 1,2,4-triphenylbenzene (TPB) oligomers are reported (see Reprints 1 and 2 and Preprint 1 for details). The unsubstituted

<input checked="" type="checkbox"/>
<input type="checkbox"/>
<input type="checkbox"/>
Codes
and/or
Special

A-1

oligomers exhibit a solid state transition when cooled from room temperature to 110K, as indicated by a change in crystallographic space group. No transition is observed for the substituted oligomers other than the usual contraction of the unit cell. The transition observed for the unsubstituted oligomers is interpreted in terms of a conformational change from an "average" planar structure to a static non-planar one. Comparisons of the room and low temperature crystal data are presented.

In collaboration with a group at the Frank J. Seiler Research Laboratory, United States Air Force Academy, the crystal structure analysis of the molten salt precursor, 1-methyl-3-ethylimidazolium chloride (MEICl), was completed as part of an investigation of the ion-ion interactions in room temperature melts, where mole fraction N of AlCl₃ is less than 0.5 (see Reprint 3 for details). Hygroscopic crystals of MEICl were grown in acetonitrile and sealed under helium gas in a capillary tube. The asymmetric unit contains four MEI⁺...Cl⁻ ion pairs. The MEI⁺ ions cluster in four distinct layers perpendicular to the c-axis. Similarly, the arrangement of Cl⁻ ions is a layered one. Each Cl⁻ ion interacts with three MEI⁺ ions and each MEI⁺ ion is associated with three nearest Cl⁻ ions. The distance of a Cl⁻ ion from a ring carbon atom averages 3.55 Å. Cl⁻ ions are situated in reasonable hydrogen-bonded positions rather than at random, suggesting this interaction to be a weak hydrogen bond. Evidence for hydrogen bonding of Cl⁻ ions at the three ring C-H bonds in basic MEICl/AlCl₃ melts is presented.

In the area of research on electro-active materials, the effect of alkyl substitution on the amino group and the placement of bulky groups on the aromatic ring in nitroaniline derivatives have been investigated through a determination of the crystal structures of 2-[2-(N,N-dimethylamino)-5-nitrophenyl]benzothiazole, 2-[2-(N-methylamino)-5-nitrophenyl]benzothiazole, 2-[2-(N,N-diethylamino)-5-nitrophenyl]benzothiazole, and 2-(trimethylsilylethynyl)-4-nitro-N,N-dimethylaniline (see Preprint 2 for details). In all four compounds, the alkyl groups attached to the amino nitrogen atom prevent the formation of intermolecular (N)-H...O hydrogen bonds between amino and nitro groups. Instead, the molecules exhibit (C)-H...O intermolecular interactions between the nitro group and hydrogen atoms of the aromatic ring and alkyl groups. Two distinct types of packing, herringbone patterns and planar stacks, are observed with the closest interactions associated with the planar stacking of molecules. The dialkylamino substituents extend above and below the molecular plane, which is comprised of essentially coplanar ring systems.

In the area of computational chemistry, semiempirical AM1 calculations have been performed for the second hyperpolarizabilities, χ , of poly-p-phenylene and polythiophene oligomers (see Preprint 3 for details). Calculated values are compared with experimental degenerate four wave mixing results and static field estimates from these experimental results. The relative calculated values agree well with experimental values when the latter are corrected for dispersion effects.

Another area of the computational chemistry effort is the study of the electronic structure and statistical properties of quasi-particles in polymeric materials. Solitons, antisolitons, polarons, and bipolarons, in one way or another, are known to play a role in the conduction of electric current in these polymeric materials. Pristine and doped polyacetylenes have been used initially to study the geometrical and electronic distortions associated with quasi-particles in oligomers and infinite polymers. The computational approach has been based on the semiempirical self-consistent LCAO-MO theory at the AM1 level of approximation for finite systems and the corresponding LCAO-CO theory in the tight binding approximation for infinite systems (see Preprint 4 for details).

II. RESEARCH OBJECTIVES

The structures of poly(p-phenylene benzobisthiazole) (PBZT) and poly(p-phenylene benzobisoxazole) (PBO) have been of interest for the past decade. Numerous publications have advanced the understanding of the fiber and film structures of these rigid rod chains [1-3]. Our approach has been to apply the linked-atom least-squares (LALS) method to PBZT and PBO fibers exhibiting the highest order observed to date. The results, representing the equilibrium crystal structure, serve as a vehicle by which one can measure progress in reaching a fully ordered structure by processing improvements. The goal is to understand changes in structure and morphology imparted by chemical or physical means (in fiber processing, for example), and to relate these changes to the properties observed for these rigid-rod materials.

The study of oligomers of poly-p-phenylene (PPP) is part of the continuing research on the structure and morphology of rigid-rod polymers. Aerospace applications of these materials require a broad range of operating temperatures and conditions. Basic morphological information is needed about factors such as the relative orientation of phenyl rings, crystal packing forces, and the nature of the structural transitions observed at low temperatures in crystalline samples. Tedious synthetic procedures coupled with a high melting point and low solubility have made PPP a difficult polymer to prepare and fabricate. Paraphenyls of specific chain length which incorporate pendant groups have recently been

prepared by a new synthesis procedure utilizing intermolecular cyclization [4]. Single crystals of sufficient size for structural analysis have been grown by sublimation and recrystallization techniques.

Research objectives in computational chemistry have been concentrated in two main areas. First, ways to compare calculated static values of the hyperpolarizability with experimental values, measured at a particular frequency, have been investigated. As expected, the effect of the radiation frequency is considerable, even for resonant frequencies. Since comparisons between calculations and experiment are usually made without allowing for the frequency effect, the discrepancies come out to be larger than they should be. This was the case particularly with oligomers of p-phenylene and thiophene, as had been previously pointed out by Goldfarb, Reale and Medrano [5].

Secondly, the discovery that doped polyacetylene and other polymers can have electrical conductivity which are several orders of magnitude larger than for pristine material prompted a world-wide research effort. It was soon realized that quasi-particles were being created by the doping process (they can also be photoregenerated), and that it was necessary to understand the associated geometrical and electronic structure, as part of the whole picture. A study of the electronic structure of quasi-particles such as solitons and polarons in infinite polymers was initiated.

III. STATUS OF RESEARCH EFFORTS

Computational Chemistry. It is possible to estimate the effect of dispersion on degenerate four wave mixing (DFWM) experiments under the assumption that most of the nonlinearity of a delocalized pi-cloud comes from the lowest excited state by the formula,

$$\chi(o) = [(w_o^2 - w^2)^4 / w_o^8] \chi(w)$$

This gives the static value $\chi(o)$ in terms of the frequency w at which the DFWM experiment was performed in obtaining $\chi(w)$. The experimental results for the above-mentioned oligomers, as a function of the number of repeat units, were thus corrected, leading to a dramatic improvement in the agreement between calculated and measured values. A paper (see Preprint 3) reporting these results has been submitted for publication in the Journal of Chemical Physics. This work has been undertaken in cooperation with H. Kurtz at Memphis State University.

For the study of quasi-particles in polymeric materials, most of the calculations performed to date have used the Su, Schrieffer and Heeger (SSH) hamiltonian [6]. The SSH approach however is still too crude for the kind of accuracy that is needed since it is basically a Huckel-type approximation with sigma bond compressibility, and electron-electron Coulomb interactions are completely neglected. On the other hand,

several self-consistent LCAO-MO calculations have been performed on finite oligomers of polyacetylene, both semiempirical and ab initio.

It was felt necessary to undertake a reliable and comprehensive study of quasi-particles, mostly in infinite polymers, since these are a better approximation to real systems. Additionally, the effect of the dopant cannot be disregarded and should be included in the calculation, which should be performed at the SCF-MO-LCAO level of theory. The repeat units used for the polymer calculation have to be quite large in order to prevent the concentration of quasi-particles to become unrealistically high. Even at the semiempirical AM1 level of approximation, these calculations are extraordinarily demanding of cpu time. The first results which were obtained have already been accepted for publication (see Preprint 4) [7].

There is still much to be done, especially with regard to the calculation of the band structure of materials containing quasi-particles, before a more complete picture begins to emerge. It is felt that our calculations are sufficiently sophisticated and reliable for systems of such large size to contribute to the understanding of the electronic structure of organic conductors.

IV. REFERENCES

1. W.W. Adams, L.V. Azaroff, and A.K. Kulshreshtha, Z. Kristallogr. 150, 321 (1980).
2. E.J. Roche, T. Takahashi, and E.L. Thomas in Fiber Diffraction Methods, edited by A.D. French and K.H. Gardner (American Chemical Society Symposium Series, No. 141, 1980), p. 303.
3. J.A. Odell, A. Keller, E.D.T. Atkins, and M J. Miles, J. Mater. Sci. 16, 3309 (1981).
4. M.R. Unroe and B.A. Reinhardt, Synthesis, 11, 981 (1987).
5. I.J. Goldfarb, H.F. Reale and J.A. Medrano, in "Theoretical Prediction of Nonlinear Optical Properties of Molecules and Polymers," Materials Research Society Symposium Proceedings, 134, 609 (1989).
6. W.P. Su, J.R. Scheiffer and A.J. Heeger, Phys. Rev. Lett., 42, 1698 (1979).
7. J.A. Medrano and D.S. Dudis, "Quasi-particles in Polymeric Conductors," Proceedings of the International Conference on Organic Superconductors, Plenum Press, 1990.

CUMULATIVE LIST OF PUBLICATIONS

1. "Structure of a Dioxabicyclic Fluoro Octane Derivative," P.G. Lenhert and A.V. Fratini, *Acta Cryst.*, C43, 1929-1932 (1987).
2. "Hydrogen-Bonded Ion-Ion Interactions in a Molten Salt Precursor: The Crystal Structure of 1-Methyl-3-Ethylimidazolium Chloride," C.J. Dymek, D.A. Grossie, A.V. Fratini and W.W. Adams, *AFWAL Tech. Rep.* 88-4165, June 1988.
3. "Structural Transformations in Crystalline Oligomers of Polyparaphenylene," K.N. Baker, A.V. Fratini, H.C. Knachel and W.W. Adams, *Proceedings of Materials Research Society*, 134, 497 (1989).
4. "Molecular Packing and Crystalline Order in Polybenzobisoxazole and Polybenzobisthiazole Fibers," A.V. Fratini, P.G. Lenhert, T.J. Resch and W.W. Adams, *Proceedings of Materials Research Society*, 134, 431 (1989).
5. "Single-Crystal Diffraction Analysis of 2-(Trimethylsilyl-ethynyl)-4-Nitro-N,N-Dimethylaniline," D.A. Grossie, A.V. Fratini, and W.W. Adams, *Tech. Rep.* WRDC-TR-89-4120 July 1989.
6. "Crystal Structures of Poly-Paraphenylene Oligomers Containing Pendant Phenyl Groups," K.N. Baker, A.V. Fratini and W. W. Adams, *Tech. Rep.* WRDC-TR-89-4121 Sept. 1989.
7. "Evidence for the Presence of Hydrogen-Bonded Ion-Ion Interactions in the Molten Salt Precursor, 1-Methyl-3-Ethylimidazolium Chloride," C.J. Dymek, D.A. Grossie, A.V. Fratini and W.W. Adams, *J. Molecular Structure*, 213, 25-34 (1989).
8. "Crystal Structures of Poly-Paraphenylene Oligomers Containing Pendant Phenyl Groups," K.N. Baker, A.V. Fratini and W. W. Adams, *Polymer*, 31, 1623-1631 (1990).

PROFESSIONAL PERSONNEL

1. Dr. A. V. Fratini, Principal Investigator, Professor of Chemistry, University of Dayton.
2. Dr. K. Baker, Postdoctoral Associate, University of Dayton.
3. Dr. J. Medrano, Senior Research Associate, University of Dayton.
4. Mr. T. Resch, Research Student, University of Dayton.
5. Ms. L. Staley, Research Student, University of Dayton.

PRESENTATIONS

1. Annual Meeting of the American Crystallographic Association, University of Washington, Seattle, WA, July 23-29, 1989.
2. Dayton Section of American Chemical Society, Dayton, OH, March 1989.
3. Dayton Section of American Chemical Society, Dayton, OH, February 1990.
4. AFOSR/NLO Review, Washington, DC, April 1988.
5. AFOSR/NLO Review, Long Beach, CA, September 1989.
6. 22ND Central Regional Meeting, American Chemical Society, Saginaw Valley State University, University Center, MI, June 1990.
7. American Crystallographic Association Annual Meeting, New Orleans, LA, April 1990.
8. Materials Research Society Meeting, Boston, MA, November 1988.

STRUCTURAL TRANSFORMATIONS IN CRYSTALLINE OLIGOMERS OF POLYPARAPHENYLENE

KENNETH N. BAKER*, HOWARD C. KNACHEL*, ALBERT V. FRATINI*, and W. WADE ADAMS**

*Department of Chemistry, University of Dayton, 300 College Park, Dayton, OH 45469.

**Materials Laboratory, Wright Research and Development Center, WPAFB, OH 45433-6533.

ABSTRACT

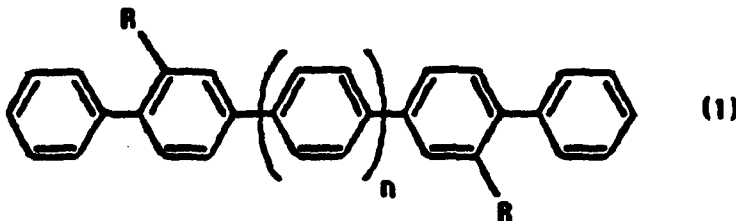
We report the room and low temperature crystal structures of the unsubstituted p-quinquephenyl (PQP) and p-sexiphenyl (PSP), and substituted 2,2',4,4'-diphenyl-p-quinquephenyl (DPQP), 2,2',6,6'-diphenyl-p-septiphenyl (DPSP), and 1,2,4-triphenylbenzene (TPB) polyparaphenylene oligomers. The unsubstituted oligomers exhibit a solid state transition when cooled from room temperature to 110K, as indicated by a change in crystallographic space group. No transition is observed for the substituted oligomers other than the usual thermal contraction of the unit cell. The transition observed for the unsubstituted oligomers is interpreted in terms of a conformational change from an "averaged" planar structure to a static non-planar one. Comparisons of room temperature and low temperature crystal data are presented.

INTRODUCTION

Oligomers of polyparaphenylene (PPP) have been of interest in our laboratory as part of continuing research on the structure and morphology of rigid-rod polymers. Aerospace applications requiring a broad range of operating temperatures and conditions require that any structural transition temperatures must be known. Much basic morphological information is still needed about factors such as the orientation of one coaxial ring to another and crystal packing forces in high performance polymers of this type.

Tedious synthetic procedures coupled with a high melting point and low solubility have made PPP a difficult polymer to prepare and fabricate [1,2]. P-polyphenyls with a specific chain length and incorporating pendant groups have been recently prepared using a new synthesis procedure utilizing intramolecular cyclization [3].

We have obtained high purity samples of PPP oligomers from which single crystals of sufficient size for structure analysis were sublimed or recrystallized. In a continuing investigation of the molecular structure, crystal packing, and structural transformations of PPP oligomers, we have studied p-quinquephenyl (PQP), p-sexiphenyl (PSP), 2,2',4,4'-diphenyl-p-quinquephenyl (DPQP), 2,2',6,6'-diphenyl-p-septiphenyl (DPSP), and 1,2,4-triphenylbenzene (TPB). The first four compounds have the general structure (1)



where $n = 1$ and $R = H$ for PQP, $n = 1$ and $R = \text{phenyl}$ for DPQP, $n = 2$ and $R = H$ for PSP, and $n = 3$ and $R = \text{phenyl}$ for DPSP. TPB was included in this present study since its room temperature structure has not been reported.

EXPERIMENTAL METHODS

Samples of PQP, PSP, DPQP, DPSP, and TPB were obtained from Bruce Reinhardt, Materials Laboratory, Wright Patterson Air Force Base. PQP and PSP samples were sublimed to obtain good quality crystals; otherwise, the samples needed no additional purification. Data were collected on an Enraf Nonius CAD4 diffractometer interfaced to a Digital Equipment Corporation Micro PDP-11 computer. Data refinement and structure determination were accomplished using the Structure Determination Package (SDP)[4] software on a Digital Equipment Corporation VAX 11/730 computer. The final R values and the corresponding ratio of the number of unique reflections to the number of parameters varied are 0.050 (663:136), 0.062 (623:163), 0.049 (1061:190), 0.046 (1537:244), and 0.036 (1839:219) for PQP, PSP, DPQP, DPSP, and TPB, respectively. Complete structural information will be given in another publication[15]. Cooling of the crystal was accomplished with an Enraf Nonius FR558NH liquid nitrogen cryostat for the CAD4 instrument.

RESULTS AND CONCLUSIONS

Table I summarizes current results along with published results for biphenyl(BP), p-terphenyl(PTP), and p-quaterphenyl(PQuatP) and one can see several trends. As the number of phenyl units in the oligomer chain increases, one observes a direct increase of approximately 4.1 Å in the c lattice dimension of the monoclinic unit cell per paraphenylene unit. This distance is slightly less than the length of a phenylene unit so one would expect the oligomer axis to be approximately aligned with the c crystallographic axis. The unit cell diagrams included in Figure 1 confirm that the oligomer axis is preferentially aligned with the c crystallographic axis.

The low temperature unit cell is a superlattice of the room temperature unit cell with parameters a and b doubled to account for the greater displacement of the non-planar oligomer. The low temperature crystal structures of PTP[8] and PQuatP[10] were solved using a triclinic unit cell. At room temperature the crystal structure indicates a planar oligomer probably resulting from the average of several non-planar conformations. At low temperature a specific non-planar geometry is preferred.

Figure 2 summarizes the melting points of p-polyphenyls and their respective transition temperatures. A steady rise in temperature is observed as the oligomer increases in length so that the predicted transition temperatures for PQP and PSP should be above room temperature. However we report here that the structures of PQP and PSP remain planar at room temperature and Differential Scanning Calorimetry (DSC) measurements indicate that there is no transition other than melting at higher temperatures. Upon cooling of PQP and PSP single crystals to 110K, unit cells very similar to the room temperature unit cells were found initially. However, after 24 hours a crystal phase transition had occurred. Both DSC analysis and X-ray powder diffraction patterns taken as low as 143K and held for several days revealed no structural transition. We conclude that the transition temperature must exist between 143K and 110K, as indicated by the error bars in Figure 2, and is time dependent. This transition could be non-first order as observed for biphenyl[5,6] in which a soft mode exists below its transition temperature. More experiments are planned to study this phenomenon.

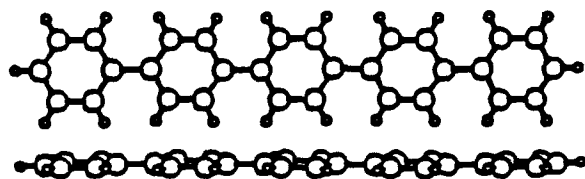
As is the case for most high temperature-resistant polymers, PPP degrades before it melts; however, for comparison purposes there is interest in knowing the theoretical melting point of the polymer. Literature reports PPP to be infusible[11], but by the extrapolation of experimental melting points of PPP oligomers (Figure 3) we estimate the melting point of PPP to be 1020K. Extrapolated melting points of 620K and 1260K have been reported for poly(tetrafluoroethylene)[12] and Kevlar™[13], respectively. Those extrapolations are based on melting point depression associated with end group concentration in polymers[14].

The low temperature crystal structure of DPQP is isostructural with its room temperature crystal structure indicating no structural transition. In a paper to be published elsewhere[15] we report that the addition of pendant groups to the PPP oligomer results in a distortion of planarity of the unsubstituted oligomer, but the torsion angles change less than an average of

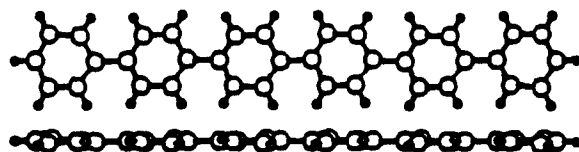
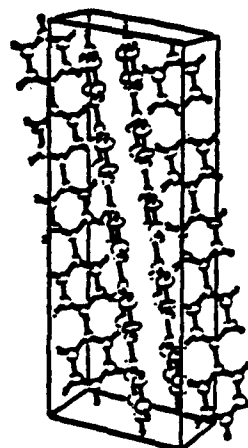
TABLE I
VARIABLE TEMPERATURE CRYSTAL DATA

Compound	Temperature(K)	Space Group	a(Å)	b(Å)	c(Å)	alpha(°)	beta(°)	gamma(°)
BP	298(5)	P2 ₁ /c*	9.51(2)	5.63(1)	8.12(2)	90	95.1(3)	90
BP	40(6)	P2 ₁ /c*	9.51(2)	11.26(2)	16.24(4)	90	95.1(3)	90
PTP	298(7)	P2 ₁ /c*	13.613(6)	5.613(2)	8.106(4)	90	92.2(2)	90
PTP	191(7)	P2 ₁ /c*	13.53(3)	11.09(3)	16.01(3)	90	92.0(2)	90
PQuatP	298(9)	P2 ₁ /c*	17.910(10)	5.610(4)	8.110(6)	90	95.80(6)	90
PQuatP	243(10)	P2 ₁ /c*	17.70(3)	11.16(2)	15.97(3)	90	95.61(8)	90
PQP	298	P2 ₁ /c	22.056(4)	5.581(1)	8.070(1)	90	97.91(1)	90
PQP	110	monoclinic, C centered	22.014(3)	11.029(4)	15.968(6)	90	98.18(2)	90
PSP	298	P2 ₁ /c	26.241(5)	5.568(1)	8.091(3)	90	98.17(2)	90
PSP	110	monoclinic, C centered	26.282(8)	10.999(4)	15.995(9)	90	99.79(4)	90
PSepP	298	P2 ₁ /c*	30.232(19)	5.574(3)	8.065(5)	90	94.85(5)	90
PSepP	110	work in progress						
DFQP	298	P2 ₁ /c	6.304(3)	31.437(9)	7.651(3)	90	106.18(4)	90
DFQP	110	P2 ₁ /c	6.265(2)	31.345(9)	7.510(2)	90	106.08(2)	90
DFSP	298	P1	11.713(2)	13.596(2)	6.138(2)	102.33(2)	96.51(2)	102.71(1)
DFSP	110	work in progress						
TPB	298	Pbca	10.368(6)	17.898(4)	18.474(5)	90	90	90
TPB	110	work in progress						

* For comparison purposes, the P2₁/s space groups were transformed to P2₁/c.



PQP



PSP

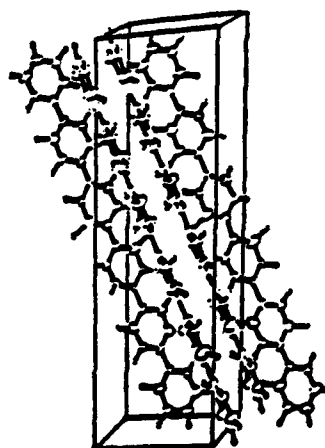


Figure 1. Flat, side and unit cell views of PQP and PSP.

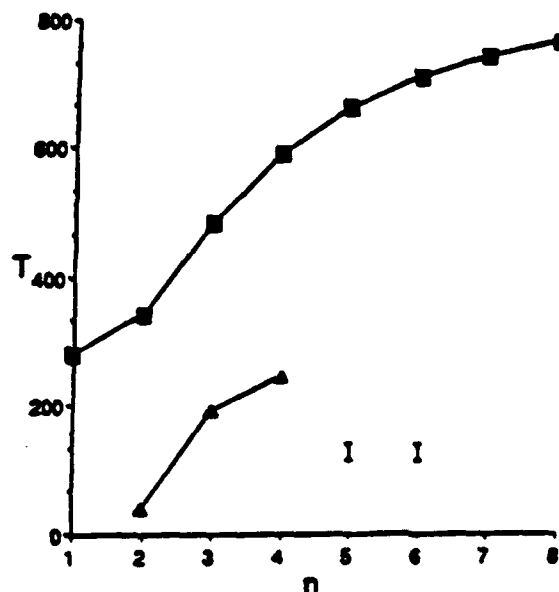


Figure 2. Plot of transition (\rightarrow , K) and melting point (\leftarrow , K) vs. oligomer length (n). Melting point data, taken from DSC measurements, are as follows: 279K[2], 343K[2], 483K[2], 591K[2], 661K[3], 710K[3], 741K[3], and 764K[3] for $n = 1 - 8$, respectively. Transition temperatures are 40K[6], 191K[7], and 243K[10] for $n = 2 - 4$, respectively. Error bars at $n = 5$ and 6 indicate temperature range for observed transition.

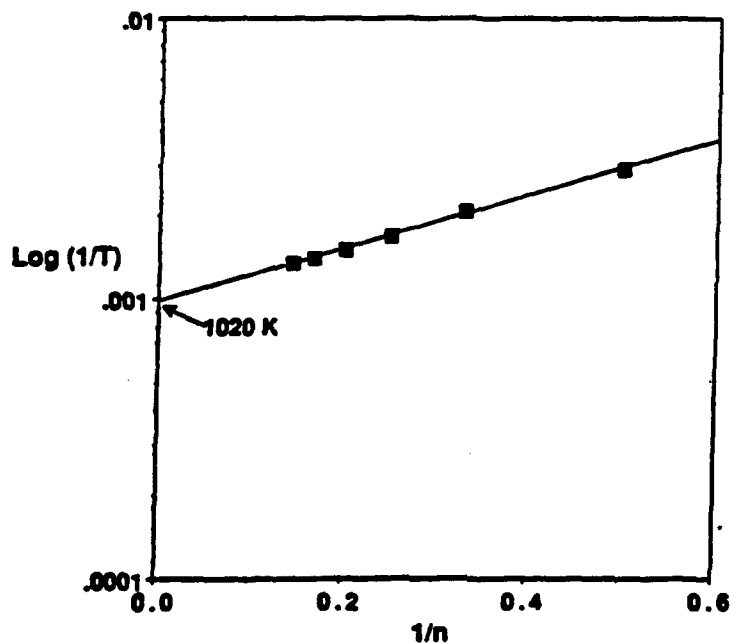


Figure 3. Plot of log of inverse melting point ($\log(1/T)$, K) vs. inverse oligomer length ($1/n$) showing the extrapolated melting point of high polymer PPP.

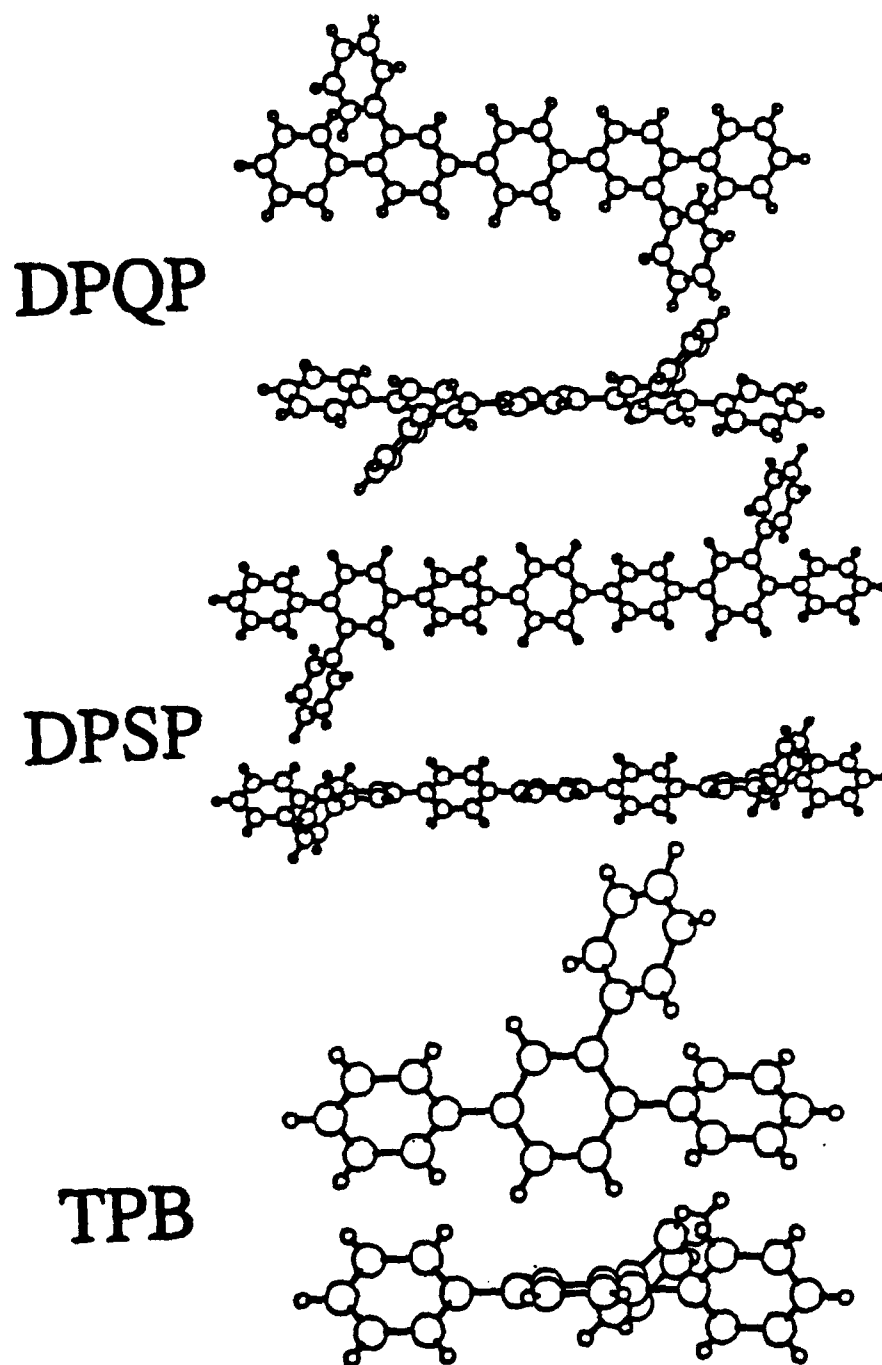


Figure 4. Molecular views of DPQP, DPSP and TPB.

10° between room and low temperature. As the length of the substituted PPP oligomer increases, a systematic decrease in symmetry is observed as a change in space group. The substituted oligomers are presented in Figure 4 and the molecules form a herringbone pattern in the unit cell. More compounds in this series are being studied.

Molecular modeling studies of PPP oligomers are complementing structure investigations. The calculated torsion angle for biphenyl is approximately twice that calculated for the rigid-rods poly(p-phenylenebenzobisthiazole) (PBZT) and poly(p-phenylenebenzobisoxazole) (PBO)[16,17]. The torsion angles calculated for a phenyl substituted biphenyl molecule in its lowest energy conformation agree with crystallographic data for substituted PPP oligomers. PPP conformations simulated in the absence of crystal packing forces have the rings perpendicular to each other. This suggests that the constraints within the unit cell are strong enough to overcome the ortho-hydrogen repulsion. Recent calculations show PPP to have a high theoretical axial tensile modulus and a high compressive strength, which encourages continued interest in PPP oligomers as potential structural materials[17].

REFERENCES

1. G.K. Noren and J.K. Stille, *J. Polym. Sci. Macromol. Rev.* **5**, 385 (1971).
2. J.G. Speight, P. Kovacic, and F.W. Koch, *J. Macromol. Sci. Rev. Macromol. Chem.* **5**, 295 (1971).
3. M.R. Umroe and B.A. Reinhardt, *Polymer* **11**, 981 (1987).
4. B.A. Frenz and Associates, Inc. (1985), College Station, Texas, 77840.
5. A. Bree and M. Edelson, *Chem. Phys. Lett.* **46** (3), 500 (1977).
6. H. Cailleau, J.L. Baudour, and C.M.E. Zeyen, *Acta Cryst.* **B35**, 426 (1979).
7. H. Cailleau and A. Dworkin, *Mol. Cryst. Liq. Cryst.* **50**, 217 (1979).
8. J.L. Baudour, Y. Delugeard, and H. Cailleau, *Acta Cryst.* **B32**, 150 (1976).
9. B.A. Bolton and P.N. Prasad, *Chem. Phys.* **35**, 331 (1978).
10. J.L. Baudour, Y. Delugeard, and P. Rivet, *Acta Cryst.* **B34**, 625 (1978).
11. P. Kovacic and A. Kyriakis, *J. Am. Chem. Soc.* **85**, 454 (1963).
12. H.W. Starkweather, *Macromolecules* **19**, 1131 (1986).
13. K. Gardner (Private Communication).
14. P.J. Flory, *Principles of Polymer Chemistry* (Cornell University Press, Ithaca, New York, 1953) p. 570.
15. K.N. Baker, H.C. Knachel, A.V. Frantini, and W.W. Adams, to be published.
16. B.L. Farmer (Private Communication).
17. S.G. Wierschke, *AEWAL-TR-88-4201* (October 1988).

Crystal structures of poly-paraphenylene oligomers containing pendant phenyl groups

Kenneth N. Baker and Albert V. Fratini

Department of Chemistry, University of Dayton, Dayton, OH 45469, USA

and W. Wade Adams*

Polymer Branch, Materials Laboratory, Wright Research and Development Center, WPAFB, OH 45433-6533, USA

(Received 11 July 1989; revised 25 September 1989; accepted 30 September 1989)

The room temperature crystal structures of 1,2,4-triphenylbenzene (TPB), $C_{24}H_{18}$; 2²,4⁵-diphenyl-*p*-quinquephenyl (DPQ), $C_{42}H_{30}$; and 2²,6³-diphenyl-*p*-septiphenyl (DPS), $C_{54}H_{38}$, have been investigated as part of a research programme in rigid-rod polymers, materials which are of great interest for aerospace and electro-optical applications. The molecules are non-planar, in contrast to the planar structures found at room temperature for the unsubstituted polyphenyls. The oligomer axis does not align with any of the crystallographic axes. The pendant-oligomer bond, however, does align with the longest crystallographic axis. The pendant torsion angle is greater than 45° and increases with increasing chain length. Knowledge of molecular structure and crystal packing of oligomeric model compounds will be useful in further calculations of mechanical, optical, and electro-optical properties for the corresponding rigid-rod polymer structures.

(Keywords: polyphenyls; poly-*p*-phenylenes; crystal structure; rigid-rod polymers; conducting polymers)

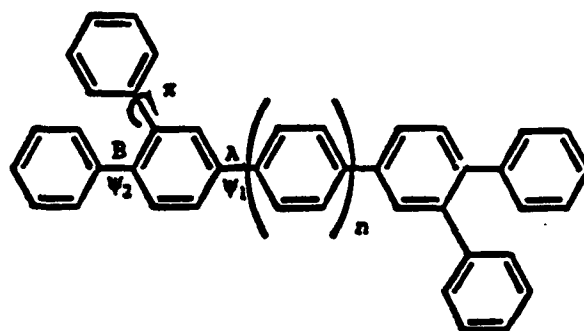
INTRODUCTION

The past few years have seen the activity in the area of conducting polymers grow at a very rapid rate. The widespread interest in conducting polymers clearly reflects their perceived technological potential¹. Attention has focused on the pi-bonded polymers such as poly-paraphenylene (PPP) for several reasons. It can be oxidized to a polymeric cation rather than undergo other chemistry and thereby be made electrically conducting; it is thermally stable; pi-orbital overlap may create interesting non-linear optical (NLO) properties; and improved methods have been reported for the synthesis of oligomeric soluble prepolymer².

The generation of charge carriers in the polyphenyls occurs by doping and the subsequent formation of ionic species, e.g., a polymeric cation and a counter ion. Electrical conductivity as high as $500 \text{ ohm}^{-1} \text{ cm}^{-1}$ has been achieved with dopants such as Li, K, and AsF_6 (ref. 3). The polymer chains, as for organic molecules in general, adopt a different conformation in the ionized state compared to the neutral state. Conformation differences would lead to changes in the amount of pi-orbital overlap along the polymer axis as well as affect the electro-optical properties of the polymer.

In an ongoing study of PPP as new electrically conducting rigid-rod polymers, the room temperature structures of 2²,4⁵-diphenyl-*p*-quinquephenyl (DPQ), 2²,6³-diphenyl-*p*-septiphenyl (DPS), and 1,2,4-triphenylbenzene (TPB) have been determined. TPB was included in the present study because its room temperature crystal structure had not been reported. The first two compounds

have the general structure,



where $n=1$ for DPQ and $n=3$ for DPS. Letters (A, B, etc.) refer to the connecting bond along the main chain and the Greek letters (ψ and π) refer to the torsion angles between adjacent phenyl groups. These compounds were synthesized in order to obtain a better understanding of how rigid-rod molecules pack in solids and how chain length affects packing. In addition, recent calculations⁴ have indicated that PPP is a very stiff molecule which, if processed into fibres using high molecular weight polymer, would have very high tensile modulus.

EXPERIMENTAL

Oligomers were synthesized by Bruce Reinhardt, Materials Laboratory, Wright Patterson Air Force Base, according to a new method which involves intermolecular cyclization⁵. The highly crystalline samples required no additional purification and/or crystal growth. Density

* To whom correspondence should be addressed

measurements were made by flotation in mixed solvents containing methyl alcohol and methylene chloride.

Reflection data were collected on an Enraf Nonus CAD4 diffractometer coupled with a DEC micro PDP-11 computer and processed on a VAX 11/730 using software in the Structure Determination Package (SDP)⁵. Structure solutions were determined by MULTAN 11/82⁶ and SHELXS-86⁷. The method of refinement followed the general scheme: (1) isotropic refinement of carbon atoms using unit-weighted reflections; (2) isotropic refinement of carbon atoms using unit-weighted reflections; hydrogen atoms, with fixed thermal factors, positioned in idealized geometries and constrained to its attached carbon atom with a bond length of 0.95 Å; (3) anisotropic refinement of carbon atoms using unit weights with hydrogen atoms still constrained to attached carbon atoms; (4) anisotropic refinement of carbon atoms to convergence using $1/\sigma^2(F)$ weights with hydrogen atoms riding on attached carbon atoms. Subsequent isotropic refinement of hydrogen atoms, as expected, did not yield appreciably better results due to the reduced data-to-parameter ratio.

RESULTS

Table 1 lists crystallographic and data collection parameters, and final refinement results. Figure 1 shows the TPB molecule with the carbon atoms labelled. Tables 2 and 3 contain the atomic positions, bond distances, and bond angles, respectively. Figure 2 shows a stereo view of the molecular packing in the unit cell.

DPQ is shown in Figure 3 with the carbon atoms of the asymmetric unit labelled. Tables 4 and 5 present the atomic positions, bond distances, and bond angles, respectively. The stereo view of the molecular packing in the unit cell is shown in Figure 4. The molecule possesses a centre of symmetry.

The DPS molecule with the carbon atoms of the asymmetric unit labelled is shown in Figure 5. Atomic positions, bond distances, and bond angles are presented

Table 2 Atomic positions of 1,2,4-triphenylbenzene. Numbers in parentheses are estimated standard deviations in the least significant digits

Atom	x	y	z	B (Å ²)
C1	0.6605(2)	0.1066(1)	-0.02818(9)	3.51(3)
C2	0.6238(2)	0.0967(1)	-0.0998(1)	3.95(4)
C3	0.5698(2)	0.1542(1)	-0.1390(1)	4.38(4)
C4	0.5516(2)	0.2233(1)	-0.1076(1)	4.76(5)
C5	0.5875(3)	0.2341(1)	-0.0369(1)	5.76(5)
C6	0.6419(2)	0.1764(1)	0.0022(1)	5.17(5)
C7	0.7186(2)	0.0445(1)	0.01392(9)	3.46(3)
C8	0.6704(2)	-0.0279(1)	0.0092(1)	3.87(4)
C9	0.7261(2)	-0.0854(1)	0.04820(9)	3.81(4)
C10	0.8327(2)	-0.0736(1)	0.09264(9)	3.38(3)
C11	0.8815(2)	-0.0007(1)	0.09859(9)	3.34(3)
C12	0.8232(2)	0.0567(1)	0.05922(9)	3.65(4)
C13	0.8905(2)	-0.1397(1)	0.12927(9)	3.57(4)
C14	0.8133(2)	-0.1891(1)	0.1676(1)	4.24(4)
C15	0.8641(2)	-0.2526(1)	0.1991(1)	5.05(5)
C16	0.9928(3)	-0.2682(1)	0.1922(1)	5.53(5)
C17	1.0707(2)	-0.2197(1)	0.1547(1)	5.53(5)
C18	1.0206(2)	-0.1558(1)	0.1236(1)	4.49(4)
C19	0.9919(2)	0.01889(9)	0.14651(9)	3.41(4)
C20	0.9958(2)	-0.0032(1)	0.2188(1)	4.26(4)
C21	1.0960(2)	0.0181(1)	0.2634(1)	5.17(5)
C22	1.1940(2)	0.0621(1)	0.2362(1)	5.21(5)
C23	1.1915(2)	0.0842(1)	0.1647(1)	5.02(5)
C24	1.0910(2)	0.0629(1)	0.1201(1)	4.15(4)
H2	0.637	0.050	-0.122	5.0
H3	0.543	0.146	-0.188	5.6
H4	0.516	0.263	-0.135	6.0
H5	0.575	0.282	-0.015	6.9
H6	0.666	0.184	0.051	6.5
H8	0.599	-0.038	-0.022	5.0
H9	0.691	-0.134	0.045	4.8
H12	0.857	0.106	0.063	4.6
H14	0.724	-0.179	0.172	5.3
H15	0.810	-0.286	0.226	6.4
H16	1.028	-0.312	0.213	7.0
H17	1.160	-0.230	0.150	6.9
H18	1.076	-0.122	0.098	5.7
H20	0.929	-0.034	0.237	5.4
H21	1.097	0.003	0.313	6.6
H22	1.263	0.077	0.267	6.5
H23	1.280	0.114	0.146	6.6
H24	1.089	0.079	0.071	5.4

Table 1 Crystal data

Name	1,2,4-Triphenyl benzene	2 ² ,4 ⁴ -Diphenyl-p-quinquephenyl	2 ² ,6 ⁶ -Diphenyl-p-septiphenyl
Formula	C ₂₄ H ₁₈	C ₄₂ H ₃₀	C ₆₆ H ₅₀
FW	306.4	534.7	686.9
T _m (°C)	123	288	375
Space group	Pbca	P2 ₁ c	P1
Z	8	2	1
a (Å)	10.368(6)	6.304(3)	11.713(2)
b (Å)	17.898(4)	31.437(9)	13.596(2)
c (Å)	18.474(5)	7.651(3)	6.138(2)
α (degrees)	90.0	90.0	102.33(2)
β (degrees)	90.0	106.18(4)	96.51(2)
γ (degrees)	90.0	90.0	102.71(1)
Vol (Å ³)	3428.3(4)	1496.4(2)	918.3(8)
Density _{calc} (g cm ⁻³)	1.187	1.219	1.242
Density _{exp} (g cm ⁻³)	1.186	1.188	1.236
Number of total reflections	19 698	5204	3558
Number of unique reflections > 3σ	1839	1061	1537
Number of parameters varied	217	190	244
R ^a	0.036	0.049	0.046
RW ^b	0.050	0.061	0.062

$$R = \frac{\sum ||F_o| - |F_c||}{\sum |F_o|}$$

$$RW = \sqrt{\frac{\sum w(|F_o| - |F_c|)^2}{\sum w|F_o|^2}}$$

Table 3 Bond distances and angles for 1,2,4-triphenylbenzene. Numbers in parentheses are estimated standard deviations in the least significant digit

Atom 1	Atom 2	Distance (Å)	Atom 1	Atom 2	Distance (Å)
C1	C2	1.388(2)	C11	C12	1.396(3)
C1	C6	1.382(3)	C11	C19	1.489(2)
C1	C7	1.486(2)	C13	C14	1.387(3)
C2	C3	1.377(3)	C13	C18	1.383(3)
C2	C4	1.379(3)	C14	C15	1.382(3)
C3	C5	1.373(3)	C15	C16	1.369(3)
C3	C6	1.381(3)	C16	C17	1.373(3)
C7	C8	1.392(3)	C17	C18	1.382(4)
C7	C12	1.387(2)	C19	C20	1.394(3)
C8	C9	1.383(3)	C19	C24	1.384(3)
C9	C10	1.393(3)	C20	C21	1.380(4)
C10	C11	1.405(2)	C21	C22	1.381(3)
C10	C13	1.489(2)	C22	C23	1.380(3)
			C23	C24	1.382(2)

Atom 1	Atom 2	Atom 3	Angle (deg)	Atom 1	Atom 2	Atom 3	Angle (deg)
C2	C1	C6	117.8(2)	C12	C11	C19	118.0(2)
C2	C1	C7	121.0(2)	C7	C12	C11	122.5(2)
C2	C1	C7	121.3(2)	C10	C13	C14	120.4(2)
C2	C2	C3	121.2(2)	C10	C13	C18	121.5(2)
C2	C3	C4	120.4(2)	C14	C13	C18	118.0(2)
C2	C4	C5	119.4(2)	C13	C14	C15	121.2(2)
C2	C5	C6	120.2(3)	C14	C15	C16	120.0(2)
C2	C6	C5	121.3(2)	C15	C16	C17	119.4(3)
C2	C7	C8	121.2(2)	C16	C17	C18	120.9(2)
C2	C7	C12	121.1(2)	C13	C18	C17	120.4(4)
C2	C7	C12	117.7(2)	C11	C19	C20	121.7(2)
C2	C8	C9	120.6(2)	C11	C19	C24	119.7(2)
C2	C9	C10	121.8(2)	C20	C19	C24	118.6(2)
C2	C10	C11	118.2(2)	C19	C20	C21	121.0(2)
C2	C10	C13	117.9(2)	C20	C21	C22	119.7(2)
C11	C10	C13	123.9(2)	C21	C22	C23	120.0(2)
C10	C11	C12	119.2(2)	C22	C23	C24	120.4(2)
C10	C11	C19	122.9(2)	C19	C24	C23	120.4(2)

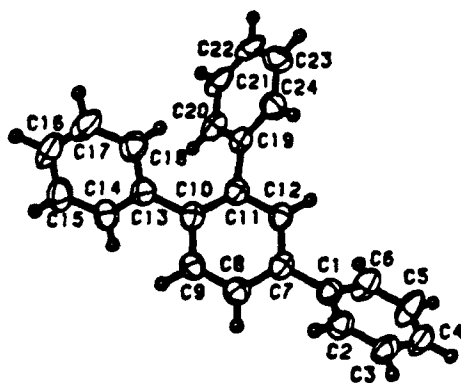


Figure 1 1,2,4-Triphenylbenzene with carbon atom ellipsoids drawn at the 30% probability level

in Tables 6 and 7, respectively. Figure 6 depicts a stereo view of the molecular packing of the structure in the unit cell. This molecule also possesses a centre of symmetry. (Observed and calculated structure factor amplitudes and other details of the structure analysis have been deposited at the British Library Copyright Receipt Office* as supplementary material to this paper.)

DISCUSSION

Table 8 summarizes the bond lengths between neighbouring phenyl units for structures determined at room

*British Library Copyright Receipt Office, 3 Sheraton Street, London W1V 4BH, UK

temperature. The values are not significantly different than the corresponding distances in the unsubstituted PPP⁸⁻¹¹. A significant shortening of these bond distances in the substituted oligomers would have indicated more double bond character and increased electron delocalization. It should be noted that the contribution of the quinoid resonance structure is believed to increase upon doping of PPP³ with alkali metals. This is accompanied by a decrease in aromaticity and an increase in electron delocalization. Thus, it is not certain whether pendant-containing PPP could therefore be doped with alkali metal ions to produce better electronic conductors and/or NLO materials.

The bond angles are very close to the expected 120° value with the largest deviations in angles associated with connecting phenyl units. The oligomer axis of each molecule is essentially coaxial and small deviations are probably due to steric hindrance of the phenyl pendant groups. Deviations of the oligomer axis carbon atoms from the best least squares line fit, plotted in Figure 7, show that DPS is distorted the most of the three oligomers. When viewed down the chain axis, DPQ has a small sinusoidal-shaped wave perpendicular to the plane of the central ring, whereas TPB and DPS are bowed. The terminal phenyl ring of TPB (C13-C18) is 7° from being collinear with the oligomer axis. These contortions of the oligomer axis are shown in Figure 8.

In all three oligomers, the oligomer axis does not align with any of the crystallographic axes; however, the bond connecting the pendant to the oligomer aligns preferentially along (or nearly so) one of the crystallographic axes. In TPB the pendant-oligomer bond aligns close to

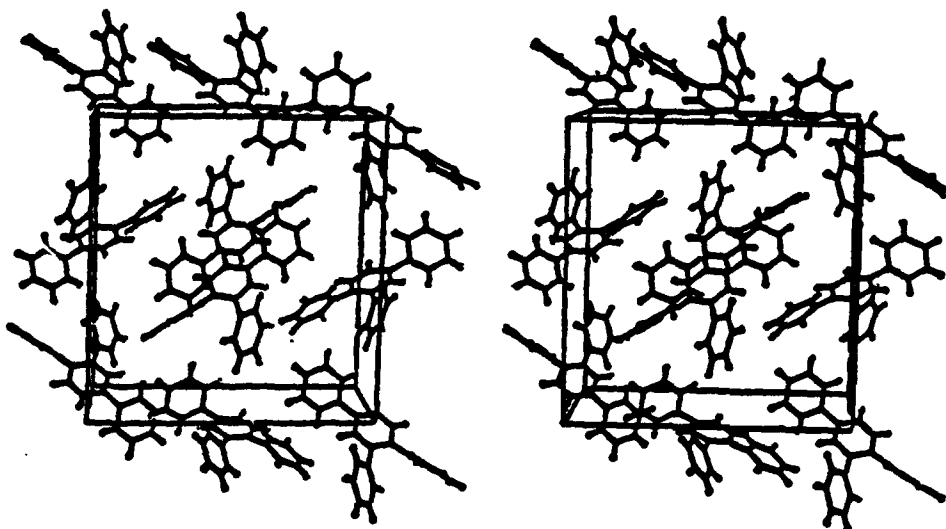


Figure 2 Stereo view of the partial contents of the unit cell of TPB. Selected molecules are omitted for clarity. The *b* axis is horizontal and the *c* axis is vertical

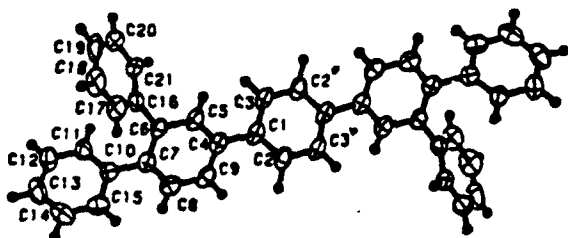


Figure 3 2,2',4,4'-Diphenyl-p-quinquephenyl with carbon atom ellipsoids drawn at the 50% probability level

Table 4 Atomic positions of 2,2',4,4'-diphenyl-p-quinquephenyl. Numbers in parentheses are estimated standard deviations in the least significant digit

Atom	x	y	z	B (Å ²)
C1	0.8032(5)	0.0213(1)	0.9088(4)	3.68(7)
C2	1.1965(5)	0.0219(1)	1.0586(5)	4.48(8)
C3	1.0016(5)	0.0428(1)	0.9683(5)	4.40(8)
C4	0.5973(5)	0.0439(1)	0.8084(4)	3.67(7)
C5	0.5685(5)	0.0868(1)	0.8359(4)	3.79(7)
C6	0.3824(5)	0.1093(1)	0.7367(4)	3.42(7)
C7	0.2203(5)	0.0877(1)	0.6023(4)	3.67(7)
C8	0.2476(5)	0.0446(1)	0.5776(4)	4.25(8)
C9	0.4317(5)	0.0227(1)	0.6810(5)	4.22(8)
C10	0.0256(5)	0.1101(1)	0.4820(4)	3.66(7)
C11	0.0476(5)	0.1467(1)	0.3885(5)	4.51(8)
C12	-0.1353(6)	0.1669(1)	0.2777(5)	5.3(1)
C13	-0.3438(6)	0.1512(1)	0.2611(5)	5.4(1)
C14	-0.3688(6)	0.1145(1)	0.3490(5)	5.37(9)
C15	-0.1869(5)	0.0937(1)	0.4609(5)	4.48(8)
C16	0.3637(5)	0.1548(1)	0.7810(4)	3.83(8)
C17	0.1831(6)	0.1700(1)	0.8328(5)	4.92(9)
C18	0.1711(7)	0.2117(1)	0.8807(6)	6.2(1)
C19	0.3376(7)	0.2395(1)	0.8793(6)	6.6(1)
C20	0.5186(7)	0.2252(1)	0.8288(6)	6.0(1)
C21	0.5316(6)	0.1832(1)	0.7798(5)	4.70(9)
H2	0.665	-0.044	0.874	4.0
H3	1.004	0.073	0.947	5.2
H5	0.678	0.101	0.926	4.5
H8	0.138	0.030	0.488	5.5
H9	0.445	-0.007	0.663	5.5
H11	0.191	0.158	0.402	5.3
H12	-0.117	0.192	0.212	6.4
H13	-0.471	0.166	0.190	6.9
H14	-0.512	0.103	0.333	6.5
H15	-0.206	0.069	0.524	5.8
H17	0.066	0.151	0.835	6.0
H18	0.048	0.222	0.917	7.9
H19	0.330	0.268	0.914	8.2
H20	0.633	0.245	0.825	7.1
H21	0.657	0.173	0.746	5.6

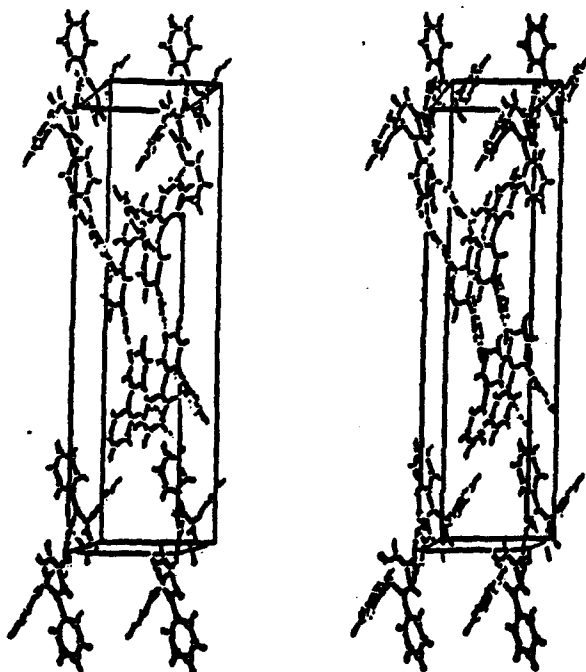


Figure 4 Stereo view of DPO showing molecular packing in unit cell. Molecules positioned on front corners are omitted for clarity. The *c* axis is horizontal and the *b* axis is vertical

a, while the pendant-oligomer bond in DPQ and DPS aligns approximately parallel to the *b* axis. In results to be published, *para*-quinquephenyl and *para*-sexiphenyl have their oligomer axes preferentially aligning with *b* (ref. 12). Thus, with the exception of TPB, the pendant-oligomer bond aligns with the longest crystallographic

Table 5 Bond distances and angles for 2²,6⁶-diphenyl-p-septiphenyl. Numbers in parentheses are estimated standard deviations in the least significant digit

Atom 1	Atom 2	Distance (Å)	Atom 1	Atom 2	Distance (Å)
C1	C2	1.381(4)	C8	C9	1.388(4)
C1	C3	1.380(4)	C10	C11	1.382(5)
C1	C4	1.392(4)	C10	C15	1.401(4)
C1	C5	1.392(4)	C11	C12	1.379(4)
C1	C6	1.490(4)	C12	C13	1.379(4)
C1	C7	1.385(4)	C13	C14	1.367(6)
C2	C3	1.386(4)	C14	C15	1.387(5)
C2	C4	1.389(5)	C16	C17	1.390(5)
C2	C5	1.405(4)	C16	C21	1.385(5)
C2	C6	1.483(4)	C17	C18	1.367(5)
C2	C7	1.385(5)	C18	C19	1.367(6)
C3	C4	1.489(4)	C19	C20	1.377(6)
			C20	C21	1.382(5)

Atom 1	Atom 2	Atom 3	Angle (deg)	Atom 1	Atom 2	Atom 3	Angle (deg)
C1	C2	C3	117.1(4)	C4	C9	C8	120.5(3)
C1	C2	C3 ^a	120.5(4)	C7	C10	C11	122.0(3)
C1	C2	C2 ^a	121.7(4)	C7	C10	C15	119.5(4)
C1	C2	C1 ^a	121.7(4)	C11	C10	C15	118.5(3)
C1	C2	C1 ^b	120.5(4)	C10	C11	C12	120.9(3)
C1	C4	C4	121.0(4)	C11	C12	C13	120.3(4)
C1	C5	C5	121.2(3)	C12	C13	C14	119.7(4)
C1	C9	C9	120.9(3)	C13	C14	C15	120.9(4)
C1	C9	C9	118.1(3)	C10	C15	C14	119.8(4)
C1	C6	C6	122.4(4)	C6	C16	C17	121.5(4)
C1	C7	C7	118.8(4)	C6	C16	C21	120.7(3)
C1	C16	C16	118.1(3)	C17	C16	C21	117.9(3)
C1	C16	C16	123.0(3)	C16	C17	C18	121.1(5)
C1	C8	C8	118.7(4)	C17	C18	C19	120.7(4)
C1	C10	C10	122.1(3)	C18	C19	C20	119.4(4)
C1	C10	C19	119.4(4)	C19	C20	C21	120.3(4)
C7	C9	C9	121.6(3)	C16	C21	C20	120.7(4)

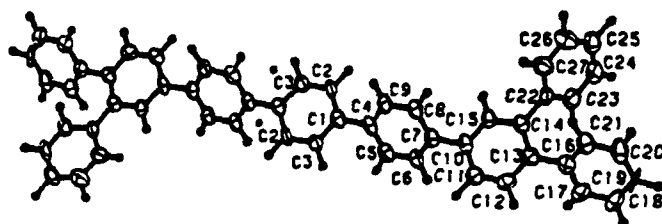


Figure 5 2²,6⁶-Diphenyl-p-septiphenyl with carbon atom ellipsoids drawn at the 50% probability level

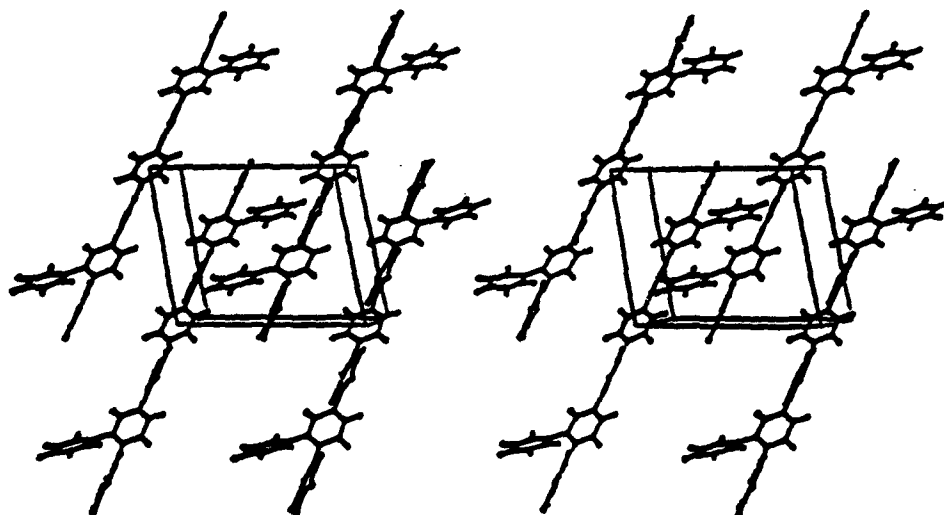


Figure 6 The c axis stereo view of DPS showing molecular packing in unit cell. Molecules on rear corners are omitted for clarity. The a axis is horizontal

Table 6 Atomic positions of 2²,6⁵-diphenyl-p-septiphenyl. Numbers in parentheses are estimated standard deviations in the least significant digit

Atom	x	y	z	B (Å ²)	Atom	x	y	z	B (Å ²)
C1	0.9955(2)	0.5334(2)	0.3887(5)	3.77(6)	C24	1.1891(3)	1.0774(2)	-0.2842(6)	5.77(9)
C2	0.5515(3)	0.6040(2)	0.5322(5)	4.39(7)	C25	1.2395(3)	1.1418(2)	-0.0761(6)	5.46(8)
C3	0.5417(3)	0.4279(2)	0.3591(5)	4.35(7)	C26	1.2498(3)	1.1005(2)	0.1086(6)	5.63(9)
C4	0.6961(2)	0.5681(2)	0.2739(4)	3.68(6)	C27	1.2106(3)	0.9936(2)	0.0831(5)	4.86(8)
C5	0.6946(2)	0.5225(2)	0.0484(5)	4.14(7)	H2	0.584	0.686	0.542	4.0
C6	0.7882(2)	0.5537(2)	-0.0607(5)	4.02(7)	H3	0.581	0.376	0.252	4.0
C7	0.8867(2)	0.6335(2)	0.0543(4)	3.64(6)	H5	0.616	0.461	-0.056	5.3
C8	0.885(2)	0.6795(2)	0.2815(5)	4.00(7)	H6	0.780	0.520	-0.225	5.1
C9	0.7949(2)	0.6472(2)	0.3898(5)	3.96(7)	H8	0.965	0.737	0.377	5.1
C10	0.9859(2)	0.6701(2)	-0.0632(4)	3.72(6)	H9	0.801	0.681	0.560	5.0
C11	1.0330(2)	0.6003(2)	-0.2050(5)	4.10(7)	H11	0.999	0.519	-0.223	5.3
C12	1.1240(2)	0.6361(2)	-0.3156(5)	4.02(7)	H12	1.164	0.586	-0.415	5.3
C13	1.1701(2)	0.7422(2)	-0.2927(5)	3.71(6)	H15	1.001	0.828	0.064	4.8
C14	1.1220(2)	0.8133(2)	-0.1541(4)	3.64(6)	H17	1.188	0.679	-0.719	5.7
C15	1.0324(2)	0.7763(2)	-0.0412(5)	3.79(6)	H18	1.337	0.717	-0.932	7.4
C16	1.2689(2)	0.7753(2)	-0.4146(5)	3.87(6)	H19	1.520	0.852	-0.735	7.6
C17	1.2621(3)	0.7288(2)	-0.6430(5)	4.42(7)	H20	1.536	0.938	-0.309	7.2
C18	1.3543(3)	0.7581(2)	-0.7584(5)	5.70(8)	H21	1.578	0.882	-0.126	6.0
C19	1.4544(3)	0.8336(2)	-0.6477(6)	6.00(9)	H23	1.105	0.920	-0.476	6.0
C20	1.4637(3)	0.8798(2)	-0.4215(6)	5.67(9)	H24	1.172	1.102	-0.430	7.4
C21	1.3727(2)	0.8515(2)	-0.3039(5)	4.57(7)	H25	1.274	1.230	-0.048	6.8
C22	1.1624(2)	0.9279(2)	-0.1274(5)	3.77(6)	H26	1.291	1.148	0.283	7.1
C23	1.1510(3)	0.9711(2)	-0.3105(5)	4.89(8)	H27	1.221	0.967	0.224	6.1

Table 7 Bond distances and angles for 2²,6⁵-diphenyl-p-septiphenyl. Numbers in parentheses are estimated standard deviations in the least significant digit

Atom 1	Atom 2	Distance (Å)	Atom 1	Atom 2	Distance (Å)
C1	C2	1.387(4)	C13	C14	1.404(4)
C2	C3	1.397(3)	C13	C16	1.487(5)
C3	C3 ^o	1.380(4)	C14	C15	1.384(4)
C3	C3 ^o	1.380(4)	C14	C22	1.493(3)
C4	C4	1.481(4)	C16	C17	1.395(4)
C4	C5	1.387(4)	C16	C21	1.404(3)
C5	C9	1.393(4)	C17	C18	1.390(5)
C6	C6	1.383(4)	C18	C19	1.372(4)
C7	C7	1.394(4)	C19	C20	1.378(5)
C7	C8	1.397(4)	C20	C21	1.384(5)
C8	C10	1.486(4)	C22	C23	1.382(4)
C10	C9	1.384(4)	C22	C27	1.380(4)
C10	C11	1.395(4)	C23	C24	1.384(4)
C10	C15	1.399(3)	C24	C25	1.386(4)
C11	C12	1.382(5)	C25	C26	1.374(5)
C12	C13	1.395(4)	C26	C27	1.393(4)

Atom 1	Atom 2	Atom 3	Angle (deg)	Atom 1	Atom 2	Atom 3	Angle (deg)
C2	C1	C3	117.1(3)	C12	C13	C14	118.7(3)
C2	C1	C4	121.5(2)	C12	C13	C16	118.6(2)
C3	C4	C4	121.4(2)	C14	C13	C16	122.8(2)
C3	C4	C5	120.9(2)	C14	C13	C15	119.3(2)
C4	C2	C3 ^o	121.8(2)	C13	C14	C22	122.2(2)
C4	C2	C2 ^o	121.1(2)	C15	C14	C22	118.5(2)
C4	C3	C1 ^o	121.1(2)	C10	C15	C14	122.4(3)
C4	C3	C1 ^o	121.8(2)	C13	C16	C17	120.5(3)
C4	C4	C9	120.9(2)	C13	C16	C21	121.6(2)
C4	C4	C9	118.2(3)	C17	C16	C21	117.8(3)
C5	C6	C6	121.5(2)	C16	C17	C18	121.1(2)
C6	C7	C7	120.3(2)	C17	C18	C19	120.1(3)
C6	C7	C8	118.2(3)	C18	C19	C20	119.9(3)
C6	C7	C10	120.8(2)	C19	C20	C21	120.8(2)
C7	C8	C10	121.0(2)	C16	C21	C20	120.3(3)
C7	C8	C9	121.1(3)	C14	C21	C23	121.2(2)
C7	C9	C8	120.6(2)	C14	C22	C27	120.4(3)
C7	C10	C11	121.6(2)	C23	C22	C27	118.4(2)
C7	C10	C15	120.7(2)	C23	C23	C24	120.9(2)
C11	C10	C15	117.7(3)	C23	C24	C25	120.5(3)
C10	C11	C12	120.6(2)	C24	C25	C26	119.5(3)
C11	C12	C13	121.4(3)	C25	C26	C27	120.1(3)
				C22	C27	C26	120.6(4)

Table 8 Summary of bond lengths between phenyl units measured at room temperature. Nomenclature of the phenyl links is relative to the centre of symmetry in the molecule such that the phenyl link is that bond which lies on the symmetry centre or the nearest phenyl link if the symmetry centre exists at a phenyl unit (see general structure). Numbers in parentheses are estimated standard deviations in the least significant digit. P means planar conformation and N means non-planar conformation

Compound name	A (Å)	B (Å)	C (Å)	α (Å)	Conformation
Biphenyl ⁹	1.495(5)	-	-	-	P
<i>p</i> -Terphenyl ¹⁰	1.505(5)	-	-	-	P
<i>p</i> -Quaterphenyl ¹¹	1.502(4)	1.486(5)	-	-	P
<i>p</i> -Quinquephenyl ¹²	1.481(5)	1.482(5)	-	-	P
<i>p</i> -Sexiphenyl ¹²	1.506(6)	1.501(8)	1.461(8)	-	P
1,2,4-Triphenyl-benzene	1.486(2)	1.489(2)	-	1.489(2)	N
2 ² ,4 ² -Diphenyl- <i>p</i> -quinquephenyl	1.490(4)	1.489(4)	-	1.483(4)	N
2 ² ,6 ² -Diphenyl- <i>p</i> -septiphenyl	1.481(4)	1.486(4)	1.487(5)	1.493(3)	N

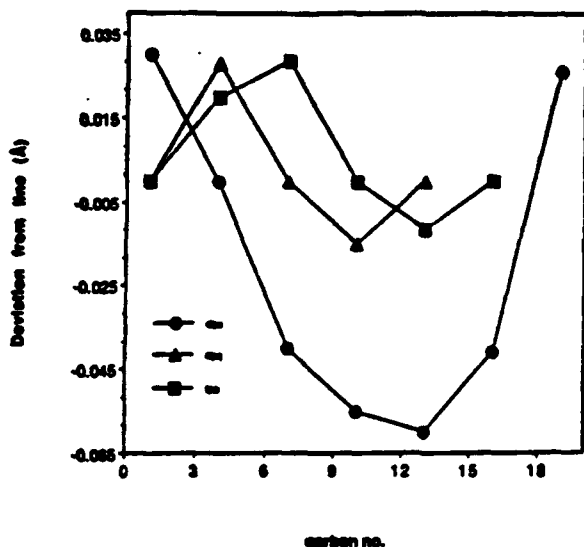


Figure 7 Deviation of the carbon atoms composing the oligomer axis from least squares line

axis. The short chain axis of TPB and lack of molecular symmetry appear to play an important role in this alignment.

The addition of the phenyl pendant groups disrupts the planarity of the polyphenyls observed in the room temperature structures of biphenyl¹², *para*-terphenyl¹⁴, *para*-quaterphenyl¹¹, *para*-quinquephenyl and *para*-sexiphenyl¹², as seen in *Tables 9* and *10*. This is most probably due to steric hindrance of the pendant groups with the oligomer chain and crystal packing forces. Hydrogen-to-hydrogen distances between phenyl rings (H2-H9 in DPS, for example) are approximately equal to 2.5 Å. Hydrogen atoms on the terminal phenyl ring closest to the pendant group are approximately equidistant from one of the *ortho* hydrogen atoms on the pendant group. In DPQ, for example, H11 and H15 on the terminal phenyl ring are both approximately 3.6 Å from H17 on the pendant ring (see *Figure 9*). The corresponding values in DPS are 3.7 Å. For the three pendant-substituted oligomers, the pendant hydrogen atom-to-terminal phenyl hydrogen atom contact increases with oligomer length (from approximately 3.5 Å in TPB to 3.7 Å in DPS).

The average torsion angle within the oligomer chain

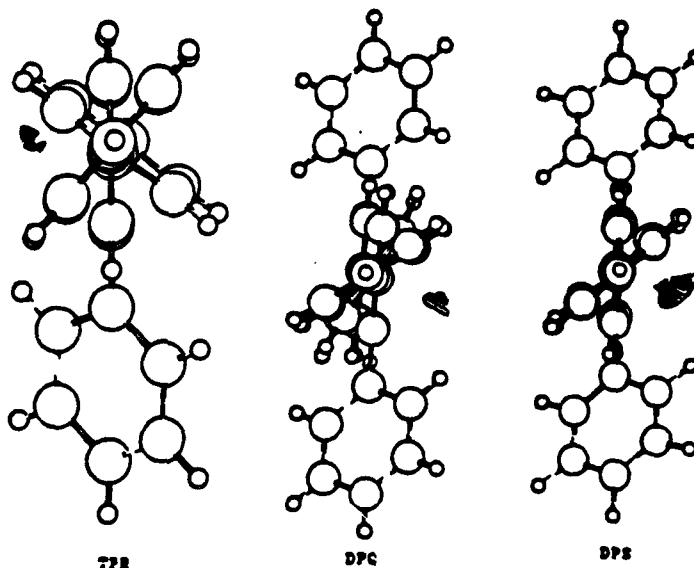


Figure 8 View down oligomer axes of TPB, DPQ, and DPS showing tortuosity of axis

Table 9 Torsion angles of straight chain polyphenyls. The torsion angles are labelled relative to the symmetry centre of the molecule such that if a symmetry centre exists on the bond connecting two phenyl units the torsion angle refers to the two adjacent rings. If a centre of symmetry exists in a phenyl unit the torsion angle refers to the nearest chain link (see general structure)

Name	Formula	Temperature (K)	ψ_1 (deg)	ψ_2 (deg)	ψ_3 (deg)
Biphenyl	$C_{12}H_{10}$	298 ¹³	0	-	-
		40 ⁹	10	-	-
<i>p</i> -Terphenyl	$C_{18}H_{14}$	298 ¹⁴	0	-	-
		110 ¹³	16	-	-
<i>p</i> -Quaterphenyl	$C_{24}H_{18}$	298 ¹¹	0	0	-
		110 ¹⁰	17.1	22.7	-
<i>p</i> -Quinquephenyl	$C_{30}H_{22}$	298 ¹²	0	0	-
		110	Work in progress		
<i>p</i> -Sexiphenyl	$C_{36}H_{26}$	298 ¹²	0	0	0
		110	Work in progress		
<i>p</i> -Septiphenyl	$C_{42}H_{30}$	298	Work in progress		
		110	Work in progress		

Table 10 Torsion angles of pendant polyphenyls. The torsion angles are labelled relative to the symmetry centre of the molecule such that if a symmetry centre exists on the bond connecting two phenyl units the torsion angle refers to the two adjacent rings. If a centre of symmetry exists in a phenyl unit the torsion angle refers to the nearest chain link. Pendant refers to the torsion angle between the pendant group and the phenyl group to which it is attached (see general structure)

Name	Formula	Temperature (K)	ψ_1 (deg)	ψ_2 (deg)	ψ_3 (deg)	π (deg)
1,2,4-Triphenyl-benzene	$C_{24}H_{18}$	298	42.8	49.8	-	48.4
		110	Work in progress			
2 ² ,3 ⁵ -Diphenyl- <i>p</i> -quaterphenyl	$C_{36}H_{26}$	298	Work in progress			
		110	Work in progress			
2 ² ,4 ³ -Diphenyl- <i>p</i> -quinquephenyl	$C_{42}H_{30}$	298	-28.0	51.2	-	55.7
		110	Work in progress			
2 ² ,5 ⁴ -Diphenyl- <i>p</i> -sexiphenyl	$C_{48}H_{34}$	298	Work in progress			
		110	Work in progress			
2 ² ,6 ⁵ -Diphenyl- <i>p</i> -septiphenyl	$C_{54}H_{38}$	298	43.2	-45.6	48.6	61.0
		110	Work in progress			

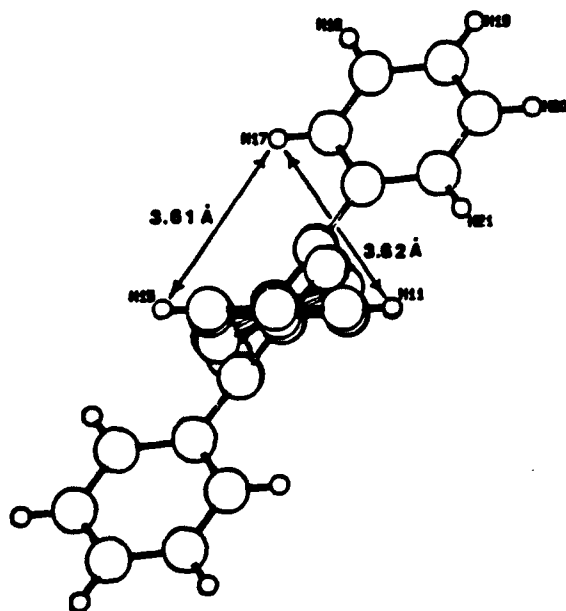


Figure 9 Hydrogen atom repulsion distances between pendant and oligomer axis for 2²,4³-diphenyl-*p*-quinquephenyl

is 45°, which is approximately twice the value of 23° predicted for PPP from structural data and further supported by *ab initio* quality quantum mechanical calculations³. The exception is DPQ which has torsion angles of approximately -28° at the centre ring, but angles of 51° for the terminal ring. The reason for this

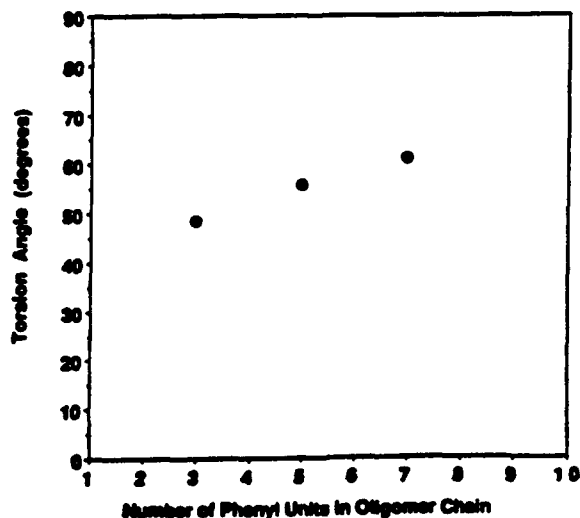


Figure 10 Graph of pendant torsion angle vs. total number of phenyl units in oligomer chain

large difference unique to this oligomer is not clear at this time.

The torsion angle between the pendant group and the oligomer chain is greater than 45°, increasing with chain length. As the hydrogen atoms of the main chain approach the hydrogen atoms of the pendant group, the pendant torsion angle decreases. This trend is not yet understood and more measurements on different model systems are under consideration. Fully-optimized

AMPAC AM1 conformational calculations for the low energy structure of *ortho*-phenyl-substituted biphenyl reveal torsion angles of approximately 40° (ref. 17). A line with a positive slope is obtained when the pendant torsion angle is plotted against the number of phenyl units in the oligomer chain (see Figure 10).

CONCLUSIONS

The non-planar structures of the phenyl-substituted oligomers contrast with average planar structures observed for the unsubstituted polyphenyls. The average torsion angle along the oligomer chain is 45°. The oligomer axis does not align with a crystallographic axis; however, the pendant connect bond prefers to align parallel to one of the crystallographic axes. The pendant torsion angle increases with chain length. More research is needed on oligomers with even numbers of phenyl units along the main chain to compare and contrast with those which have an odd number. Also the pendant groups of the title compounds occupy positions closest to the terminal phenyl unit. Similar measurements of compounds where the pendant group is attached closest to the central phenyl unit are needed to identify the major reasons for variations in the torsion angles along the oligomer axis.

ACKNOWLEDGEMENTS

Research was sponsored in part by the Air Force Office of Scientific Research, Air Force Systems Command, AFSC, under Grant Number AFOSR-88-0044. Further acknowledgements go to Timothy Resch for X-ray photography and density measurements and to Edward Soloski for d.s.c. analysis.

REFERENCES

- 1 Duke, C. B. and Gibson, H. W. in 'Kirk-Othmer Encyclopedia of Chemical Technology', 3rd Edn. Wiley, New York, 1982, vol. 18, p. 755
- 2 Unroe, M. R. and Reinhardt, B. A. *Synthesis* 1987, 11, 981
- 3 Baughman, R. H., Bredas, J. L., Chance, R. R., Elsebaumer, R. J. and Shacklette, L. N. *Chem. Rev.* 1982, 82, 209
- 4 Wierschke, S. G. in 'The Materials Science and Engineering of Rigid-Rod Polymers', (Eds W. W. Adams, R. K. Eby, and D. E. McLemore) *Mater. Res. Soc. Proc.* 1989, 134, 313
- 5 Frenz, B. A. and Associates, Inc. 'SDP/VAX Structure Determination Package', College Station, Texas 77840, and Enraf-Nonius, Delft, The Netherlands, 1985
- 6 Main, P., Ed. 'Muitan 11 82. A System of Computer Programs for the Automatic Solution of Crystal Structures from X-ray Diffraction Data', Department of Physics, University of York, York, UK, 1982
- 7 Sheldrick, G. M. in 'Crystallographic Computing 3', (Eds G. M. Sheldrick, C. Kruger and R. Goddard), Oxford University Press, Oxford, 1985, p. 175
- 8 International Tables for X-Ray Crystallography 1968, Vol. III, The Kynoch Press, Birmingham, UK, p. 276
- 9 Cailleau, H., Baudour, J. L. and Zeyen, C.M.E. *Acta Cryst.* 1979, B35, 426
- 10 Baudour, J. L. and Cailleau, H. *Acta Cryst.* 1977, B33, 1773
- 11 Delugeard, Y., Desuiche, L. and Baudour, J. L. *Acta Cryst.* 1976, B32, 702
- 12 Baker, K. N., Kaschel, H. C., Fratini, A. V. and Adams, W. W., in preparation
- 13 Trotter, J. *Acta Cryst.* 1961, 14, 1135
- 14 Rietveld, H. M., Maslen, E. N. and Clews, C. J. B. *Acta Cryst.* 1970, B26, 693
- 15 Baudour, J. L., Delugeard, Y. and Cailleau, H. *Acta Cryst.* 1976, B32, 150
- 16 Baudour, J. L., Delugeard, Y. and Rivet, P. *Acta Cryst.* 1978, B34, 625
- 17 Farmer, B. L. and Adams, W. W. in 'The Materials Science and Engineering of Rigid-Rod Polymers', (Eds W. W. Adams, R. K. Eby, and D. E. McLemore) *Mater. Res. Soc. Proc.* 1989, 134, 447

EVIDENCE FOR THE PRESENCE OF HYDROGEN-BONDED ION-ION INTERACTIONS IN THE MOLTEN SALT PRECURSOR, 1-METHYL-3-ETHYLIMIDAZOLIUM CHLORIDE

C.J. DYMEK, JR.*

The Frank J. Seiler Research Laboratory, United States Air Force Academy, Colorado Springs, CO 80840 (U.S.A.)

DAVID A. GROSSIE

Department of Chemistry, Wright State University, Dayton, OH 45435 (U.S.A.)

ALBERT V. FRATINI

Department of Chemistry, University of Dayton, Dayton, OH 45469 (U.S.A.)

W. WADE ADAMS**

Materials Laboratory, Air Force Wright Aeronautical Laboratories, Wright-Patterson Air Force Base, OH 45433 (U.S.A.)

(Received 10 January 1989)

ABSTRACT

The crystal structure analysis and IR study of the molten salt precursor, 1-methyl-3-ethylimidazolium chloride (MEICl) has been undertaken as part of an investigation of the ion-ion interactions in room temperature melts, where the mole fraction of AlCl_3 is less than 0.5. Hygroscopic crystals of MEICl have been grown in acetonitrile and sealed under helium gas in a capillary tube. The orthorhombic space group is $P2_12_12_1$, with $a=10.087(1)$, $b=11.179(1)$, $c=28.733(4)$ Å, $V=3240.0$ Å³, mol. wt. = 146.62 and $D_{\text{calc}}=1.204$ g cm⁻³ for $Z=16$. The asymmetric unit contains four $\text{MEI}^+\cdots\text{Cl}^-$ ion pairs. The MEI^+ ions cluster in four distinct layers perpendicular to the c axis. Similarly, the arrangement of Cl^- ions is a layered one. Each Cl^- interacts with three MEI^+ ions and each MEI^+ is associated with three nearest Cl^- ions. The distance of Cl^- from a ring carbon atom averages 3.55 Å. Cl^- ions are situated in hydrogen-bonded positions rather than at random, characteristic of a $\text{C-H}\cdots\text{Cl}^-$ hydrogen-bond interaction. Evidence for the presence of hydrogen bonding of Cl^- at the three ring C-H bonds in basic MEICl/ AlCl_3 melts is presented.

INTRODUCTION

Mixtures of 1-methyl-3-ethylimidazolium chloride, MEICl, and AlCl_3 , where the mole fraction (N) of AlCl_3 is between 0.33 and 0.67, are molten salts at

*Present address: European Office of Aerospace Research and Development, United States Air Force, 223/231 Old Marylebone Rd., London, NW1 5TH, Gt. Britain.

**Author to whom correspondence should be addressed.

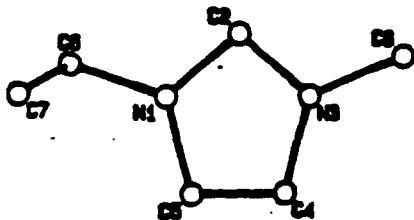


Fig. 1. Structure of one of the four MEI⁺ ions in the asymmetric unit. Selected average bond distances (Å) and bond angles (°) are: N1-C2 1.27; C2-N3 1.30; N3-C4 1.39; C4-C5 1.38; C5-N1 1.41; N1-C6 1.55; C6-C7 1.43; N3-C8 1.48; C2-N1-C5 109; N1-C2-N3 110; C2-N3-C4 111; N3-C4-C5 104; C4-C5-N1 106; C2-N1-C6 130; C5-N1-C6 121; C2-N3-C8 126; C4-N3-C8 123; and N1-C6-C7 104. MEI⁺ (3) values for N1-C6 and C6-C7 are omitted from the average bond distances presented. Maximum estimated standard deviations for individual bond distances and bond angles are 0.05 Å and 4°, respectively.

and well below room temperature [1,2]. Pure MEICl has a melting point of 87°C. These melts are of interest as electrolytes in high energy-density batteries [3,4], as solvents for studying ionic complexes [5], and as catalytic solvents for organic reactions [6]. The potential utility of these melts has prompted studies into the nature of the ionic interactions in the melts.

IR spectroscopy [7] recently showed that the MEI⁺ ion interacts with Cl⁻ ions present in basic melts ($N < 0.5$) at the C2, C4, and C5 positions shown in Fig. 1. This result differs from the ion-pair model in which Cl⁻ is hydrogen bonded solely at the C2 position. An alternative model was suggested but not satisfactorily demonstrated in which the MEI⁺ ions are stacked parallel to each other with Cl⁻ and AlCl₄⁻ anions positioned such that Cl⁻ can interact with all three ring C-H bonds. Since the IR spectra of solid and liquid (90°C) MEICl were shown to be very similar, the structure analysis of MEICl was undertaken to determine the nature of MEI⁺...Cl⁻ interactions in molten salts.

EXPERIMENTAL METHODS

Solid MEICl was prepared by the reaction of 1-methylimidazole and ethyl chloride in airless glassware as described previously [1]. The solvent of recrystallization was acetonitrile rather than ethyl acetate, a procedure which enhanced crystal quality. Unfortunately, the crystals were observed to retain a coating of mother liquor even after nine days under vacuum.

A small, irregularly-shaped crystal of MEICl with dimensions 0.25 mm × 0.25 mm × 0.35 mm was mounted in a glass capillary under dry box conditions. Preliminary examination and data collection were performed with Mo K α radiation ($\lambda = 0.71073$ Å) on an Enraf-Nonius CAD4 diffractometer equipped with a graphite crystal incident beam monochromator.

Cell constants and an orientation matrix for data collection were obtained

from least-squares refinement, using the setting angles of 25 reflections in the range $5.0 < \theta < 16.3^\circ$. The orthorhombic cell parameters and calculated volume are: $a = 10.087(1)$, $b = 11.179(1)$, $c = 28.733(4)$ Å, $V = 3240.0$ Å³. For $Z = 16$ and $MW = 146.62$, the calculated density is 1.20 g cm⁻³, which compares with the measured density of 1.204 ± 0.004 g cm⁻³ obtained by flotation in a benzene/carbon tetrachloride mixture. From the observed systematic absences and subsequent least-squares refinement, the space group was determined to be $P2_12_12_1$ (No. 19).

The data were collected at room temperature using the $w/2\theta$ scan technique. The scan rate was calculated from the results of a fast pre-scan, and varied from 0.69 to 2.78° min⁻¹ (in omega). Data were collected to a maximum 2θ of 50.0° ($h = 0-12$, $k = 0-13$, $l = 0-34$).

Three representative reflections were measured every 30 min as a check on crystal and electronic stability. The intensities of these standards remained constant within experimental error throughout data collection and no decay correction was applied. The extremely hygroscopic crystal moved slowly inside the capillary during data collection. This movement was carefully monitored by periodically examining the orientation check reflections. Reorientation of the crystal occurred on average every 125 reflections; 3284 unique reflections were collected. Lorentz and polarization corrections were applied to the data. The linear absorption coefficient was 3.9 cm⁻¹ for Mo $K\alpha$ radiation and no absorption correction was made.

The structure was solved by direct methods [9]. Hydrogen atoms were located and added to the structure factor calculations but their positions were not refined. The structure was refined by full matrix least-squares [10] where the function minimized was $\sum w(|F_o| - |F_c|)^2$ and the weight w is defined as the reciprocal of the standard deviation of F_o , squared. Atomic scattering factors were taken from Cromer and Waber [11] and the values for $\Delta f'$ and $\Delta f''$ were those of Cromer [12].

865 Reflections having intensities greater than 3.0 times their standard deviation were used in the refinements. The final cycle of refinement included 159 variable parameters and converged (largest parameter shift was 0.07 times its estimated standard deviation) with unweighted and weighted agreement factors of 0.10 and 0.13, respectively. The standard deviation of an observation of unit weight was 3.63. Because of unresolved problems associated with the refinement of C26 and C27, their positions were held fixed during the final cycle of refinement. The highest peak in the final difference Fourier map had a height of 0.44 e Å⁻³ with an estimated error based on ΔF of 0.10, while the largest negative peak had a height of 0.41 e Å⁻³. The two largest positive density peaks were located in the vicinity of C26 and C27; others were randomly located throughout the unit cell.

Fractional coordinates and equivalent isotropic thermal parameters for the 36 nonhydrogen atoms are reported in Table 1. Observed and calculated struc-

TABLE 1

Fractional coordinates and equivalent isotropic thermal parameters and their estimated standard deviation

	Atom	x	y	z	B (Å ²) ^a
MEI* (1)	N1	0.834(3)	0.673(2)	0.5846(8)	6.3(7)
	C2	0.758(3)	0.742(3)	0.562(1)	7(1)
	N3	0.680(2)	0.800(2)	0.5907(7)	4.8(6)
	C4	0.701(3)	0.765(2)	0.6355(8)	3.4(6)
	C5	0.804(3)	0.680(3)	0.6325(9)	5.6(8)
	C6	0.944(3)	0.599(3)	0.568(1)	8(1)
	C7	0.913(4)	0.478(4)	0.568(1)	15(2)
	C8	0.581(3)	0.883(3)	0.577(1)	6.3(9)
MEI* (2)	N11	-0.065(2)	0.014(2)	0.4069(8)	5.5(7)
	C12	-0.118(3)	-0.054(3)	0.3799(9)	5.3(8)
	N13	-0.072(2)	-0.050(2)	0.3393(7)	5.0(6)
	C14	0.019(3)	0.047(3)	0.334(1)	6.4(9)
	C15	0.044(4)	0.078(3)	0.381(1)	9(1)
	C16	-0.090(3)	0.052(3)	0.460(1)	6.8(9)
	C17	0.008(4)	-0.032(3)	0.481(1)	11(1)
	C18	-0.129(3)	-0.121(3)	0.2984(9)	6.1(9)
MEI* (3)	N21	0.752(3)	0.289(3)	0.341(1)	9.4(9)
	C22	0.813(3)	0.366(3)	0.3668(9)	6.0(9)
	N23	0.783(2)	0.340(2)	0.4104(7)	4.1(6)
	C24	0.685(3)	0.250(3)	0.4096(9)	4.8(8)
	C25	0.671(4)	0.217(3)	0.364(1)	9(1)
	C26	0.807 ^b	0.250 ^b	0.285 ^b	12(1)
	C27	0.723 ^b	0.279 ^b	0.262 ^b	16(2)
	C28	0.822(3)	0.398(2)	0.4538(9)	5.0(8)
MEI* (4)	N31	0.642(2)	-0.060(2)	0.1583(7)	4.0(5)
	C32	0.565(2)	-0.001(2)	0.1866(8)	3.0(6)
	N33	0.482(2)	0.063(2)	0.1623(7)	3.7(5)
	C34	0.495(3)	0.043(3)	0.1169(9)	4.4(7)
	C35	0.589(3)	-0.039(3)	0.115(1)	5.0(8)
	C36	0.764(3)	-0.145(3)	0.167(1)	7(1)
	C37	0.714(3)	-0.232(3)	0.197(1)	8(1)
	C38	0.390(3)	0.154(3)	0.184(1)	7(1)
	C11	0.2339(9)	0.7793(8)	0.5556(3)	5.8(2) ^a
	C12	0.476(1)	0.9408(8)	0.7042(3)	6.6(2) ^a
	C13	-0.173(1)	0.8055(8)	1.0402(3)	6.6(2) ^a
	C14	-0.4661(1)	0.9774(8)	1.3019(3)	6.4(2) ^a

^aAn asterisk indicates that the atoms were refined anisotropically and are given in the form of the isotropic equivalent thermal parameter defined as: $(4/3)[a^2B_{11} + b^2B_{22} + c^2B_{33} + ab(\cos\gamma)B_{12} + ac(\cos\beta)B_{13} + bc(\cos\alpha)B_{23}]$.

^bParameter was fixed during the final cycle of least-squares refinement.

ture factor amplitudes and other details of the structure analysis are available from B.L.L.D. as Supplementary Publication No. SUP 26375 (6 pages).

Infrared spectra were recorded on an IBM IR/32 FTIR spectrometer. The liquid MEICl sample was a thin film between NaCl plates with no spacers.

DISCUSSION

MEI⁺ cation

The asymmetric unit consists of four $\text{MEI}^+ \cdots \text{Cl}^-$ ion pairs. Figure 1 shows a view of one of the four substituted imidazolium ions. The endocyclic bond distances and angles in the four MEI^+ ions vary markedly from ring to ring (1.21–1.51 Å and 101–114°). The exocyclic alkyl groups are attached to the ring with bond distances of 1.43–1.74 Å. In $\text{MEI}^+(2)$ and $\text{MEI}^+(4)$ ions, the β carbon of each ethyl substituent is above the mean plane of the five-membered ring, with torsion angles (C12–N11–C16–C17 and C32–N31–C36–C37) of 96.3 and 55.7°, respectively, while in the $\text{MEI}^+(1)$, the beta carbon is below the ring, with a torsion angle (C2–N1–C6–C7) of -107.3° . Atoms C26 and C27 of the ethyl substituent in ($\text{MEI}^+(3)$) are disordered. This observation reflects one of the difficulties in the crystallographic examination of these molten salt precursors.

Unit cell

As shown in Fig. 2, the ion pairs pack into the unit cell in ways similar to both planar molecules and simple inorganic salts. The MEI^+ ions cluster in four distinct layers, perpendicular to the *c* axis, with interlayer separations of 6.741–7.568 Å as defined by the average distances between ring centroids. Within a layer, each molecule is separated from its neighbor by 3.792–4.091 Å as measured along the diagonal, while the edge-to-edge separation is 7.381–7.704 Å. The middle layers differ in orientation in the same manner as the first and fourth layers.

As described for the MEI^+ ions, the arrangement of Cl^- ions is a layered one, comprising four different patterns of anions. The first two patterns at $z = -0.05$ and 0.05 are related by space group symmetry, each consisting of a pair of Cl^- ions situated approximately on *ab* cell diagonals. The third and fourth patterns are found at $z = 0.30$ and 0.70 , the former consisting of four ions located approximately on the *ac* and *bc* faces of the unit cell, while the latter is comprised of a plane of five ions, one close to each cell edge and the fifth approximately in the center of the cell. These four patterns occur cyclically along the *c*-axis, the first occurrence of the first and second patterns being split by the bottom *ab* face of the unit cell. The fourth pattern occurs after this, fol-

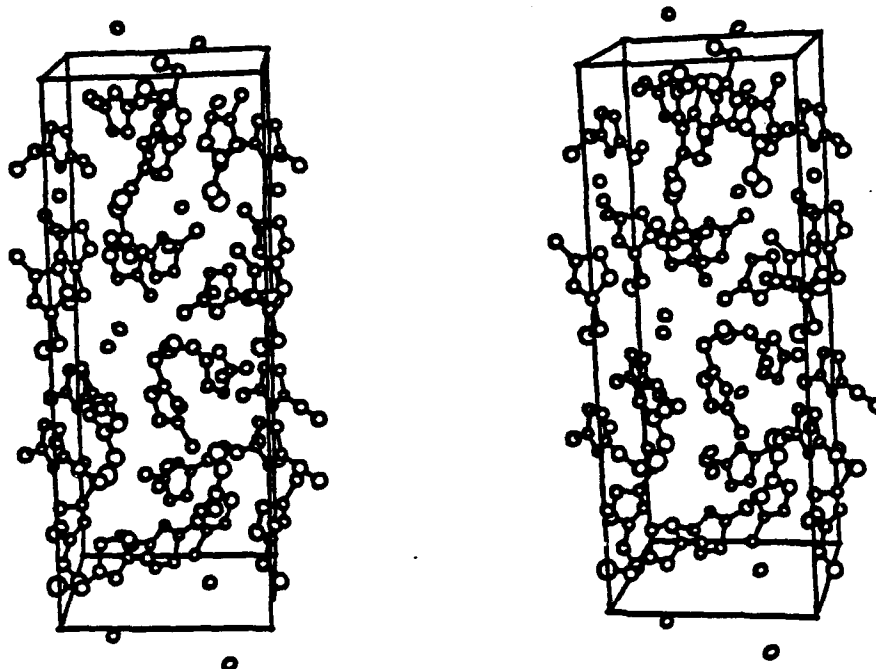


Fig. 2. Stereoview of the MEI Cl unit cell. The c axis is vertical and a is horizontal.

lowed by the third. In the center of the cell, the first and second patterns repeat, after which the third and fourth patterns repeat, and so on.

Interlayer interactions

The relative orientations and connectivity of the MEI $^+$ and Cl $^-$ layers are alternately depicted in Fig. 3. In this drawing, the cations are shown arranged in rows (designated a-h) in which the MEI $^+$ rings share a common plane. The rows in the plane of the drawing (a, c, e and g) represent a cross-section of the layers formed by the staggered stacks of MEI $^+$ running parallel to the plane of the drawing. The alternating rows running perpendicular to the plane of the drawing (b, d, f and h) represent a similar cross-section. The heavy dashed line (the c axis of the unit cell) is at the intersection of these two cross-sections. Note that the rows labelled a and e are equivalent. The light dashed lines connect Cl $^-$ and MEI $^+$ ions which are nearest neighbors. By examining the Cl $^-$ ions on the intersection line, it can be seen that each Cl $^-$ interacts with three MEI $^+$ ions, two of which share a plane which is perpendicular to the plane of the third. Also, each MEI $^+$ is associated with three nearest Cl $^-$ ions which are in the same plane as the MEI $^+$ ring.

There are two rows of Cl $^-$ ions associated with each row of MEI $^+$ ions. One has Cl $^-$ ions interacting with just a single ring carbon atom (alternating between C2 and C5) of the MEI $^+$ ion in an associated row, while another (on the

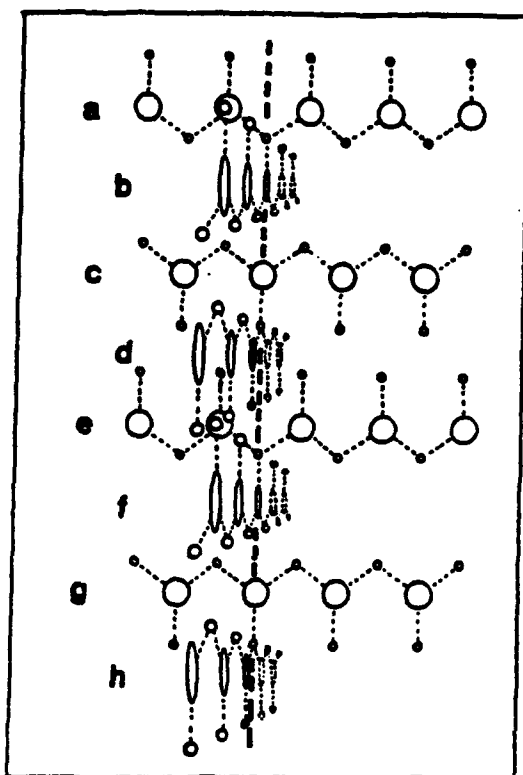


Fig. 3. MEICl structure showing relative orientation and connectivity of adjacent layers. Rows a and e are equivalent. The heavy dashed line represents the direction of *c* axis.

side of the MEI^+ row) has each Cl^- interacting with ring carbon atoms from two adjacent MEI^+ ions in the row. In Fig. 3 these would be the top and bottom Cl^- rows, respectively, interacting with row a of MEI^+ ions. These rows are drawn with uniformly spaced Cl^- ions; however, in the crystal the spacings are alternately large and small. In the top row, the Cl^- ions interacting with C2 are directly above the MEI^+ , while those interacting with C5 are forced to shift in the direction of the C5-H bond and as a consequence away from positions directly above the MEI^+ . If the interaction of Cl^- with MEI^+ were non-specific, the Cl^- ions would be expected to be uniformly spaced to achieve maximum separation. This uneven spacing is seen as evidence for Cl^- ions interacting specifically with MEI^+ through hydrogen bonding.

Ion-ion interactions

Figure 3 shows that the *stack model* in which Cl^- ions are positioned between stacked MEI^+ ions is not supported by the crystal structure and that the $\text{C2-H}\cdots\text{Cl}^-$ hydrogen-bonded ion-pair model is preferred. The triple interactions of each ion in the structure are illustrated in Fig. 4. The distance of

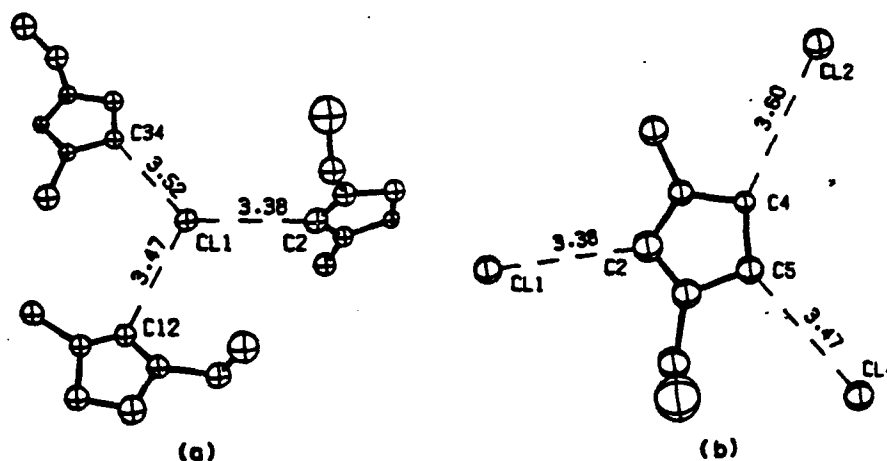


Fig. 4. (a) Representative triple interaction of Cl1 with three nearest MEI⁺ ions. (b) interaction of MEI⁺ (1) with three nearest Cl⁻ ions. Distances (Å) shown are C...Cl⁻ contacts.

a Cl⁻ from a ring carbon atom averages about 3.55 Å, ranging from 3.34 to 3.80 Å. This is in good agreement with the accepted criteria for C-H...Cl⁻ hydrogen bonding [8]. The fact that the Cl⁻ ions are situated in potential hydrogen-bonded positions (C-H...Cl⁻ angle ranges from 132 to 167°) rather than at random also strongly suggests this interaction to be hydrogen bonding. Further evidence for a hydrogen-bonded interaction is provided by ring C-H stretching bands which shift to lower frequencies (by about 100–150 cm⁻¹) and become broader and more intense as more Cl⁻ is present in basic MEICl/AlCl₃ melts [7]. Thus, the C2-H...Cl⁻ hydrogen-bonded ion pair model should account for a C-H...Cl⁻ type interaction at all three ring carbon atoms. Structural evidence for the presence of discrete hydrogen-bond ion pairs ($r\{C2-H...I^{-}\}=2.93$ Å) in crystals of 1-methyl-3-ethylimidazolium iodide has recently been reported [13].

Extension of model to liquid phase

The shift in frequency and broadening of the MEI⁺ ring C-H stretching band observed in basic MEICl/AlCl₃ melts [7] is certainly consistent with the aforementioned hydrogen-bonding model. An equally compelling observation is the comparison of the IR spectra of solid and liquid MEICl shown in Fig. 5. This previously presented [7] but unpublished result supports the conclusions that the interactions with Cl⁻ affecting the ring C-H stretches in MEI⁺ are virtually the same in the solid and liquid phases of MEICl. The presence of AlCl₄⁻ in basic melts may alter the MEI⁺...Cl⁻ interaction only slightly since the peaks of the ring C-H stretching bands in liquid MEICl and basic MEICl/AlCl₃ melts are also virtually the same (the "Cl⁻ interaction band" is at 3049

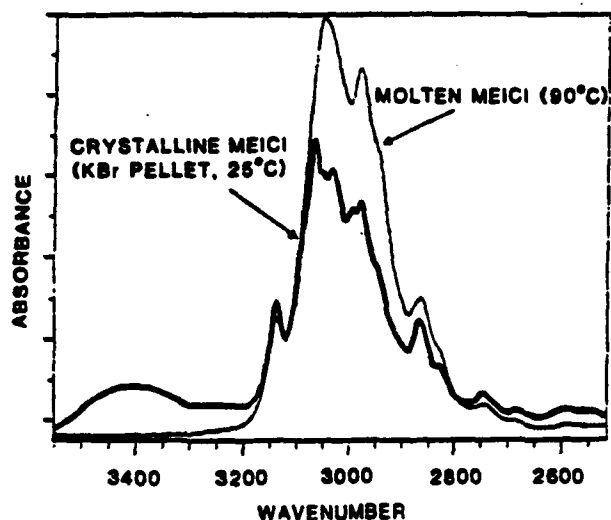


Fig. 5. FTIR spectra of solid and liquid MEICl [7].

cm^{-1} [7]). Thus the $\text{MEI}^+ \cdots \text{Cl}^-$ interactions in basic melts are characterized as hydrogen-bonding of Cl^- at the three ring C-H bonds.

CONCLUSIONS

The structure of crystalline MEICl is characterized by layers containing MEI^+ ions interspersed with layers of Cl^- ions. The directions of the stacks in adjacent layers are rotated 90° . Each MEI^+ ion appears to be hydrogen bonded to three nearest Cl^- ions. The results suggest that in basic MEICl/ AlCl_3 molten salts, the Cl^- ions also interact with MEI^+ by hydrogen bonding at the three ring carbon atoms.

REFERENCES

- 1 J.S. Wilkes, J.A. Levisky, R.A. Wilson and C.L. Hussey, *Inorg. Chem.*, 21 (1982) 1263.
- 2 A.A. Fannin, Jr., D.A. Floreani, L.A. King, J.S. Landers, B.J. Pierama, D.J. Stetch, R.L. Vaughn, J.S. Wilkes and J.L. Williams, *J. Phys. Chem.*, 88 (1984) 2614.
- 3 G.F. Reynolds and C.J. Dymek, Jr., *J. Power Sources*, 15 (1985) 109.
- 4 C.J. Dymek, Jr., G.F. Reynolds and J.S. Wilkes, *J. Electrochem. Soc.*, 134(7) (1987) 1658.
- 5 C.L. Hussey, *Adv. Molten Salt Chem.*, 15 (1983) 185.
- 6 J.A. Boon, J.A. Levisky, J.L. Pflug and J.S. Wilkes, *J. Org. Chem.*, 51 (1986) 480.
- 7 K.M. Dieter, C.J. Dymek Jr., N.E. Heimer, J.W. Rovang and J.S. Wilkes, Ionic structure and interactions in 1-methyl-3-ethylimidazolium chloride/ AlCl_3 molten salts. *Proc. Joint Int. Symp. on Molten Salts, The Electrochemical Society, 1987, Vol. 87-7, page 414.*
- 8 R. Taylor and O. Kennard, *J. Am. Chem. Soc.*, 104 (1982) 5063.

- 9 P. Main (Ed.). MULTAN 11/82. A System of Computer Programs for the Automatic Solution of Crystal Structures from X-ray Diffraction Data. University of York, Gt. Britain. 1982.
- 10 Enraf-Nonius. SDP/VAX. A System of Programs for Crystal Structure Determination. 1982.
- 11 D.T. Cromer and J.T. Waber. International Tables for X-Ray Crystallography, Kynoch Press, Birmingham, 1974, Table 2.2 B, p. 99.
- 12 D.T. Cromer, *ibid.*, Table 2.3.1, p. 149.
- 13 A.K. Abdul-Sada, A.M. Greenway, P.B. Hitchcock, T.J. Mohammed, K.R. Seddon, and J.A. Zora. *J. Chem. Soc., Chem. Commun.*, (1986) 1753.

MOLECULAR PACKING AND CRYSTALLINE ORDER IN
POLYBENZOBISOXAZOLE AND POLYBENZOBISTHIAZOLE FIBERS

ALBERT V. FRATINI^{*}, P. GALEN LENHERT^{**}, TIMOTHY J. RESCH^{*},
AND W. WADE ADAMS

Department of Chemistry, University of Dayton, 300 College
Park, Dayton, OH 45469

Department of Physics, Vanderbilt University, Nashville, TN
37235

Wright Research and Development Center, Materials Laboratory,
WPAFB, OH 45433-6533

ABSTRACT

The structures of poly(p-phenylenebenzobisthiazole) (PBZT) and poly(p-phenylenebenzobisoxazole) (PBO) fibers have been investigated by fiber diffraction techniques. d-spacings were obtained from equatorial and meridional scans recorded on a four-circle diffractometer. Intensity data were derived from x-ray rotation patterns taken on Weissenberg and vacuum cylindrical cameras. Unit cells were found to be monoclinic and non-primitive, each containing two chains per cell of dimensions $a = 11.79(2)$, $b = 3.539(5)$, $c = 12.514(9)$ Å, $\gamma = 94.0(2)^\circ$ for PBZT; and $a = 11.20(1)$, $b = 3.540(2)$, $c = 12.050(3)$ Å, $\gamma = 101.3(1)^\circ$ for PBO. The fiber axes correspond to c. The conformational torsion angle between the bisthiazole and phenylene units and the orientation of chains within the unit cells were obtained from a 'linked-atom least-squares' (LALS) refinement procedure. A packing model is proposed for each polymer in which two independent molecular chains are displaced longitudinally by discrete rather than random increments. Primitive unit cells ($Z = 1$), besides requiring perfect axial registry of molecular chains, suffer from the occurrence of short intermolecular contacts and are rejected from further consideration.

INTRODUCTION

The structures of poly(p-phenylene benzobisthiazole) (PBZT) and poly(p-phenylene benzobisoxazole) (PBO) have been of interest for the past decade. Numerous publications have advanced the understanding of the fiber and film structures of these rigid rod chains [1-3]. Based on diffraction patterns which show molecular transform scattering on layer lines and diffuse (biaxial) reflections along the equator, the as-spun polymer is viewed as a nematic solid with a high degree of orientational order but with axial translational disorder. Heat treatment induces crystallization of the chains, as seen by axial bright field lattice imaging [4,5]. The crystallization process is reported to be more extensive for PBO than for PBZT; thus a considerable amount of axial disorder is expected in the final fiber structure of PBZT [6]. The extent of ordering still does not approach the 3D crystallinity of the chemically similar, extended-chain poly-2,5-benzoxazole (ABPBO) and poly-2,6-benzothiazole (ABPT) molecules, as well as the stiff-chain poly(p-phenylene terephthalamide) (PPTA) fibers [6,7].

Our approach has been to apply the linked-atom least-squares (LALS) method to PBZT and PBO fibers exhibiting the

highest order observed to date. The results, representing the equilibrium crystal structure, serve as a vehicle by which one can measure progress in reaching a fully ordered structure by processing improvements. The goal is to understand changes in structure and morphology imparted by chemical or physical means (in fiber processing, for example), and to relate these changes to the properties observed for these rigid-rod materials.

EXPERIMENTAL DETAILS

Materials. PBZT samples were obtained from the E.I. DuPont and Hoechst Celanese Companies (AFTECH I and II). PBO fibers were spun by W.-F. Hwang (currently with the Dow Chemical Company) while he was affiliated with the University of Dayton Research Institute [6]. Fibers were spun at elevated temperatures from liquid crystalline solutions in methanesulfonic acid. Heat treatment temperatures ranged from 525 to 700°C for PBZT, and 600 to 710°C for PBO.

Fiber densities were measured by the flotation method in mixed carbon tetrachloride-chloroform and chloroform-tetrachloro ethylene solvents. Comparable densities were obtained in each solvent system.

X-Ray Photography. Fiber bundles of sub-millimeter diameters were prepared by winding single filaments around a cardboard support. Specimens were mounted so that the fiber axis was normal to the incident beam. X-ray diffraction patterns were recorded on Weissenberg, Buerger precession and 57.3 mm radius vacuum cylindrical cameras using Ni-filtered $\text{CuK}\alpha$ radiation. The latter camera was employed to resolve, at least partially, diffuse overlapping spots and to reduce the effects of air scatter, whereas the primary function of the precession camera was to survey fiber specimens and not to collect diffraction intensities. The precession camera recorded a plane in reciprocal space in which c is vertical and parallel to the fiber direction. The multiple-film method was used to collect the entire range of intensities.

Diffractometer Scans. Nickel-filtered $\text{CuK}\alpha$ radiation was produced by a Rigaku RU200 rotating anode generator with a 0.3 x 3mm source size. Equatorial and meridional scans were recorded on a Picker four-circle diffractometer which had previously been modified for modulus studies [8]. An advantage of this technique is the ability to observe weak reflections at high 2θ by adjusting step scan intervals and counting times. Overlapping reflections were resolved by using a curve fit program which also corrected for background, L_p factors, absorption, and air and Compton scattering. Areas under the peak profiles afforded estimates of the intensities of equatorial reflections.

Microdensitometry. Integrated intensities of equatorial and off-axis reflections, corrected for background and L_p factors, were obtained by scanning fiber rotation photographs on a Joyce-Loebl microdensitometer. Details of the procedure have been discussed elsewhere [7]. Reflections which could not be resolved were treated as an overlapping group and assigned a composite intensity value.

RESULTS

The chemical structures of the molecules and atom label designations are shown in Figure 1.

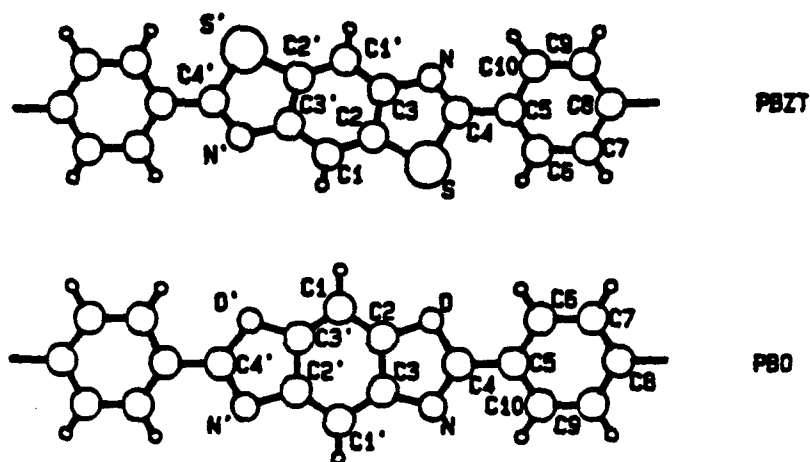


Figure 1. Chemical structures of PBZT and PBO showing atom label designations.

The measured monofilament fiber densities, of PBZT and PBO are $1.57 \pm 0.01 \text{ g/cm}^3$ and $1.50 \pm 0.01 \text{ g/cm}^3$, respectively. No detectable differences were observed in the values for as-spun and heat treated fibers.

PBZT and PBO samples yielded well-defined diffraction data. Representative fiber rotation patterns are shown in Figure 2. Strong equatorial and multiple meridional reflections are general features of the diffraction patterns of both polymers. Heat treated fibers show a limited number of off-axis (hkl) reflections, indicating the presence of 3D order. For example, hk2 reflections as well as discrete hk5 reflections are clearly visible for each polymer (see Figure 2).

Figure 3 presents equatorial scans which show reflections beyond a 2θ of 90° . Corresponding meridional scans, published elsewhere in these Proceedings [8], revealed up to twelve orders of diffracted intensity. The curve fit program used the least-squares method to match a combination of Gaussian and Lorentzian peak profiles to the corrected intensities. Figures 4 and 5 show representative curve fits for several regions of overlapping intensity along the equator.

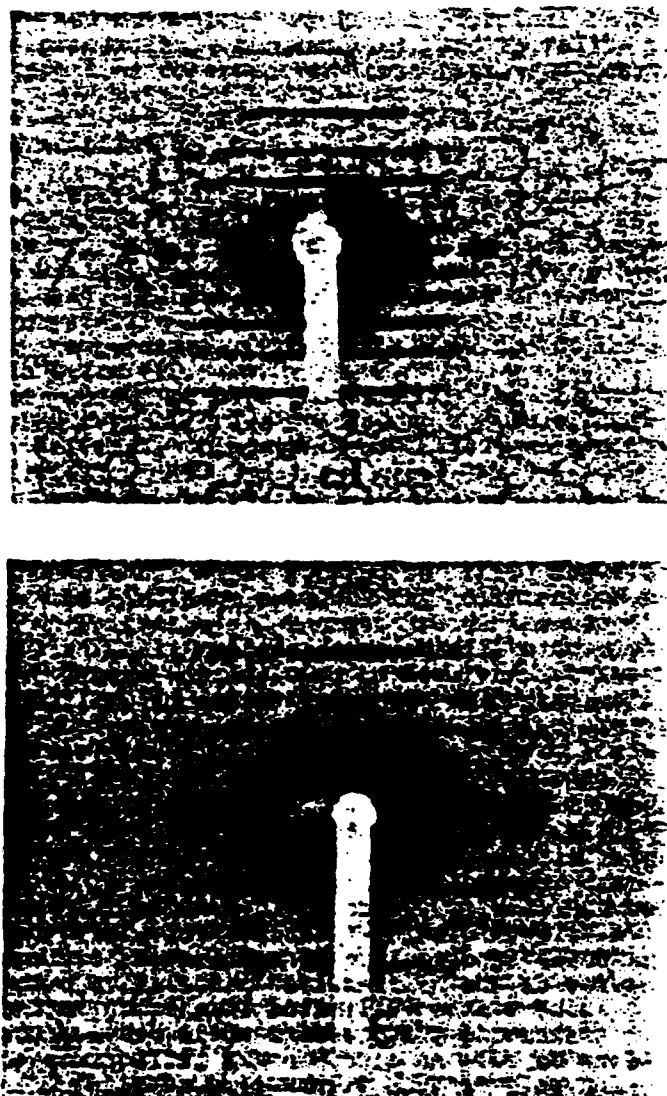


Figure 2. Fiber rotation patterns (fiber axis vertical) of PBZT (top) and PBO (bottom): $\text{CuK}\alpha$ radiation, Ni filter, camera radius 28.6 mm.

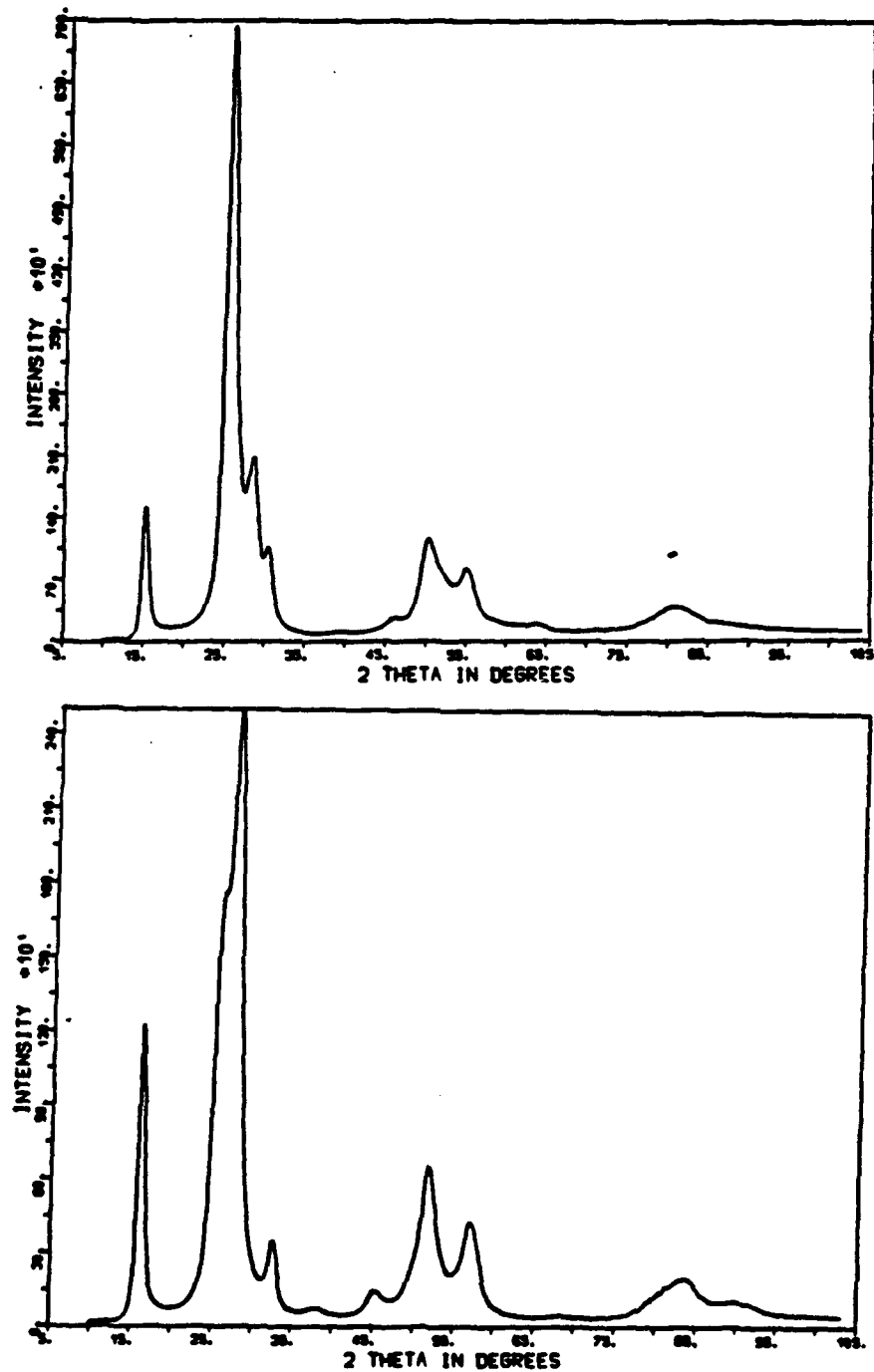


Figure 3. Equatorial scan of heat treated PBZT (top) and PBO (bottom) fiber bundle (CuK α radiation with Ni filter, intensity after experimental corrections).

436

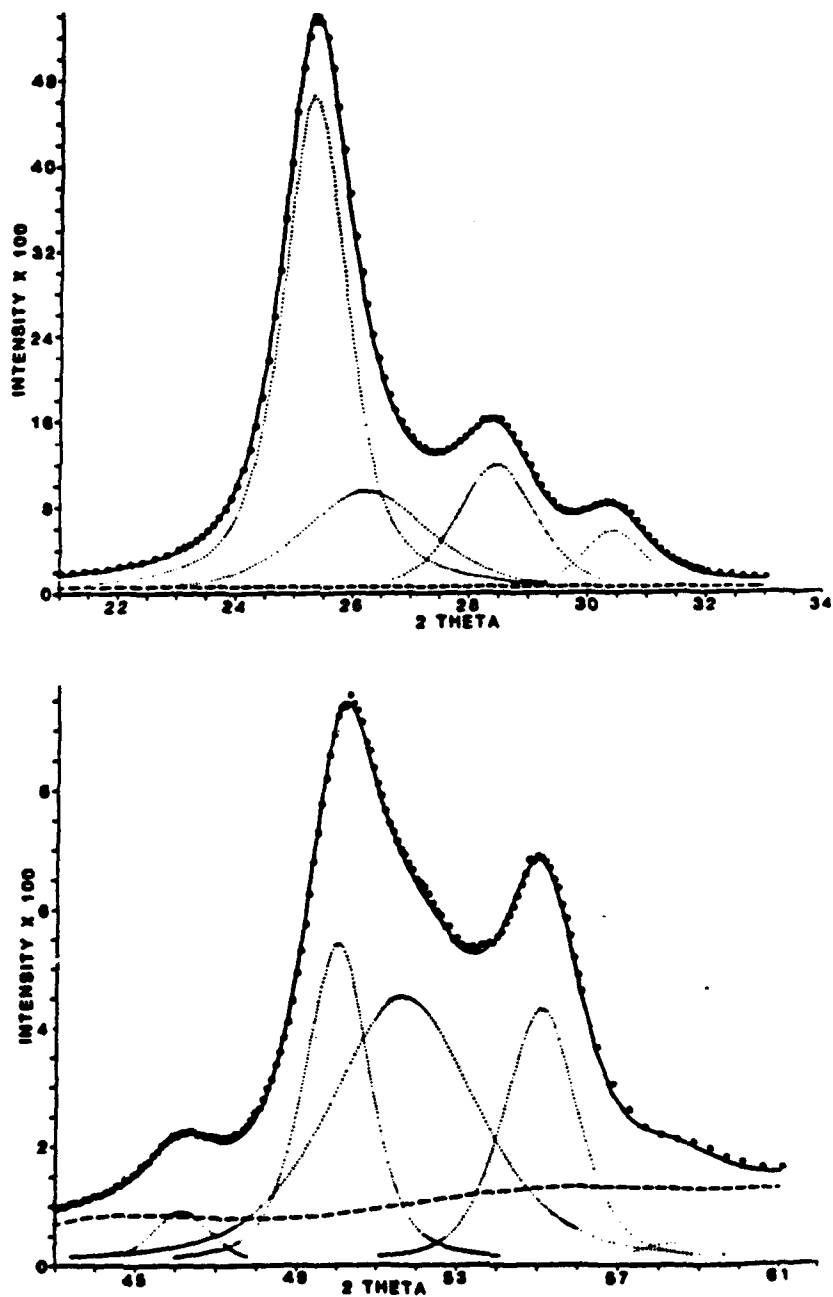


Figure 4. Curve fit analysis of two equatorial regions for PBZT. Circles denote experimental points, dashed line is background, dotted curves show individual peak as calculated, and solid line is the sum of peak plus background. Two theta in degrees.

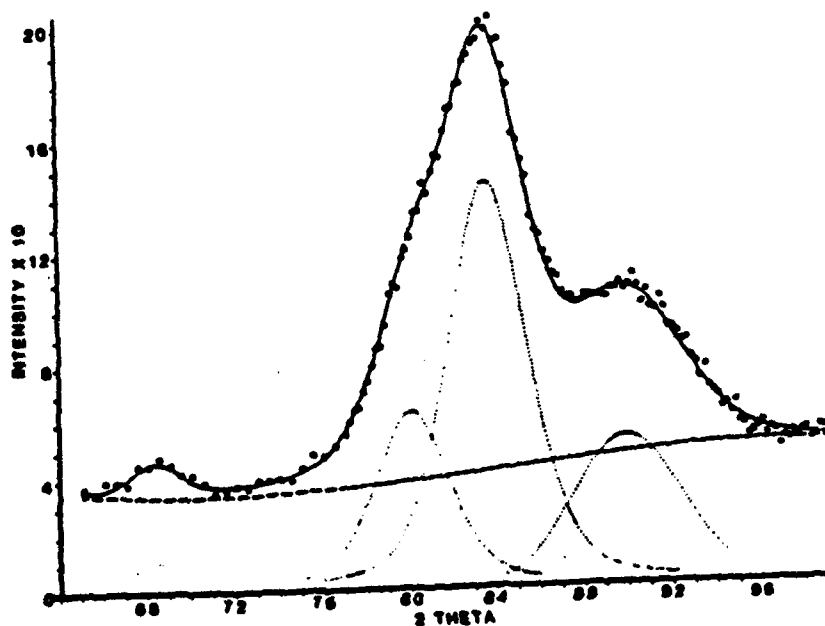
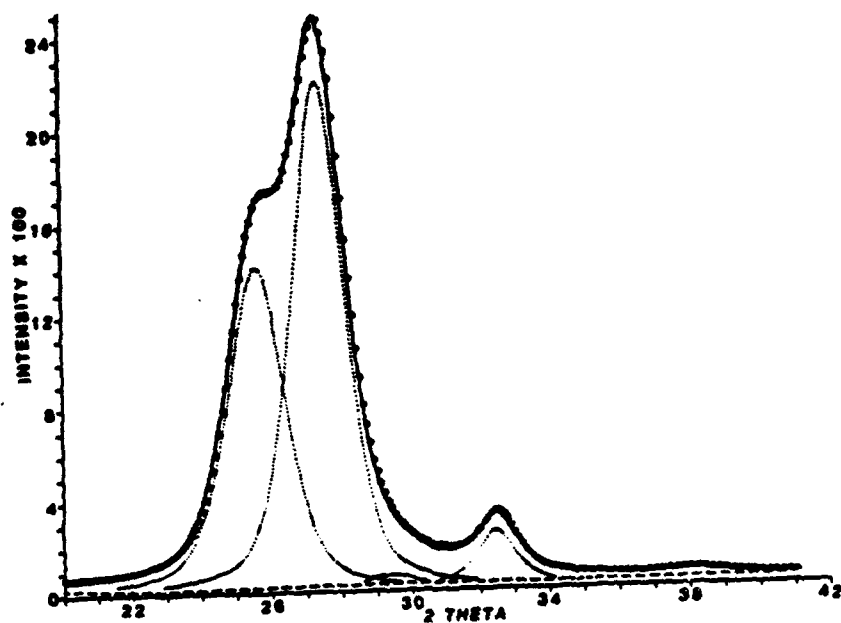


Figure 5. Curve fit analysis of two equatorial regions for PBO. Circles denote experimental points, dashed line is background, dotted curves show individual peak as calculated, and solid line is the sum of peak plus background. Two theta in degrees.

d-spacings, obtained by least-squares, were satisfactorily indexed using both primitive and non-primitive* cells. Cell constants were obtained by minimizing the sum of the squares of the differences between observed and calculated d-spacings. A weighting scheme based on the intensities and widths of fitted peak profiles was applied in which completely resolved reflections were assigned larger weights than partially resolved or unresolved reflections. Best-fit lattice parameters for non-primitive unit cells are listed in Table I. The measured equatorial d-spacings used to compute them are tabulated in Tables II and III, along with calculated values using alternate indexing schemes. Spacings along c were obtained independently from a least-squares fit of meridional reflections. Odell's assignment of indexes for PBZT, shown in Table II, was judged to give a less satisfactory match between observed and calculated values. The same conclusion was reached for PBO, Cell B, presented in Table III.

Table I. Non-primitive Unit Cells for PBZT and PBO

	PBZT	PBO
a (Å)	11.79(2)	11.20(1)
b (Å)	3.539(5)	3.540(2)
c (Å)	12.514(9)	12.050(3)
γ (deg)	94.0(2)	101.3(1)
Crystal system	monoclinic	monoclinic
Molecules per cell (Z)	2	2
Cell volume (Å ³)	536.4	468.4
Calculated density (g cm ⁻³)	1.71	1.66
Observed density (g cm ⁻³)	1.57	1.50
Formula Repeat	[C ₁₄ H ₆ N ₂ S ₂] _n	[C ₁₄ H ₆ N ₂ O ₂] _n

The indexes corresponding to the best-fit primitive cells are given in Table IV, which for PBZT is similar to Unit Cell I previously reported by Roche₃ (a = 5.83, b = 3.54, c = 12.35Å, $\gamma = 96^\circ$, D_{calc} = 1.74 g cm⁻³)[2]. The best-fit primitive cell for PBO is essentially that reported by Krause et.al. (a = 5.65, b = 3.58, c = 11.74Å, and $\gamma = 102.5^\circ$ [6]). For reasons discussed later, primitive cells were deemed unacceptable and eliminated from further consideration.

The LALS technique has been employed in the analysis of the structure of ordered polymers [9]. Its application to PBZT and PBO involved reducing the number of variables by constraining bond lengths and bond angles to the values shown in Table V, which are obtained from model compound studies [10,11]. The

* The terms 'primitive, non-primitive and monoclinic' are not used in the strict crystallographic sense since the asymmetric unit lacks the requisite point symmetry. In space group P2, for example, a polymer chain located at 0,0,z is required to have a two-fold rotation axis coincident with the unique axis. Neither PBZT nor PBO possesses the required symmetry. In this paper, as well as in those of earlier researchers, the terms primitive and non-primitive imply a cell containing one and two chains per cell, respectively. The term monoclinic simply denotes a cell with two 90° angles for which a satisfactory fit exists between observed and calculated d-spacings.

Table II. Comparison between Observed and Calculated Equatorial Spacings (Å) for Two PBZT Non-primitive Unit Cells

Observed d-spacing	Index and Calculated d-spacing				Observed Intensity (c)
	this work (a)		Odell (b)		
5.828	200	5.882	200	5.87	15.1
3.509	010	3.531	-110	3.534	100.0
3.129	-210	3.125	110	3.185	29.3
2.932	400,210	2.939	400	2.935	11.2
1.964	600	1.961	-	-	2.3
1.823	-	1.825	-220	1.767	14.9
1.768	020,-610	1.766	020	1.745	27.9
1.666	220,610	1.662	120	1.643	13.0
1.579	-420	1.563	220	1.593	1.3
1.455	420	1.469	-	-	0.93
1.187	030	1.177	-	-	16.0
1.121	-430	1.120	-	-	0.94

(a) Calculated using cell in Table I.

(b) Odell's cell, hkl's and observed spacings taken from [3].

(c) Derived from peak areas from diffractometer scans and scaled to a maximum of 100.

Table III. Comparison between Observed and Calculated Equatorial Spacings (Å) for Two Best-Fit PBO Non-primitive Cells

Observed d-spac	Index and Calculated d-spacing				Observed Intensity (c)
	this work (a)		Cell B (b)		
5.501	200	5.491	200	5.505	26.2
3.481	010	3.472	010	3.481	71.7
3.256	-210	3.233	110	3.259	100.0
2.756	400	2.746	400,210	2.752	11.3
2.360	-410	2.392	-	-	0.74
1.996	410	1.975	-	-	5.8
1.835	600	1.830	600	1.835	5.4
1.768	-120	1.769	-	-	30.6
1.702	-320	1.702	120	1.702	7.7
1.615	-420	1.617	-320	1.611	22.3
1.371	800	1.373	800	1.376	0.56
1.198	810	1.199	-	-	5.1
1.157	030	1.157	030,-130	1.160	11.7
1.091	230	1.091	-430	1.093	4.7

(a) see Table I.

(b) Cell B: $a = 11.032(8)$, $b_3 = 3.485(3)$, $c = 12.050(2)$ Å,
 $\gamma = 93.6(1)^\circ$, $V = 462.4$ Å³, $D_{\text{calc}} = 1.68$ g cm⁻³.

(c) Derived from peak areas from diffractometer scans and scaled to a maximum of 100.

Table IV. Comparison between Observed and Calculated Spacings (Å) for the Best-Fit Primitive Cells

PBZT			PBO		
Index (a)	Observed d-spacing	Calculated d-spacing	Index (b)	Observed d-spacing	Calculated d-spacing
100	5.828	5.882	100	5.501	5.491
010	3.509	3.531	010	3.481	3.473
-110	3.129	3.125	-110	3.256	3.234
200	2.932	2.941	200	2.756	2.746
300	1.964	1.961	-210	2.360	2.393
-	1.823	-	-	1.996	-
020	1.768	1.765	300	1.835	1.830
310,120	1.666	1.662	-310,-120	1.768	1.768
-220	1.579	1.563	-	1.702	-
-	1.455	-	-220	1.615	1.617
030	1.187	1.177	400,-410	1.371	1.372
-230	1.121	1.120	410	1.198	1.199
			030,320	1.157	1.155
			130	1.091	1.091

(a) $a = 5.896(11)$, $b = 3.539(5)$, $c = 12.514(9)$ Å, $\gamma = 94.0(2)^\circ$,
 $V = 260.5$ Å³, $D_{\text{calc}} = 1.70$ g cm⁻³. Based on 9 degrees of
 freedom.

(b) $a = 5.598(6)$, $b = 3.540(3)$, $c = 12.050(4)$ Å, $\gamma = 101.2(1)^\circ$,
 $V = 234.2$ Å³. $D_{\text{calc}} = 1.66$ g cm⁻³. Based on 14 degrees of
 freedom.

Table V. Fixed Bond Distances (Å) and Bond Angles (°) in Polymer Repeat Units (a)

Bond	PBZT	PBO	Angle	PBZT	PBO
C2-S(O)	1.736	1.383	C2-S(O)-C4	88.9	104.1
C4-S(O)	1.758	1.370	C3-N-C4	110.8	104.4
C3-N	1.385	1.399	C2-C1-C3'	117.3	112.5
C4-N	1.292	1.300	C1-C2-S(O)	128.6	127.0
C1-C2	1.376	1.385	C3-C2-S(O)	109.0	107.1
C1-C3'	1.389	1.385	C1-C2-C3	122.4	125.8
C2-C3	1.422	1.405	C1'-C3-N	124.6	129.7
C4-C5	1.469	1.464	C2-C3-N	115.1	108.6
C5-C6	1.383	1.387	C1'-C3-C2	120.4	121.7
C5-C10	1.392	1.387	N-C4-S(O)	116.3	115.6
C6-C7	1.385	1.387	C5-C4-S(O)	119.9	122.2
C7-C8	1.371	1.387	C5-C4-N	123.8	122.2
C8-C9	1.378	1.387	C4-C5-C6	121.6	120.0
C9-C10	1.377	1.387	C4-C5-C10	119.3	120.0
			C6-C5-C10	119.1	120.0
			C5-C6-C9	120.0	120.0
			C6-C7-C8	120.0	120.0
			C7-C8-C9	120.0	120.0
			C8-C9-C10	120.0	120.0
			C9-C10-C5	120.0	120.0

(a) C-H distances are fixed at 0.94 Å; C-C-H angles at 120°. Atoms in parentheses correspond to PBO.

overall isotropic temperature factor B was fixed at 6.0\AA^2 . A scale factor, one torsion angle per polymer repeat (τ), and three angles which define the orientation of chains in the unit cell were refined. Final fractional atomic coordinates of the repeat units are presented in Table VI.

DISCUSSION

Based on the observed fiber period and model compound data, the chain direction in both polymers is parallel to the fiber axis (c-axis). The length of the c-axis corresponds to the repeat distance of a single mer unit, which is comprised of a bisbenzazole and attached p-phenylene segment.

The b-axis is roughly the perpendicular distance between the faces of two overlapping heterocyclic rings, while the a-axis is the approximate distance between equivalent edges of side-by-side heterocyclic rings. The structure and cell parameters of PBO are similar to those of PBZT, except that the a and c-axes in PBZT are slightly larger, probably due to conformational differences between chains and the larger size of the sulfur atom.

Refinement of Primitive Cells. Analysis of the packing of molecules in primitive cells revealed some serious shortcomings. First, inclusion of longitudinal and lateral disorder to any significant degree in the final structure is precluded since primitive cells require perfect registry of adjacent chains. In addition, close intermolecular contacts, which could not be eliminated by refinement of the variable parameters, were observed. The closest contacts (H1...H1', 1.73Å; H7...H9, 1.96Å; and H6...H10, 1.99Å for PBZT, and H1...H1', 1.76Å; H6...H10, 1.90Å; and H7...H9, 1.90Å for PBO) occurred between neighboring molecules positioned along a. Thirdly, a close examination of the x-ray photographs (see Figure 2) showed an inner row of diffraction maxima which could not be indexed in a primitive cell. This latter observation is consistent with the appearance of a weak innermost equatorial peak ($d = 11.5\text{\AA}$) for PBZT film, which was indexed 100 in a non-primitive cell [3]. For these reasons, further refinement of primitive cells was discontinued.

It should also be noted that refinement of primitive cells for each polymer produced non-planar structures with reasonable torsion angles ($\tau = 18.9^\circ$ for PBZT and 12.0° for PBO).

Refinement of Non-Primitive Cells. The problems just described for primitive cells are virtually eliminated with non-primitive unit cells ($Z=2$). The close H...H intermolecular contacts are relieved, increasing to over 2.0Å for the closest H...H contact. Contacts larger than 2.1Å are considered to be acceptable. The non-primitive cells are constructed by doubling the length of the a-axis of the primitive cells. This permits a second chain to be added at $0.5, 0, w$ (relative to the first at $0, 0, 0$), thereby allowing axial shifts between well-aligned chains. w can range over one translational interval along c. If w is zero, the non-primitive cell reduces to a primitive one, and if w is 0.5, the cell becomes centered and hkl reflections are absent if $h+l$ is odd.

Additional lateral disorder can also be incorporated into the overall structure by allowing the second chain to have a

Table VI. Fractional Atomic Coordinates of Repeat Units

PBZT			
Atom	X	Y	Z
C4'	0.0000	0.0000	0.0000
N'	-0.0877	0.0140	0.0613
C3'	-0.0562	0.0080	0.1679
C2'	0.0622	-0.0115	0.1866
S'	0.1320	-0.0221	0.0646
C1	-0.1312	0.0197	0.2533
C2	-0.0859	0.0116	0.3545
C3	0.0325	-0.0080	0.3732
C1'	0.1076	-0.0197	0.2879
S	-0.1558	0.0222	0.4765
C4	-0.0240	0.0001	0.5410
N	0.0639	-0.0139	0.4798
C5	-0.0185	-0.0017	0.6583
C6	-0.0925	-0.2341	0.7189
C7	-0.0856	-0.2305	0.8294
C8	-0.0050	0.0047	0.8795
C9	0.0692	0.2375	0.8199
C10	0.0631	0.2363	0.7100
H1	-0.2097	0.0327	0.2424
H1'	0.1861	-0.0327	0.2990
H6	-0.1463	-0.3910	0.6846
H7	-0.1374	-0.3930	0.8691
H9	0.1277	0.4082	0.8555
H10	0.1170	0.4056	0.6654
PBO			
Atom	X	Y	Z
C4'	0.0000	0.0000	0.0000
N'	-0.1002	-0.1142	0.0555
C2'	-0.0643	-0.0755	0.1668
C3'	0.0619	0.0671	0.1710
O'	0.1026	0.1149	0.0626
C1'	-0.1334	-0.1553	0.2623
H1'	-0.2224	-0.2558	0.2622
C3	-0.0642	-0.0787	0.3579
C2	0.0620	0.0641	0.3538
C1	0.1311	0.1438	0.2582
H1	0.2201	0.2444	0.2583
N	-0.1000	-0.1210	0.4692
C4	0.0003	-0.0086	0.5247
O	0.1030	0.1085	0.4620
C5	0.0032	-0.0074	0.6461
C6	0.1060	0.1835	0.7017
H6	0.1780	0.3203	0.6588
C7	0.1087	0.1847	0.8168
H7	0.1828	0.3223	0.8568
C8	0.0088	-0.0050	0.8763
C9	-0.0940	-0.1959	0.8207
H9	-0.1661	-0.3326	0.8637
C10	-0.0970	-0.1971	0.7057
H10	-0.1709	-0.3347	0.6656

different azimuthal orientation relative to the first chain. The refinement of this angle was not undertaken due to the small number of observed reflections, especially off-axis reflections. In the case of PBO, an azimuthal rotation of the second chain by 180° could occur in a more or less random fashion. Such would not be the case for PBZT since the bithiazole unit is centrosymmetric and a flip of the second chain by 180° can be seen to be equivalent to a translation along c.

PBZT. Figure 6 shows a c-axis view of the packing. As expected from the crystal structures of model compounds, PBZT adopts a non-planar conformation in the non-primitive cell given in Table I. Shifts of $w = \pm 0.3$ (approximately $\pm 4\text{\AA}$) by the second chain produce optimum intermolecular contacts (minimum H...H contacts are 2.4\AA). The mean torsion angle (τ) is 46° . Shifts of $w = \pm 0.5$ ($\pm 6\text{\AA}$) are also possible, but produce a slightly higher R index.

Recent semi-empirical calculations on an isolated PBZT unit support a non-planar conformation for the polymer by predicting a torsion angle of 29° for the minimum energy conformation [12]. Molecular mechanics calculations reach a similar conclusion, the torsion angle being 20° . Semi-empirical calculations also reveal a small barrier (0.11 kcal/mole) at 0° , and a larger one (0.74 kcal/mole at 90°) [12]. The small barrier is consistent with the proposal that the conformation may be subject to packing considerations in the polymer and processing conditions.

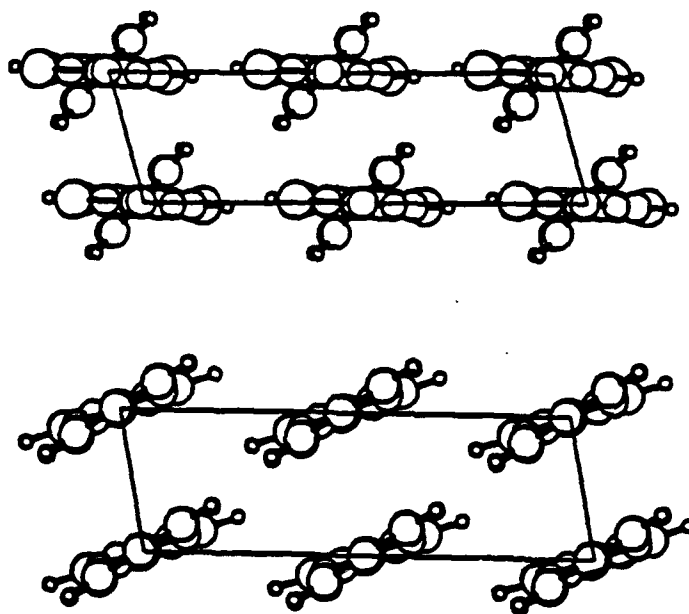


Figure 6. c-axis view of the molecular packing of PBZT (top) and PBO (bottom). The a-axis is horizontal.

PBO. PBO molecules also adopt a slightly non-planar conformation in a cell shown in Table I. The mean torsion angle (τ) is 13° . This contrasts with the planar conformation observed in the crystal structures of model compounds [11]. Shifts of $w = +/-0.10$ ($+/-1.2\text{\AA}$) and $+/-0.5$ ($+/-6\text{\AA}$) yield the optimum intermolecular contacts. Shifts of $w = +/-0.3$ ($+/-3.6\text{\AA}$) are also possible but only at the expense of a higher R index. Figure 6 also presents a view of the molecular packing.

The final orientation angles, R index (calculated on the basis of observed reflections only and equal to $(\sum |\Delta F| / \sum |F_o|)$) and observed and calculated structure factor amplitudes are given in Table VII.

For molecules stacked directly above one another, the theoretical prediction of the minimum energy arrangement is that chains are out of register by 1.5 Å for PBZT and as much as 3.0 Å for PBO [13]. D. Martin is currently using electron diffraction data to investigate quantitatively the type of disorder [14].

Table VII. Observed and Calculated Structure Factor Amplitudes for PBZT and PBO

PBZT			PBO			
hkl	F _o	F _c (a)	hkl	F _o	F _c (b)	
2 0 0	87	92	2 0 0	86	86	
0 1 0	139	144	0 1 0	104	108	
-2 1 0	76	66	-2 1 0	132	136	
12 1 0			12 1 0			
14 0 0	48	51	14 0 0	38	40	
6 0 0	12	2	6 0 0	24	20	
-6 1 0			$\left. \begin{array}{l} -2 2 0 \\ -1 2 0 \\ 0 2 0 \end{array} \right\}$			
10 2 0	59	53			69	56
16 1 0						
12 2 0	36	22	14 2 0			
2 0 2	5	7	-2 2 0	44	41	
			0 1 2	19	9	
			3 1 3	28	19	
			14 0 4			
			12 1 4	18	7	
			-1 1 5			
			1 1 5	21	26	

- (a) F_c values are based on shifts of $w = +0.30$ for the second chain. The placement of the first chain in the unit cell is accomplished by placing the root atom (C4' in each case) at the origin with the bond to its precursor (C8') pointing along the positive x-axis and its precursor (C7' for PBZT and C9' for PBO) in turn lying in the (x,-y) half-plane. Orientation angles X, Y and Z are -40.8° , -92.7° and 9.3° , respectively. They refer to the angle about a, b and c, respectively, required to bring the chain into its correct orientation. Positive rotation is counterclockwise when viewed from positive infinity. Chain continuity is maintained via coincidence constraints imposed on pairs of atoms related by translational symmetry along c. The R index is 12.0% based on 8 Bragg maxima.
- (b) $w = 0.10$ for the second chain. X, Y and Z angles are 90.3° , -91.3° and 158.1° , respectively. R is 11.4% based on 11 reflections.

ACKNOWLEDGEMENT

Support for this work was provided by the Air Force Office of Scientific Research under Grant AFOSR-88-0044. One of us (PGL) is the recipient of a AFSC University Resident Research Program Appointment.

REFERENCES

1. W.W. Adams, L.V. Azaroff, and A.K. Kulshreshtha, *Z. Kristallogr.* **150**, 321 (1980).
2. E.J. Roche, T. Takahashi, and E.L. Thomas in Fiber Diffraction Methods, edited by A.D. French and K.H. Gardner (American Chemical Society Symposium Series, No. 141, 1980), p. 303.
3. J.A. Odell, A. Keller, E.D.T. Atkins, and M.J. Miles, *J. Mater. Sci.* **16**, 3309 (1981).
4. K. Shimamura, J.R. Minter, and E.L. Thomas, *J. Mat. Sci. Lett.* **18**, 54 (1983).
5. W.W. Adams, S. Kumar, D.C. Martin, and K. Shimamura, *Polymer Communications* (1989), in press.
6. S.J. Krause, T.B. Haddock, D.L. Vezie, P.G. Lenhert, W.-F. Hwang, G.E. Price, T.E. Helminiak, J.F. O'Brien, and W.W. Adams, *Polymer* **29**, 1354 (1988).
7. A.V. Fratini, E.M. Cross, J.F. O'Brien, and W.W. Adams, *J. Macromol. Sci. -Phys.* **B24(1-4)**, 159 (1985-1986).
8. P.G. Lenhert and W.W. Adams, *Proc. Mater. Res. Soc. Symp.*, **134**, (1989).
9. A.V. Fratini, E.M. Cross, R.B. Whitaker, and W.W. Adams, *Polymer* **27**, 861 (1986).
10. M.W. Wellman, W.W. Adams, R.A. Wolff, D. Dudis, D.R. Wiff, and A.V. Fratini, *Macromolecules* **14**, 935 (1981).
11. M.W. Wellman, W.W. Adams, D.R. Wiff, and A.V. Fratini, AFML-TR-79-4184, February (1980).
12. B.L. Farmer, S.G. Wierschke, and W.W. Adams, *Polymer*, 1989.
13. D. Bhaumik, W.J. Welsh, H.H. Jaffe and J.E. Mark, *Macromolecules* **14**, 951 (1981).
14. D.C. Martin, Ph.D. dissertation, University of Massachusetts, (1989).

**CRYSTAL STRUCTURES AND PHASE TRANSITIONS
OF POLY (PARAPHENYLENE) OLIGOMERS**

Kenneth N. Baker, Albert V. Fratini, Timothy Resch and Howard C. Knachel
Department of Chemistry
University of Dayton
300 College Park
Dayton, Ohio 45469-2357

W. Wade Adams
Polymer Branch
Nonmetallic Materials Division
Wright-Patterson Air Force, Ohio 45433-6533

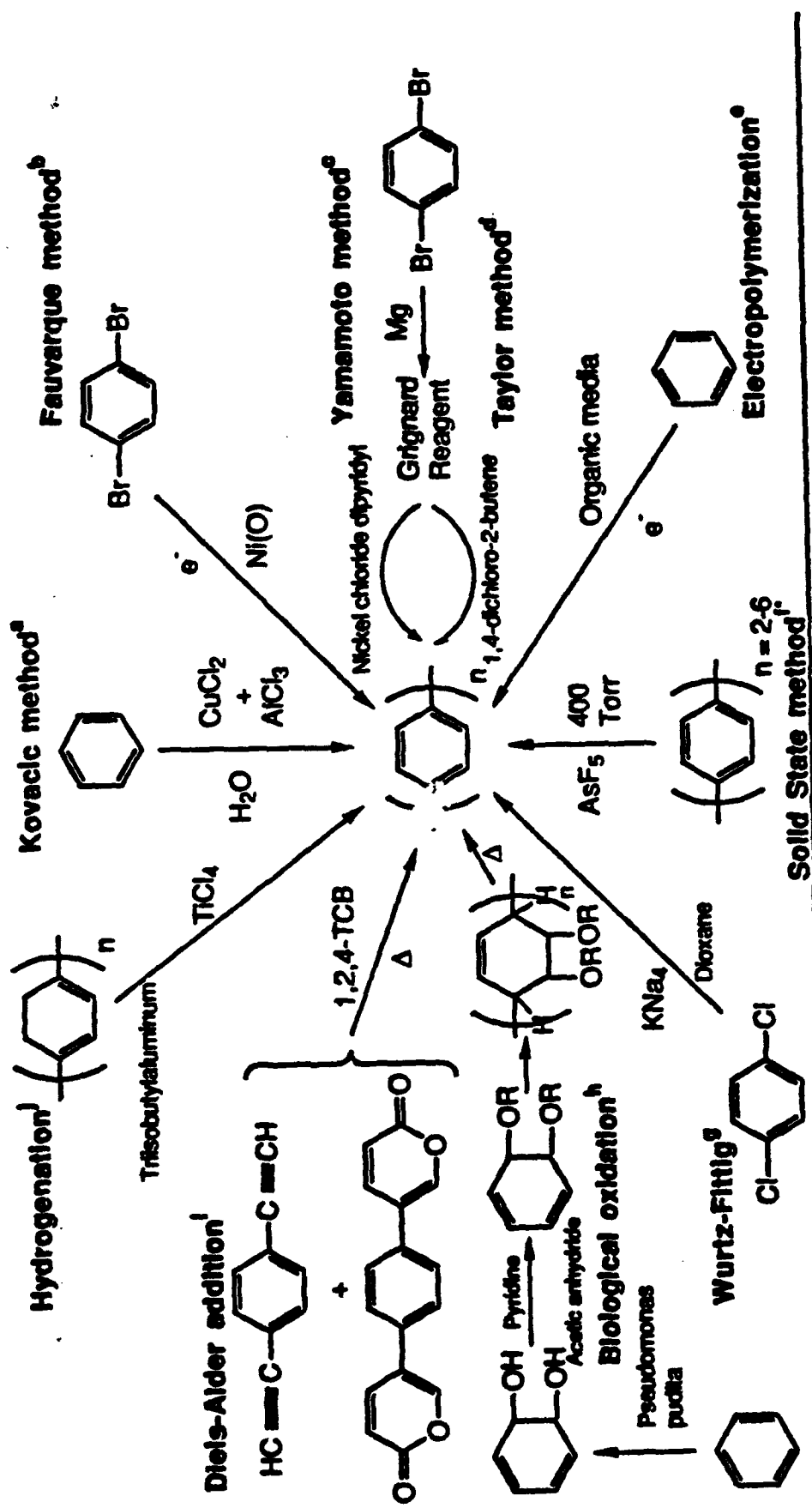
ABSTRACT

The room temperature crystal structures and the temperature related structural transitions of p-quinquephenyl (PQP), $C_{30}H_{22}$; p-sexiphenyl (PSexiP) $C_{36}H_{26}$; p-septiphenyl (PSeptiP) $C_{40}H_{30}$, have been investigated as part of a research effort toward rigid rod polymers which are of great interest for aerospace and electro-optical applications. The molecules are planar at room temperature, observe the herringbone type of crystal packing and have a setting angle θ of 56° , which is similar to that reported for the polymer poly(paraphenylene) (PPP). In contrast to PPP, the oligomers align in the unit cell parallel to the (010) face and intersect the (100) face at an angle ω . At room temperature the cell dimension a increases by 4.1\AA for each additional benzene ring added to the oligomer, while b and c remain more or less constant. At low temperature the unit cell parameters b and c are approximately doubled and a remains the same as in the room temperature cell. Unit cell changes are similar to that observed in previous measurements on the shorter polyphenyls. A time-dependent structural transition, in contrast to the lower oligomers, was observed for PQP, PSexiP, and PSeptiP at 110 K; however, efforts to determine the exact transition temperature were unsuccessful and a low temperature structure could not be refined. High temperature measurements indicate the oligomers to be thermotropic liquid crystals and the crystal \rightarrow smectic transition temperatures were obtained for PQP, PSP, PSeptiP, and p-octiphenyl (POP) $C_{46}H_{34}$.

Poly (paraphenylene) (PPP) has been reviewed quite extensively.¹⁻³ It can be synthesized by many routes illustrated in Figure 1 with the two most common being the Kovacic method⁴ and the Yamamoto method⁵. PPP is an insoluble and infusible dark brown material commonly called "brick dust". Its lower oligomers shown in Table I and derivatives with phenyl pendant groups⁶ exhibit measurable melting points and limited solubilities, but is difficult to process. Yet PPP has been applied to many structural uses ranging from solid state lubricants⁷⁻¹⁰ to fibers¹¹ and ribbons¹². Tensile bars have been fabricated out of PPP powder by powder-forming techniques¹³ and hydrostatic pressing¹⁴ which exhibit tensile strengths up to 35 MPa (5000 psi). Recent calculations¹⁵ indicate that if PPP could be obtained in high molecular weight and fabricated into fibers, it would possess excellent compressive strength, surpassing other rigid-rod polymers such as poly (paraphenylenebenzobisoxazole) (PBO) and poly (paraphenylenebenzobisthiazole) (PBT), but have a limited tensile modulus. Objects made from PPP powder exhibit ablation-compaction properties which allow fabricated parts to undergo controlled uniform shrinkage from up to 80% of the original.¹⁶

In general, the mechanical properties of fabricated PPP fall in between those of polyimide and graphite.¹⁴ PPP has excellent heat and solvent stability in addition to the good macroscopic structural properties mentioned above. However the polymer has even more interesting microscopic molecular properties. PPP becomes highly conducting n- or p- type materials when it complexes with either electron donors (Na^+ , K^+ , or Li^+) or acceptors (AsF_5 , SbF_5 , BF_5^- , or PF_6^-), respectively.¹⁷ The highest conductivity occurs with AsF_5 increasing the conductivity of the virgin polymer from approximately 10^{-12} $\text{ohm}^{-1} \text{m}^{-1}$ to greater than 10^4 $\text{ohm}^{-1} \text{m}^{-1}$ for the doped polymer - an increase of 16 orders of magnitude! Different model structures have been proposed for the two types of conducting materials. An intercalation model (see Figure 2) has been suggested by Pradere, et al.¹⁸ based upon the diffraction pattern of heavily doped PPP with AsF_5 . Fibers of PPP increased in diameter by approximately 50% upon AsF_5 doping suggesting diffusion of dopant molecules inside the fiber.

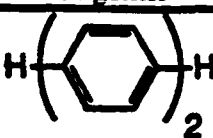
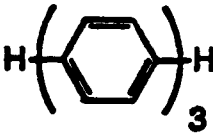
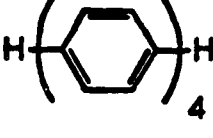
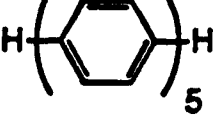
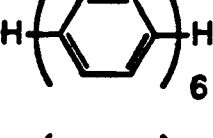
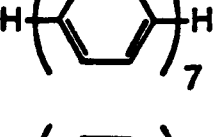
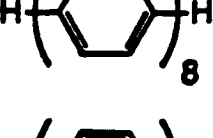
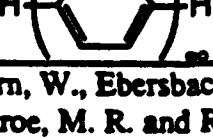
Figure 3 shows the other model proposed by Baughman, et al.¹⁹ in which the K^+ ions aggregate in columns between two parallel polymer chains. In this model the K^+ ions do not stack over the center of the phenyl rings but over the midpoint of the HC-CH bonds parallel to the molecular axis. This model lends credibility to the belief that PPP conduction is strongly influenced by the ability of the molecule to form the quinoid resonance structure^{23,24} since the quinoid resonance structure would have greater electron density over the HC-CH bonds parallel to the molecular axis in contrast to the benzoid structure where "doughnuts" of electron density exist above and below the ring planes.



a Kovacs, P. and Kyrstals, A. J. Amer. Chem. Soc. 1965, 85, 454.
 b Fauvarque J.-F.; Petit, M.-A.; Pfluger, F.; Juland, A.; and Chevrol, C. Makromol. Chem., Rapid Commun. 1983, 4, 455.
 c Yamamoto, T.; Hayashi, Y.; and Yamamoto, A. Bull. Chem. Soc. Jpn. 1978, 51, 2091.
 d Taylor, S. K.; Bennett, S. G.; Koury, J.; and Kovacic, P. J. Polym. Sci., Polym. Lett. Ed. 1981, 19, 85.
 e Aeyach, S. and Lacaze, P. C. J. Polym. Sci., Polym. Chem. 1969, 27, 515.
 f Shacklette, L. W.; Eckhardt, H.; Chance, R. R.; Miller, G. G.; Ivoy, D. M.; and Baughman, R. H. J. Chem. Phys. 1960, 73, 4098.
 g Edwards, G. A. and Goldfinger, G. J. Polym. Sci. 1955, 16, 569.
 h Bailard, D. G. H.; Courtis, A.; Shirley, J. M.; and Taylor, S. C. Macromolecules 1988, 21, 294.
 i VanKerckhoven, H. F.; Gilliams, Y. K.; and Stille, J. K. Macromolecules 1972, 5, 451.
 j Marvel, C. S. and Hartzell, G. E. Chem. Abstracts 1959, 53, 14966f.

Figure 1. Synthesis routes to PPP.

TABLE I
PPP Oligomer Melting Points and Solubility

Oligomer	Melting Point, °C	Solubility, g/L
	70 ^a	440 in Toluene ^a
	210 ^a	8.5 in Toluene ^a
	320 ^a	0.22 in Toluene ^a
	395 ^a 388 ^b 388 ^c	<0.1 in Toluene ^a good in 1,2,4-Trichlorobenzene ^b unavailable ^c
	475 ^a 437 ^b 429 ^c	<0.01 in Toluene ^a poor in 1,2,4-Trichlorobenzene ^b unavailable ^c
	545 ^a 468 ^b	insoluble ^a very limited in 1,2,4-TCB ^b
	491 ^b	very limited in 1,2,4-TCB ^b
	infusible ^d	insoluble ^d

^a Kern, W., Ebersbach, H. W., and Ziegler, I. *Makromol. Chem.* 1959, 31, 154.

^b Unroe, M. R. and Reinhardt, B. A. *Synthesis* 1987, 11, 981.

^c Kambe, H., Mita, R., and Yokota, R. *Thermal Anal.* 1971, 3, 387.

^d Kovacic, P. and Kyriakis, A. *J. Amer. Chem. Soc.* 1963, 85, 454.

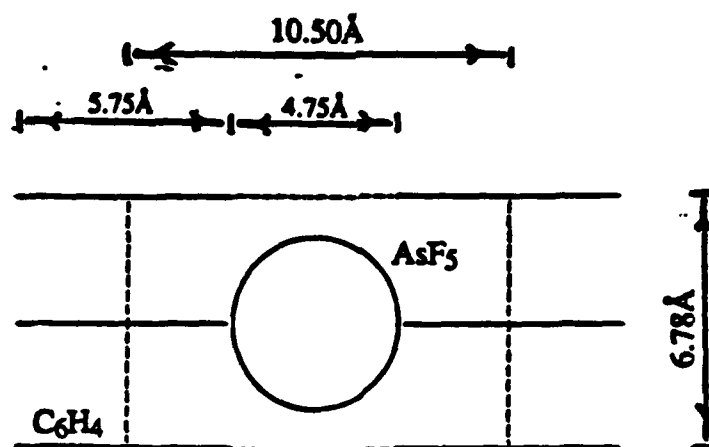


Figure 2. Intercalation model of arsenic pentafluoride doped PPP showing d-values obtained from diffraction pattern. Figure is adapted from reference 18.

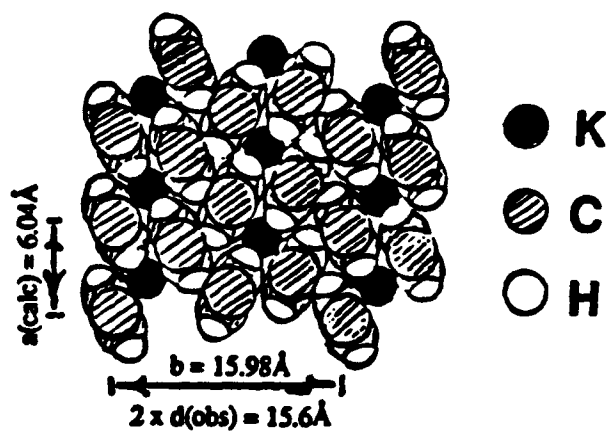


Figure 3. Stacking model of potassium doped PPP showing d-values. Figure is adapted from reference 19.

The electronic properties of PPP also suggest that it has good nonlinear optical (NLO) properties. Recent calculations^{22,23} on the electronic band structures of p-quinaterphenyl, p-quinaterpyrrole, and p-quinaterthiophene indicate that the undoped oligomer is more polarizable than its heteroatom counterparts. Moreover, when doped with sodium atoms the polarizabilities of these oligomers increase. The largest increase is with p-quinaterphenyl which doubles its mean polarizability to 159.34 ev and almost triples its linear polarizability along the molecular axis to 790.00 ev. This significant increase in linear polarizability (α) is expected to lead to an even larger increase in the third order polarizability (γ), due to the scaling relationship between α and γ .²³ PPP has a band-gap of 3.2 ev²⁴ which decreases when the oligomer length²⁵ and the quinoid character of the oligomer backbone²⁶ increases. Calculations^{27,28}, optical measurements²⁹, and EPR studies³⁰ demonstrate that upon heavy doping with alkali metals or AsF₅ spinless bipolarons are formed in coexistence with polarons. Optical measurements²⁶ suggest a polaron-exciton defect to occur over about five phenyl rings.

Since PPP is the simplest type of rigid-rod polymer it represents the least complicated case of shape anisotropy. Paul Flory writes:

"These homologues (of PPP) offer unique examples that (i) are rigid with respect to the rectilinear axis, (ii) are effectively cylindrically symmetric about this axis, and (iii) are devoid of possible vitiating effects of polar groups."³¹

PPP oligomers are thermotropic liquid crystals to which theoretical calculations involving the relationship of shape anisotropy to intermolecular forces³² and experimentation³³ are devoted to better understand and someday exploit liquid crystal transitions.

The foundation of this work lies in the Air Force Ordered Polymer program which has as one of its objectives the research and development of new materials for aerospace applications. PPP has been around a long time but due to its intractability has not been exploited as well as other materials. Also the existing synthesis methods produce ortho and meta substituted products in addition to the desired para substituted isomer. For this reason a new synthesis procedure was developed to produce pure para substituted product. This procedure proved very successful not only in preparing pure para oligomers of PPP up to nine benzene rings long in high yield, but also in the selective substitution of pendant phenyl rings on the oligomer chain in an effort to increase the solubility of PPP allowing for routine processing of the polymer by conventional means. The latter goal (to increase PPP's solubility) has not been significantly realized to-date, but it has given us an excellent opportunity to study the structure of extended oligomer chains of PPP.

Why would one perform a crystal structure when structural information can be obtained through IR or NMR spectrometry? With a good crystal structure one can obtain accurate unit cell parameters, atomic coordinates, and bond distances and angles. In a

concise description of the technique, X-rays record areas of high electron density from which atoms can be located. So the basic information obtained from such a study is atomic coordinates from which we obtain bond distances, bond angles, dihedral angles, ring planarity, and atomic thermal factors which describe the dynamics the atoms are experiencing. If unit cell information is included, close packing diagrams and interatomic distances and angles are obtained. This information is important to both synthetic and theoretical chemists whom are designing other systems. For example, the polymers poly(paraphenylene sulfide) PPS, poly(paraphenylene vinylene) PPV, and poly(paraphenylene bithiophene) PPBT are being considered for their NLO and conduction properties. Structural information about para substituted phenyl units is important to optimize the molecular geometry in order to achieve the desired effect, whether it be π electron conjugation or structural strength. Our work on the pendant PPP oligomers has been published elsewhere and in this report is recent findings on the crystal structures and phase transitions of the non-substituted PPP oligomers p-quinquephenyl (PQP), p-sexiphenyl (PSP), and p-septiphenyl (PSeptiP).

EXPERIMENTAL METHODS

Samples of PQP, PSP, and PSeptiP were obtained from Bruce Reinhardt of the Polymer Branch in polycrystalline form. The samples were further purified by sublimation in order to obtain single crystals suitable for structure determination. Density measurements were made by flotation in solvent mixtures containing dichloromethane ($\rho = 1.316 \text{ g/cm}^3$) and methanol ($\rho = 1.0 \text{ g/cm}^3$).

Crystals were selected from representative samples, discriminating on the basis of size and well defined crystal faces. They were observed under crossed polarized filters to determine extinction boundaries. Single crystals when viewed under crossed polarized filters are birefringent and when rotated on the microscope stage will go completely dark at some angle of rotation. Crystals not meeting this criteria were rejected as being twinned or polycrystalline aggregates. Good crystals were mounted on glass fibers using cyanoacrylate adhesive, the fibers were inserted into standard brass or stainless steel pins and the pins mounted into goniometers for X-ray analysis.

Upon mounting the goniometer on the Enraf-Nonius CAD4 diffractometer and centering the crystal in the X-ray beam, a rotation photograph was taken using two complete rotations of the crystal. Observation of this photograph usually revealed:

- a) if the crystal diffracted well enough and far enough out in the 2θ range to collect a suitable data set for structure determination and
- b) if the beam collimator needed to be changed so that the cross-section of the X-ray beam matched the crystal size.

Automatic search routines for strong diffraction peaks were initiated on crystals which showed promise. Once a suitable unit cell was found, reflection data sets were collected on the CAD4 interfaced to a DEC Micro PDP-11 computer. Data sets collected at room temperature (approximately 22°C) were followed by low temperature data sets (110 K or -163°C). The crystal was cooled to low temperature using the Enraf-Nonius FR558 Liquid Nitrogen Cryostat.

Raw reflection data were copied onto a VAX 11/730 computer and processed using software in the Structure Determination Package (SDP)³⁴. Structure solutions were found by the software MULTAN 11/82³⁵ and/or SHELXS-86³⁶ and were subsequently refined by full matrix least-squares treatment of all non-hydrogen atoms. Hydrogen atoms were placed in idealized positions since subsequent isotropic refinement of hydrogen atoms did not yield appreciably better results due to the reduced data-to-parameter ratio.

The temperature programmable Enraf-Nonius FR553 Guinier-Simon camera equipped with another Enraf-Nonius FR558 Liquid Nitrogen Cryostat was used to obtain variable low temperature structural data on PQP, PSP, and PSeptiP. The moving film/ramping temperature option on the camera's controller facilitates the determination of

structural transitions. Differential scanning calorimetry (DSC) measurements were performed on a Dupont 910 apparatus interfaced with an Omnitherm 35053 three module controller.

RESULTS

Table II summarizes the crystallographic and data collection parameters, and final refinement results for the structures determined at room temperature. Complete data sets could not be collected at low temperature due to problems with the crystals. Space group and unit cell information for the room and low temperature polyphenyls are summarized in Table III. Experiments are in progress to obtain better structural data for the low temperature structures of PQP, PSP, and PSeptiP.

Figure 4 shows the PQP molecule with the carbon atoms of the asymmetric unit labelled. Tables IV and V contain the atomic positions, bond distances and bond angles respectively. Figure 5 shows a stereoview of the crystal packing in the unit cell. PSP is shown in Figure 6 with the carbon atoms of the asymmetric unit labelled. Atomic positions are in Table VI and bond distances and angles are contained in Table VII. The stereodrawing of the crystal packing within the unit cell is shown in Figure 7.

The PSeptiP molecule with the carbon atoms of the asymmetric unit labelled is shown in Figure 8. Atomic positions, bond distances and bond angles are presented in Tables VIII and IX, respectively. Reflection data for PSeptiP were not of sufficient quality to refine all of the carbon atoms anisotropically. Figure 9 depicts a stereoview of the crystal packing in the unit cell.

Literature reports PPP to be infusible⁴, but for comparison purposes its theoretical melting point has been determined to be 1020 K by the extrapolation of experimental melting points of PPP oligomers (see Figure 10). Using similar methods, extrapolated melting points of 620 K and 1260 K have been reported for poly (tetrafluoroethylene)³⁷ and Kevlar³⁸, respectively. It should be noted that these polymers mentioned above are expected to degrade before reaching these theoretical melting points. Extrapolations of this kind are based on melting point depression association with end group concentration in polymers.³⁹ An extrapolated crystal density of 1.36 g/cm³ has been calculated (see Figure 11) using experimental densities from crystalline oligomer model compounds. This theoretical density is smaller than that measured for PBO and PBT (1.65 and 1.69 g/cm³, respectively) which is consistent with calculations¹⁵ that PPP fibers would have a lower modulus since modulus is directly proportional to density. However the force constant, K, which is derived from the energy/strain curve fit, is larger for PPP than for PBO or PBT making PPP more resistant to strain. Indeed, calculations¹⁵ on PPP indicate that it will not fail with up to 15% tensile strain and 3% compressive strain.

TABLE II
Crystallographic Data

NAME	p-Quinquephenyl	p-Sexiphenyl	p-Septiphenyl
Formula	C ₃₀ H ₂₂	C ₃₆ H ₂₆	C ₄₂ H ₃₀
FW	382.51	458.61	534.70
Melting Point, °C	388	437	468
Crystal System	Monoclinic	Monoclinic	Monoclinic
Space Group	P2 ₁ /c	P2 ₁ /c	P2 ₁ /c
Z	2	2	2
a, Å	22.056(4)	26.241(5)	30.65(2)
b, Å	5.581(1)	5.568(1)	5.564(3)
c, Å	8.070(1)	8.091(3)	8.056(5)
α, °	90.0	90.0	90.0
β, °	97.91(1)	98.17(2)	100.57(5)
γ, °	90.0	90.0	90.0
Volume, Å ³	982.9(5)	1170.2(8)	1350.1(8)
Density _{cal} , g/cm ³	1.292	1.302	1.315
Density _{exp} , g/cm ³	1.291	1.288	1.311
Crystal Dimensions, mm	0.29x0.28x0.05	0.35x0.50x0.05	0.10x0.10x0.50
Crystal Shape	Flat Plate	Rectangular Plate	Needle
Cell Determined	25 Reflections 9°<2θ<36°	25 Reflections 9°<2θ<25°	25 Reflections 9°<2θ<36°
Radiation	Mo (graphite)	Mo (graphite)	Mo (graphite)
Scan Type	ω/2θ	ω/2θ	ω/2θ
Scan Rate, °/min.	1.27-5.49	1.27-5.49	1.27-5.49
Scan Angle, °	0.80+0.34Tanθ	0.80+0.34Tanθ	0.80+0.34Tanθ

	45KV/20ma	45KV/20ma	45KV/20ma Preprint 1
Power	45KV/20ma	45KV/20ma	45KV/20ma
Detector Aperture	4.00mm	4.00mm	4.00mm
Check Reflections	3 every 200 refl. 12° $\Delta\theta$ $\Delta 24^\circ$	3 every 200 refl. 12° $\Delta\theta$ $\Delta 24^\circ$	3 every 200 refl. 22° $\Delta\theta$ $\Delta 26^\circ$
Orientation Reflections	3 every 2 hrs. 16° $\Delta\theta$ $\Delta 36^\circ$	3 every 2 hrs. 18° $\Delta\theta$ $\Delta 24^\circ$	3 every 2 hrs. 22° $\Delta\theta$ $\Delta 26^\circ$
Temperature, °C	22	22	22
2θ Range, °	2-50	2-50	2-50
Data Collected, h, k, l	±31, 0-7, ±11	±31, 0-6, ±9	0-36, ±6, ±9
Total Number of Reflections	5776	4593	3188
Unique Number of Reflections >3σ	663	623	527
Number of Parameters Varied	136	163	73
Average Decay Correction	1.006	1.004	1.004
Absorption Coefficient, cm ⁻¹	0.7	0.7	0.7
Absorption Correction	none	none	none
R	0.050	0.062	0.067
RW	0.060	0.091	0.074
Maximum Shift/error in final cycle	0.03	0.01	0.01

$$R = \frac{\sum ||F_o| - |F_c||}{\sum |F_o|}$$

$$RW = \sqrt{\frac{\sum w(|F_o| - |F_c|)^2}{\sum w(F_o)^2}}$$

TABLE III
VARIABLE TEMPERATURE CRYSTAL DATA

Compound	Temperature (K)	Space Group	a(Å)	b(Å)	c(Å)	$\alpha(^{\circ})$	$\beta(^{\circ})$	$\gamma(^{\circ})$
Biphenyl	298 ^a	P2 ₁ /c*	9.51(2)	5.63(1)	8.12(2)	90	95.1(3)	90
	40 ^b	P2 ₁ /c*	9.51(2)	11.26(2)	16.24(4)	90	95.1(3)	90
P-Terphenyl	298 ^c	P2 ₁ /c*	13.613(6)	5.613(2)	8.106(4)	90	92.2(2)	90
	191 ^c	P2 ₁ /c*†	13.53(3)	11.09(3)	16.01(3)	90	92.0(2)	90
P-Quaterphenyl	298 ^d	P2 ₁ /c*	17.91(1)	5.610(4)	8.110(6)	90	95.80(6)	90
	243 ^e	P2 ₁ /c*†	17.70(3)	11.16(2)	15.97(3)	90	95.61(8)	90
P-Quinquephenyl	298	P2 ₁ /c	22.056(4)	5.581(1)	8.070(1)	90	97.91(1)	90
	110	monoclinic, C centered	22.014(3)	11.029(4)	15.968(6)	90	98.18(2)	90
P-Sexiphenyl	298	P2 ₁ /c	26.241(5)	5.568(1)	8.091(3)	90	98.17(2)	90
	110	monoclinic, C centered	26.282(8)	10.999(4)	15.995(9)	90	99.79(4)	90
P-Septiphenyl	298	P2 ₁ /c*	30.65(2)	5.564(3)	8.056(5)	90	100.6(5)	90
	110	orthorhombic, C centered	30.064(6)	11.005(2)	15.972(2)	90	90	90

* For comparison purposes, the P2₁/a space groups were transformed to P2₁/c.

† Space group of structure refinement is P1 and is converted to a pseudo-monoclinic cell with molecules centered on the (001) face for comparison purposes.

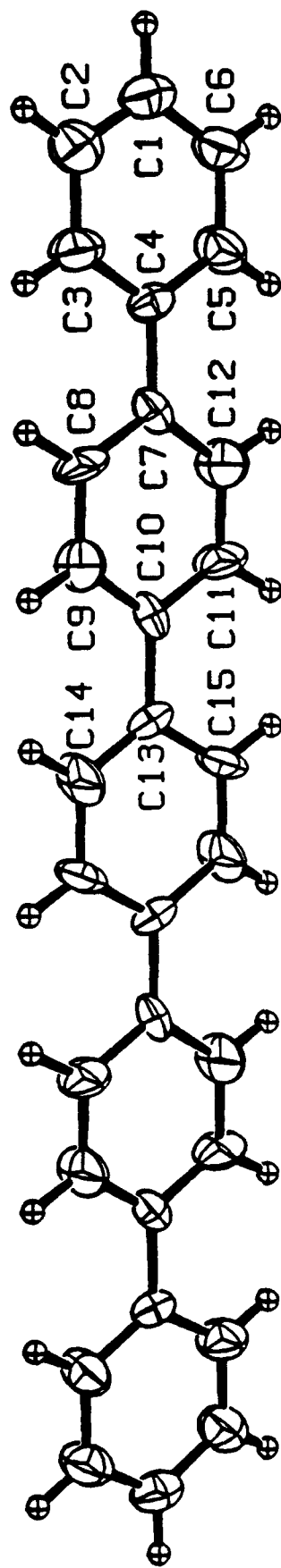
^a Bree, A. and Edelson, M., *Chem. Phys. Lett.* 1977, 46(3), 500.

^b Cailleau, H., Baudour, J. L. and Zeyen, C.M.E., *Acta Cryst.* 1979, B35, 426.

^c Cailleau, H. and Dworkin, A. *Mol. Cryst. Liq. Cryst.* 1979, 50, 217.

^d Bolton, B.A. and Prasad, P.N. *Chem. Phys.* 1978, 35, 331.

^e Baudour, J. L., Delugeard, Y., and Rivet, P. *Acta Cryst.* 1978, B34, 625.



P-QUINQUEPHENYL

Figure 4. P-quinquephenyl with carbon atom ellipsoids drawn at the 50% probability level

TABLE IV

Positional Parameters, Equivalent Isotropic Thermal Factors, and
Their Estimated Standard Deviations for p-Quinquephenyl

Atom	x	y	z	B(Å ²)
C3	0.3384(2)	-0.1788(9)	0.2567(5)	4.1(1)
C4	0.3163(2)	0.0007(8)	0.3521(4)	2.63(8)
C7	0.2515(2)	0.0042(7)	0.3830(4)	2.71(8)
C8	0.2115(2)	-0.1726(9)	0.3206(6)	5.1(1)
C9	0.1511(2)	-0.1737(8)	0.3475(5)	4.8(1)
C10	0.1263(2)	-0.0020(7)	0.4393(4)	2.62(8)
C11	0.1663(2)	0.1751(9)	0.5007(6)	4.8(1)
C12	0.2267(2)	0.1775(9)	0.4743(5)	5.0(1)
C13	0.0614(2)	-0.0037(7)	0.4698(4)	2.59(7)
C14	0.0204(2)	-0.1789(8)	0.4079(5)	4.6(1)
C15	0.0397(2)	0.1773(9)	0.5622(5)	4.3(1)
C1	0.4390(2)	-0.0065(9)	0.2967(5)	4.1(1)
C2	0.3989(2)	-0.1807(9)	0.2300(5)	4.6(1)
C6	0.4180(2)	0.1739(9)	0.3906(5)	4.4(1)
H1	0.481	-0.012	0.281	5.4*
H2	0.413	-0.302	0.162	6.0*
H3	0.312	-0.302	0.209	5.3*
H5	0.343	0.299	0.485	5.5*
H6	0.445	0.297	0.436	5.4*
H8	0.226	-0.301	0.260	6.6*
H9	0.125	-0.298	0.298	6.2*
H11	0.152	0.304	0.562	6.1*
H12	0.253	0.302	0.523	6.9*
H14	0.034	-0.297	0.337	5.8*
H15	0.066	0.305	0.601	5.1*

Starred atoms were refined isotropically.

Anisotropically refined atoms are given in the form of the isotropic equivalent displacement parameter defined as: $(4/3)[a^2B_{1,1} + b^2B_{2,2} + c^2B_{3,3} + ab(\cos \gamma)B_{1,2} + ac(\cos \beta)B_{1,3} + bc(\cos \alpha)B_{2,3}]$

TABLE V

Bond Distances (Å) and Bond Angles (°) for p-Quinquephenyl

Atom 1	Atom 2	Distance	Atom 1	Atom 2	Distance	Atom 1	Atom 2	Distance
C3	C4	1.392(6)	C10	C13	1.482(5)	C8	C9	1.376(6)
C3	C2	1.378(6)	C11	C12	1.373(6)	C1	C2	1.374(6)
C3	H3	0.950(4)	C11	H11	0.950(5)	C8	H8	0.951(5)
C4	C5	1.386(6)	C12	H12	0.951(4)	C1	C6	1.379(7)
C4	C7	1.481(5)	C13	C14	1.378(6)	C9	C10	1.372(6)
C5	C6	1.388(6)	C13	C15	1.380(6)	C1	H1	0.951(4)
C5	H5	0.951(5)	C14	C15'	1.378(6)	C9	H9	0.951(4)
C7	C8	1.372(6)	C14	H14	0.950(5)	C2	H2	0.950(5)
C7	C12	1.376(6)	C15	H15	0.950(4)	C6	H6	0.950(4)
C10	C11	1.373(6)	C15	C14'	1.378(6)			

Atom 1	Atom 2	Atom 3	Angle	Atom 1	Atom 2	Atom 3	Angle
C4	C3	C2	120.7(4)	C12	C11	H11	117.8(4)
C4	C3	H3	120.3(4)	C7	C12	C11	122.8(5)
C2	C3	H3	119.1(4)	C7	C12	H12	118.4(4)
C3	C4	C5	117.7(3)	C11	C12	H12	118.8(5)
C3	C4	C7	121.3(3)	C10	C13	C14	122.8(4)
C5	C4	C7	121.0(4)	C10	C13	C15	119.9(3)
C4	C5	C6	121.4(4)	C14	C13	C15	117.3(4)
C4	C5	H5	119.1(4)	C13	C14	C15'	122.0(4)
C6	C5	H5	119.5(4)	C13	C14	H14	117.7(4)
C4	C7	C8	120.9(4)	C15'	C14	H14	120.2(4)
C4	C7	C12	124.3(4)	C13	C15	C14'	120.8(4)
C8	C7	C12	114.9(4)	C13	C15	H15	119.0(4)
C7	C8	C9	122.1(4)	C14'	C15	H15	120.1(4)
C7	C8	H8	119.4(4)	C2	C1	C6	119.1(4)
C9	C8	H8	118.5(4)	C2	C1	H1	120.7(4)
C8	C9	C10	123.2(5)	C6	C1	H1	120.3(4)
C8	C9	H9	118.3(5)	C3	C2	C1	121.1(4)
C10	C9	H9	118.4(4)	C3	C2	H2	119.5(4)
C9	C10	C11	114.6(4)	C1	C2	H2	119.3(5)
C9	C10	C13	123.4(4)	C5	C6	C1	120.0(4)
C11	C10	C13	122.1(4)	C5	C6	H6	119.9(5)
C10	C11	C12	122.6(4)	C1	C6	H6	120.2(4)
C10	C11	H11	119.6(4)				

Numbers in parentheses are estimated standard deviations in the least significant digits.

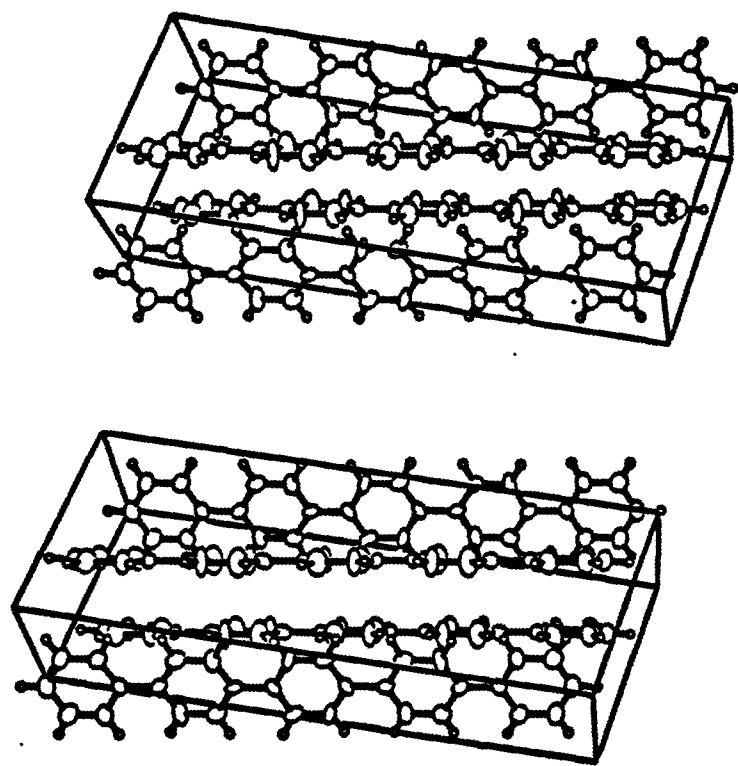
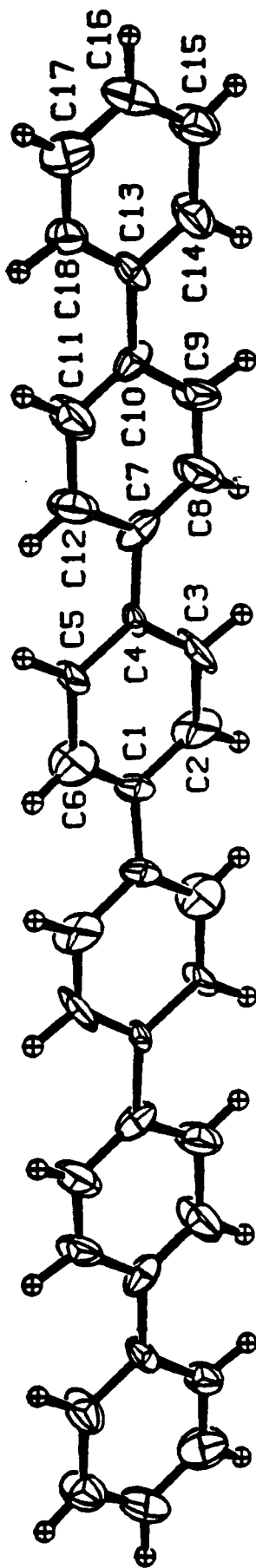


Figure 5. Stereoview of PQP showing molecular packing in unit cell. The *a* axis is vertical and the *b* axis is horizontal.



P-SEXIPHENYL

Figure 6. P-sexiphenyl with carbon atom ellipsoids drawn at the 50% probability level

TABLE VI

Positional Parameters, Equivalent Isotropic Thermal Factors and
Their Estimated Standard Deviations for p-Sexiphenyl

Atom	x	y	z	B(Å ²)
C1	0.0276(2)	0.007(1)	0.0409(6)	2.5(1)
C2	0.0620(2)	-0.174(1)	0.0066(8)	4.5(2)
C3	0.1117(3)	-0.174(1)	0.0849(8)	4.5(2)
C4	0.1321(2)	0.001(1)	0.1953(6)	1.6(1)
C5	0.0982(2)	0.179(1)	0.2214(8)	3.9(2)
C6	0.0456(3)	0.179(2)	0.1529(9)	5.7(2)
C7	0.1875(3)	-0.008(1)	0.2729(7)	3.6(2)
C8	0.2220(3)	-0.181(2)	0.2399(9)	5.4(2)
C9	0.2696(2)	-0.178(1)	0.3188(8)	4.4(2)
C10	0.2910(2)	0.002(1)	0.4253(7)	3.1(1)
C11	0.2569(3)	0.175(1)	0.4563(9)	5.3(2)
C12	0.2051(2)	0.173(1)	0.3828(9)	4.6(2)
C13	0.3443(2)	0.001(1)	0.5074(7)	2.7(1)
C14	0.3781(2)	-0.174(1)	0.4752(8)	4.1(2)
C15	0.4320(2)	-0.177(2)	0.5448(9)	4.7(2)
C16	0.4488(3)	0.003(2)	0.6560(9)	5.3(2)
C17	0.4149(3)	0.179(2)	0.6951(9)	4.9(2)
C18	0.3661(2)	0.183(1)	0.6192(8)	3.4(1)
H2	0.052	-0.296	-0.074	5.2*
H3	0.133	-0.304	0.064	5.6*
H5	0.111	0.314	0.286	4.5*
H6	0.023	0.293	0.189	7.1*
H8	0.212	-0.293	0.153	6.8*
H9	0.290	-0.316	0.310	5.7*
H11	0.270	0.306	0.525	6.5*
H12	0.182	0.293	0.411	5.8*
H14	0.365	-0.306	0.408	5.8*
H15	0.455	0.291	0.510	5.1*
H16	0.484	0.005	0.707	6.4*
H17	0.426	0.295	0.779	6.6*
H18	0.345	0.316	0.639	4.2*

Starred atoms were refined isotropically.

Anisotropically refined atoms are given in the form of the isotropic equivalent displacement parameter defined as: $(4/3)[a^2B_{1,1} + b^2B_{2,2} + c^2B_{3,3} + ab(\cos \gamma)B_{1,2} + ac(\cos \beta)B_{1,3} + bc(\cos \alpha)B_{2,3}]$

TABLE VII

Bond Distances (Å) and Bond Angles (°) for p-Sexiphenyl

Atom 1	Atom 2	Distance	Atom 1	Atom 2	Distance	Atom 1	Atom 2	Distance
C1	C1'	1.506(6)	C9	H9	0.951(7)	C5	H5	0.950(6)
C1	C2	1.41(1)	C10	C11	1.36(2)	C16	C17	1.39(1)
C1	C6	1.36(2)	C10	C13	1.461(8)	C6	H6	0.951(9)
C2	C3	1.366(9)	C11	C12	1.40(1)	C16	H16	0.950(8)
C2	H2	0.951(7)	C11	H11	0.950(7)	C7	C8	1.38(2)
C12	H12	0.950(7)	C17	C18	1.339(8)	C9	C10	1.386(9)
C3	C4	1.378(8)	C13	C14	1.37(1)	C7	C12	1.38(1)
C3	H3	0.950(7)	C13	C18	1.426(9)	C17	H17	0.951(8)
C4	C5	1.366(8)	C14	C15	1.446(9)	C8	C9	1.321(9)
C4	C7	1.501(8)	C14	H14	0.950(7)	C18	H18	0.950(7)
C15	C16	1.38(2)	C8	H8	0.950(8)	C15	H15	0.951(8)
C5	C6	1.413(9)						

Atom 1	Atom 2	Atom 3	Angle	Atom 1	Atom 2	Atom 3	Angle
C1'	C1	C2	118.7(6)	C8	C9	H9	117.2(7)
C1'	C1	C6	123.5(6)	C10	C9	H9	117.0(6)
C2	C1	C6	117.8(5)	C9	C10	C11	114.0(6)
C1	C2	C3	120.2(6)	C9	C10	C13	123.7(7)
C1	C2	H2	121.0(6)	C11	C10	C13	122.1(6)
C3	C2	H2	118.7(7)	C10	C11	C12	122.5(7)
C2	C3	C4	124.0(7)	C10	C11	H11	117.3(6)
C2	C3	H3	118.1(7)	C12	C11	H11	120.2(7)
C4	C3	H3	117.9(6)	C7	C12	C11	119.8(7)
C3	C4	C5	114.3(5)	C7	C12	H12	120.2(6)
C3	C4	C7	120.8(5)	C11	C12	H12	120.0(8)
C5	C4	C7	124.9(5)	C10	C13	C14	121.5(6)
C4	C5	C6	124.1(6)	C10	C13	C18	123.8(6)
C4	C5	H5	117.6(5)	C14	C13	C18	114.7(5)
C6	C5	H5	118.3(6)	C13	C14	C15	123.9(6)
C1	C6	C5	119.3(7)	C13	C14	H14	117.7(6)
C1	C6	H6	120.3(6)	C15	C14	H14	118.4(7)
C5	C6	H6	120.3(8)	C14	C15	C16	117.0(7)
C4	C7	C8	124.5(6)	C14	C15	H15	121.7(7)
C4	C7	C12	117.6(7)	C16	C15	H15	121.4(6)
C8	C7	C12	117.9(6)	C15	C16	C17	120.3(7)
C7	C8	C9	119.9(7)	C15	C16	H16	119.4(8)
C7	C8	H8	119.0(6)	C17	C16	H16	120.3(8)
C9	C8	H8	120.9(8)	C16	C17	C18	120.7(8)

Bond Angles (°) for P-Sexiphenyl (Continued)

<u>Atom 1</u>	<u>Atom 2</u>	<u>Atom 3</u>	<u>Angle</u>	<u>Atom 1</u>	<u>Atom 2</u>	<u>Atom 3</u>	<u>Angle</u>
C8	C9	C10	125.7(7)	C16	C17	H17	119.9(6)
C18	C17	H17	119.4(7)	C13	C18	C17	123.3(7)
C13	C18	H18	117.9(5)	C17	C18	H18	118.8(7)

Numbers in parentheses are estimated standard deviations in the least significant digits.

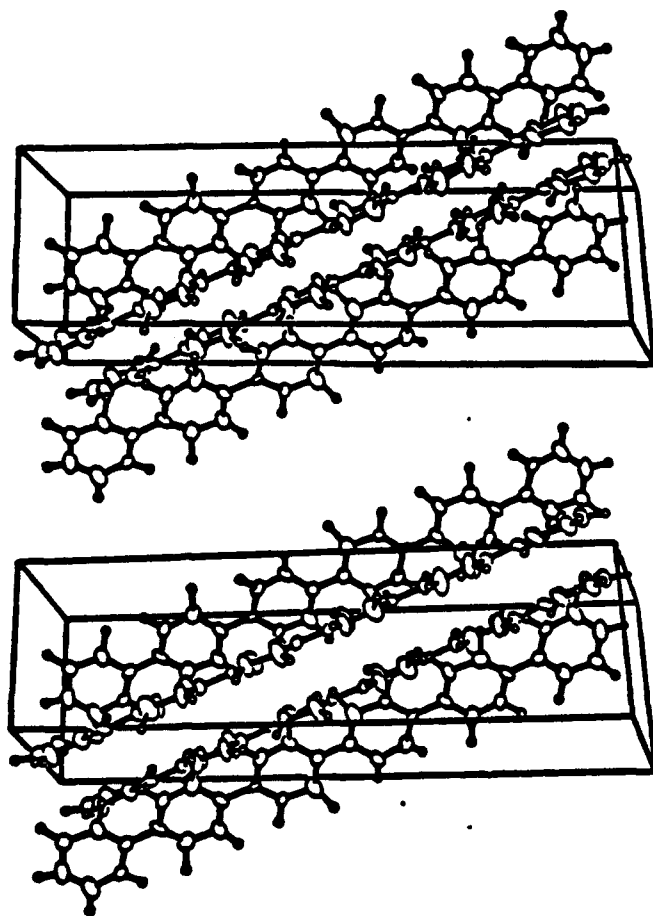
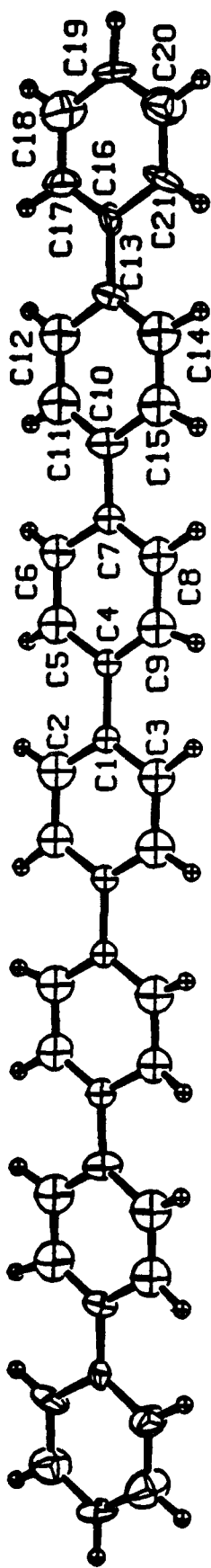


Figure 7. Stereoview of PSexiP showing molecular packing in unit cell. The a axis is vertical and the b axis is horizontal.



P-SEPTIPHENYL

Figure 8. P-septiphenyl with carbon atom ellipsoids drawn at the 50% probability level

TABLE VIII

Positional Parameters, Equivalent Isotropic Thermal Factors and
Their Estimated Standard Deviations for P-Septiphenyl

Atom	x	y	z	B(Å ²)
C1	0.044	0.501	0.480	2.1
C2	0.028	0.323	0.568	4.4
C3	0.016	0.681	0.411	3.8
C4	0.092	0.502	0.457	2.1
C5	0.121	0.320	0.524	4.3
C6	0.166	0.318	0.503	3.6
C7	0.182	0.504	0.415	2.6
C8	0.153	0.677	0.345	4.1
C9	0.109	0.677	0.366	4.3
C10	0.2289(2)	0.497(2)	0.3923(9)	2.8(2)
C11	0.259	0.322	0.456	5.0
C12	0.302	0.321	0.437	4.7
C13	0.3196(2)	0.501(2)	0.3504(9)	2.4(2)
C14	0.290	0.674	0.284	5.1
C15	0.246	0.673	0.303	4.8
C16	0.3664(2)	0.500(2)	0.327(1)	2.4(2)
C17	0.3966(3)	0.324(2)	0.401(1)	4.0(2)
C18	0.4406(3)	0.326(2)	0.384(1)	5.1(3)
C19	0.4563(3)	0.505(2)	0.293(1)	3.6(2)
C20	0.4267(3)	0.680(2)	0.219(1)	4.7(3)
C21	0.3828(2)	0.683(2)	0.236(1)	4.2(2)
H5	0.115	0.212	0.606	5.1*
H6	0.186	0.215	0.591	4.2*
H8	0.164	0.808	0.268	4.4*
H9	0.097	0.811	0.321	4.6*
H11	0.252	0.219	0.536	5.3*
H12	0.324	0.211	0.518	5.0*
H14	0.297	0.812	0.202	5.0*
H15	0.227	0.808	0.235	5.1*
H17	0.386	0.197	0.462	4.3*
H18	0.460	0.201	0.432	5.2*
H19	0.487	0.508	0.282	4.5*
H20	0.437	0.805	0.155	4.5*
H21	0.363	0.808	0.188	4.4*
H3	0.0297	0.8067	0.3196	4.0*
H2	0.047	0.197	0.647	4.0*

Starred atoms were refined isotropically.

Anisotropically refined atoms are given in the form of the isotropic equivalent displacement parameter defined as: $(4/3)[a^2B_{1,1} + b^2B_{2,2} + c^2B_{3,3} + ab(\cos \gamma)B_{1,2} + ac(\cos \beta)B_{1,3} + bc(\cos \alpha)B_{2,3}]$

TABLE IX

Bond Distances (Å) and Bond Angles (°) for P-Septiphenyl

Atom 1	Atom 2	Distance	Atom 1	Atom 2	Distance	Atom 1	Atom 2	Distance
C1	C2	1.361(9)	C11	H11	0.92(1)	C8	C9	1.39(1)
C1	C3	1.369(9)	C12	C13	1.389(9)	C18	H18	0.95(2)
C1	C4	1.522(9)	C12	H12	1.043(9)	C8	H8	1.06(2)
C2	H2	1.046(9)	C13	C14	1.360(9)	C19	C20	1.40(1)
C3	H3	1.150(9)	C13	C16	1.49(2)	C9	H9	0.88(1)
C4	C5	1.38(2)	C14	C15	1.38(2)	C19	H19	0.951(8)
C4	C9	1.36(2)	C14	H14	1.06(2)	C10	C11	1.366(9)
C5	C6	1.41(2)	C15	H15	1.06(2)	C20	C21	1.38(1)
C5	H5	0.94(2)	C16	C17	1.40(1)	C10	C15	1.38(1)
C6	C7	1.39(1)	C16	C21	1.40(1)	C20	H20	0.96(2)
C6	H6	1.03(1)	C17	C18	1.38(1)	C11	C12	1.36(2)
C7	C8	1.36(1)	C17	H17	0.96(2)	C21	H21	0.950(9)
C7	C10	1.489(8)	C18	C19	1.38(1)	C2	C3'	1.394(8)
C3	C2'	1.394(8)						

Atom 1	Atom 2	Atom 3	Angle	Atom 1	Atom 2	Atom 3	Angle
C1	C2	C3'	121.9(6)	C1	C3	C2'	119.6(6)
C2	C1	C3	118.5(9)	C11	C10	C15	114.1(5)
C2	C1	C4	121.3(5)	C10	C11	C12	123.7(4)
C3	C1	C4	120.2(4)	C10	C11	H11	119.3(4)
C1	C2	H2	126.7(4)	C12	C11	H11	115.3(4)
C1	C3	H3	115.1(4)	C11	C12	C13	122.2(3)
C1	C4	C5	120.5(3)	C11	C12	H12	117.3(3)
C1	C4	C9	121.7(3)	C13	C12	H12	118.3(3)
C5	C4	C9	117.7(3)	C12	C13	C14	114.7(5)
C4	C5	C6	121.1(5)	C12	C13	C16	122.5(7)
C4	C5	H5	123.6(7)	C14	C13	C16	122.8(8)
C6	C5	H5	113.9(8)	C13	C14	C15	122.7(4)
C5	C6	C7	120.0(4)	C13	C14	H14	123.8(3)
C5	C6	H6	113.8(3)	C15	C14	H14	113.1(3)
C7	C6	H6	122.3(3)	C10	C15	C14	122.7(3)
C6	C7	C8	117.7(3)	C10	C15	H15	123.3(3)
C6	C7	C10	119.2(4)	C14	C15	H15	114.0(4)
C8	C7	C10	123.0(4)	C13	C16	C17	122.0(8)
C7	C8	C9	121.7(8)	C13	C16	C21	120.7(8)
C7	C8	H8	117.5(8)	C17	C16	C21	117.2(7)
C9	C8	H8	120.7(7)	C16	C17	C18	122.2(9)
C4	C9	C8	121.6(9)	C16	C17	H17	118.7(8)
C4	C9	H9	131.5(8)	C18	C17	H17	119.1(9)
C8	C9	H9	106.6(9)	C17	C18	C19	120.3(9)

Bond Angles (°) for P-Septiphenyl (Continued)

<u>Atom 1</u>	<u>Atom 2</u>	<u>Atom 3</u>	<u>Angle</u>	<u>Atom 1</u>	<u>Atom 2</u>	<u>Atom 3</u>	<u>Angle</u>
C7	C10	C11	124.5(7)	C17	C18	H18	120(2)
C7	C10	C15	121.5(7)	C19	C18	H18	119.4(8)
C18	C19	C20	118.3(8)	C21	C20	H20	118.0(9)
C18	C19	H19	120.5(9)	C16	C21	C20	119.6(8)
C20	C19	H19	121.3(9)	C16	C21	H21	119.3(8)
C19	C20	C21	122.4(9)	C20	C21	H21	122(1)
C19	C20	H20	119.5(8)				

Numbers in parentheses are estimated standard deviations in the least significant digits.

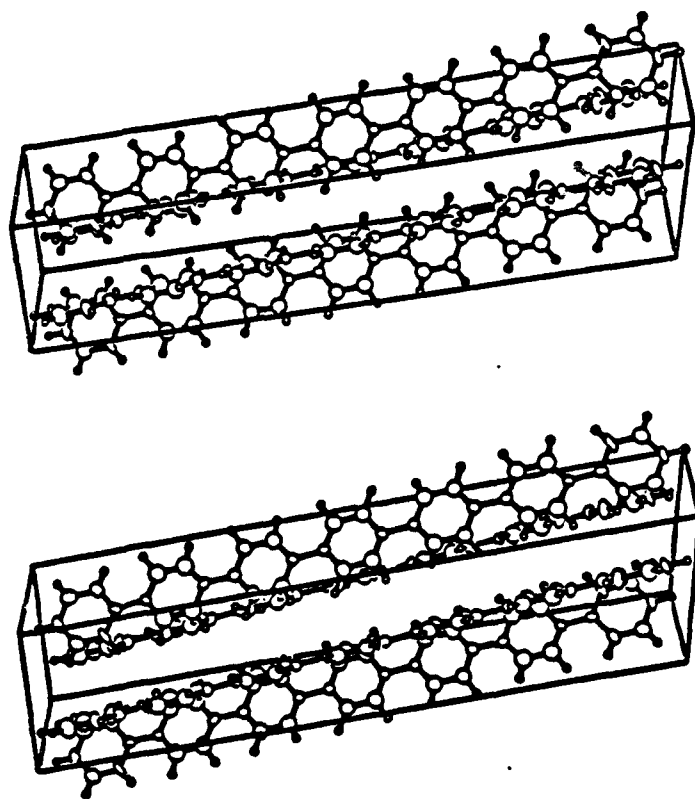


Figure 9. Stereoview of PSeptiP showing molecular packing in unit cell. The **a** axis is vertical and the **b** axis is horizontal.

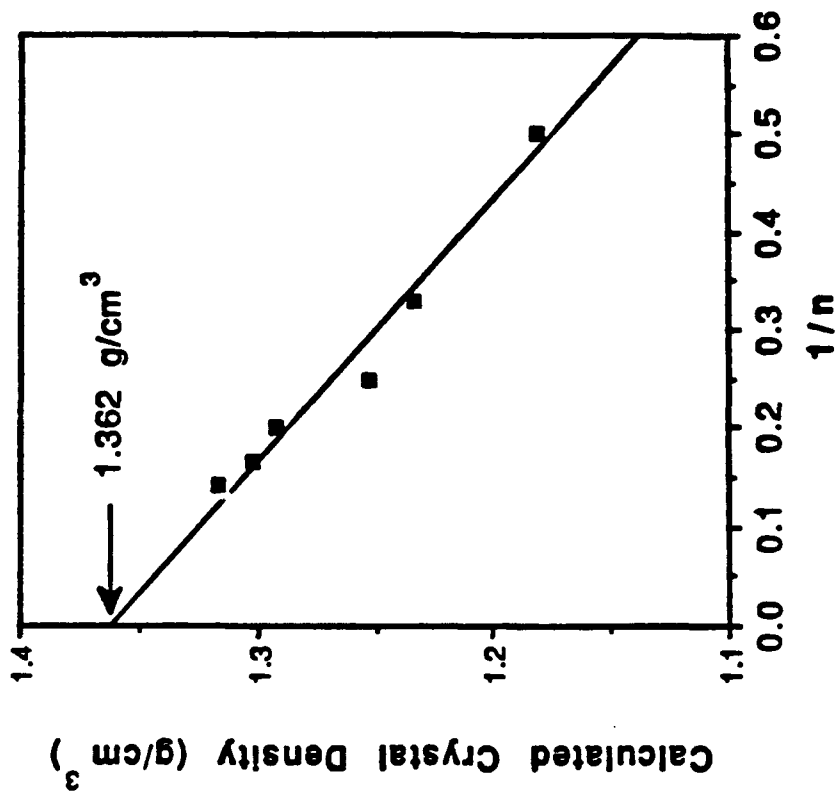


Figure 11. Plot of density vs inverse oligomer length showing the extrapolated crystal density of high polymer PPP.

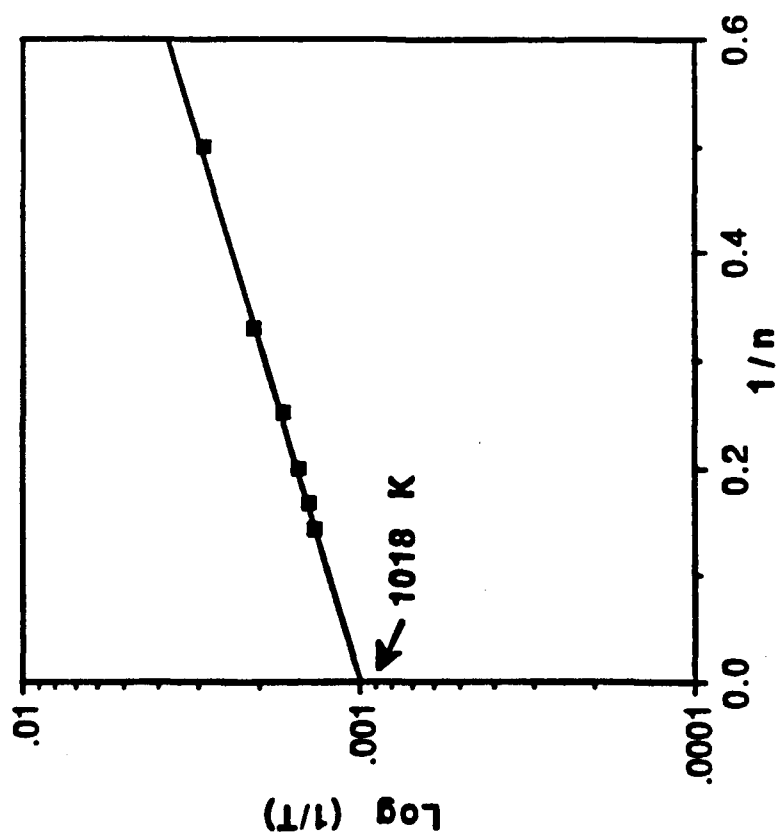


Figure 10. Plot of log of inverse melting point ($\log (1/T), K$) vs. inverse oligomer length ($1/n$) showing the extrapolated melting point of high polymer PPP.

DISCUSSION

The unit cell parameters of the $n = 5, 6,$ and 7 polyphenyl series (where n is the number of phenyl units in the molecule) agree well with the $n = 2, 3,$ and 4 oligomers, namely biphenyl, *p*-terphenyl, and *p*-quaterphenyl, allowing for space group transformations as shown in Table III. The a cell parameter is increased by approximately 4.14 \AA with the addition of a phenyl group to the end of the molecule, which is less than the length of the phenyl structural unit (approximately 4.3 \AA). Direct alignment with the long axis of the unit cell is difficult to achieve and a structural anomaly is predicted to occur such as a:

- (i) Phenyl ring deformation (chain compression or expansion),
- (ii) Molecular axis linear deviation (chain bending or kinks), and
- (iii) Cell axis alignment deviation (chain tilting).

Simple observation of the stereoviews of the oligomers in Figures 5, 7, and 9 reveals that the molecular axis is tilted away from the long crystallographic axis. Biphenyl⁴⁰, *p*-terphenyl⁴¹, and *p*-quaterphenyl⁴² also possess this anomaly. Figure 12 presents different views of PSeptiP showing how the molecules align parallel to the ac or (010) plane and the setting angle θ as the angle the benzene planes of the "averaged" oligomer make with the ac (010) plane of the unit cell. Figure 12 also shows the molecular axes intersecting with the ab (001) and bc (100) planes defining an intersection angle ω and ϕ , respectively. This angular data is tabulated below in Table X and shown in Figure 13.

TABLE X

Intersection Angles and Setting Angles for *p*-Polyphenyls

COMPOUND	$\omega, \pm 0.3^\circ$	$\theta, \pm 0.3^\circ$	$\phi, \pm 0.3^\circ$
Biphenyl	22.5	56	72.5
<i>p</i> -terphenyl	19	57	73
<i>p</i> -quaterphenyl	11.5	56.5	73
<i>p</i> -quinquephenyl	9.5	56.5	73
<i>p</i> -sexiphenyl	26	55	71
<i>p</i> -septiphenyl	6.5	57	72.5

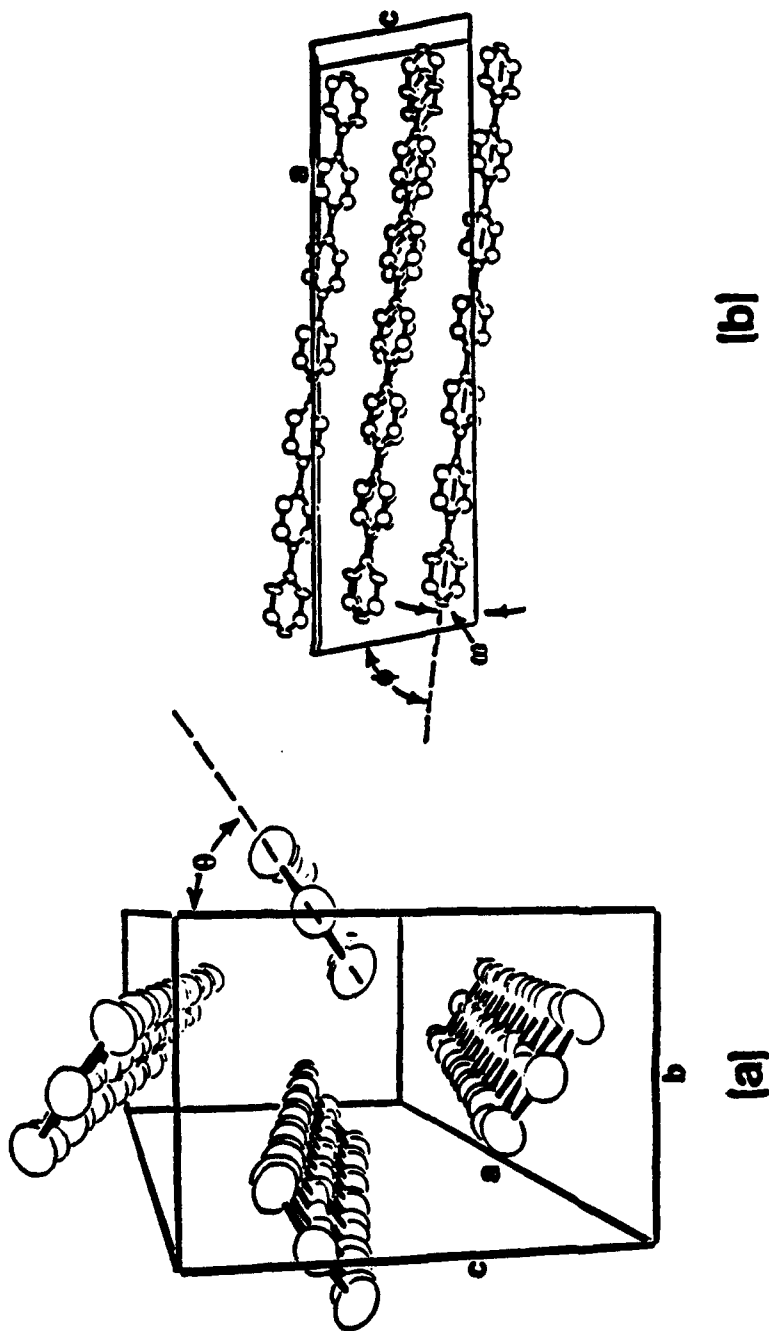


Figure 12. Diagram describing a) setting angle θ and b) intersection angles ω and ϕ for PPP oligomers.

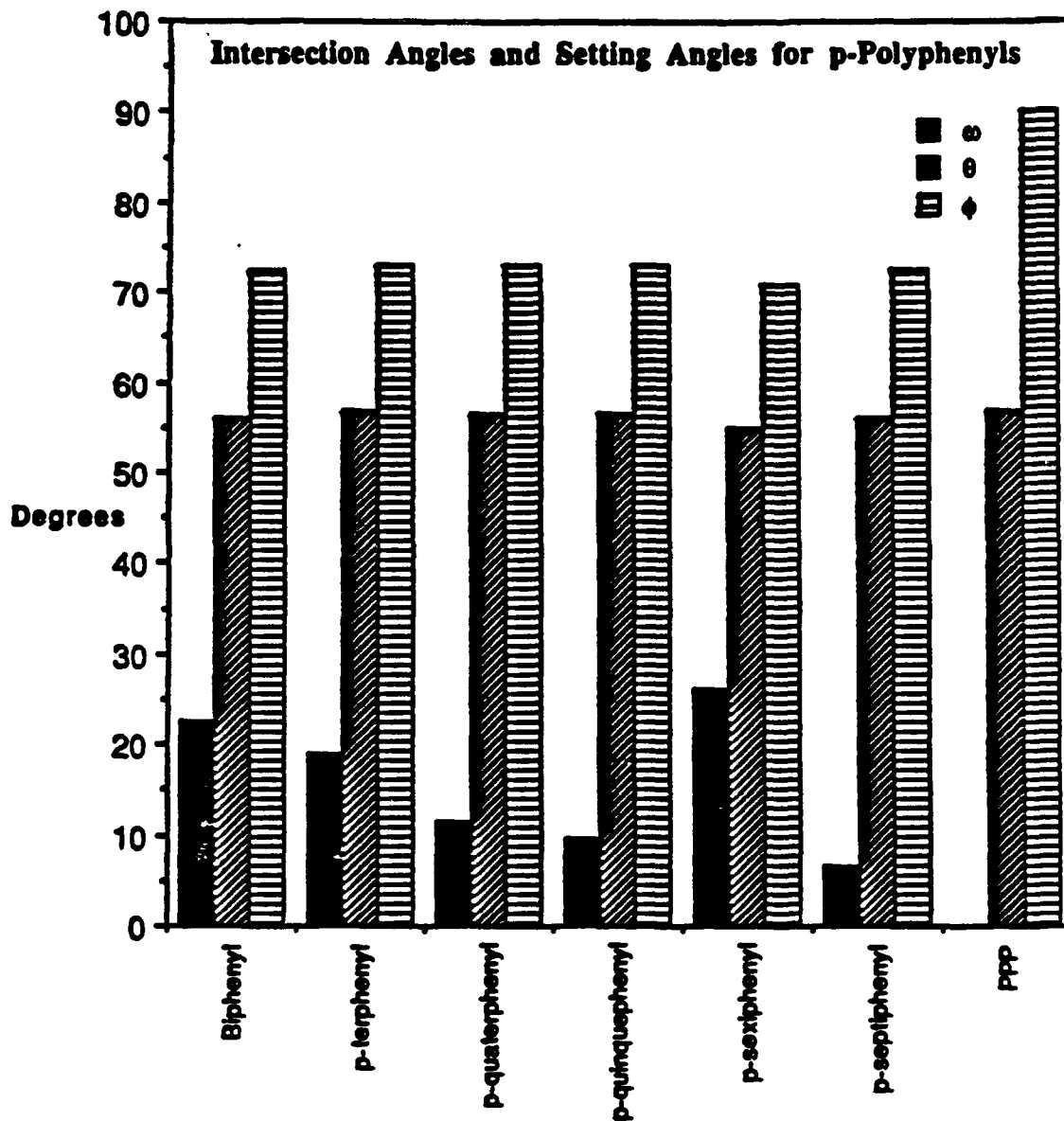


Figure 13. Intersection angles ω and ϕ and the setting angle θ for p-Polyphenyls.

PPP polymer has been determined⁴³ to have $\theta = 57^\circ$ by incorporating the setting angle into the data refinement and defining the molecular axes to be perpendicular to the (100) plane and parallel to the (010) and (001) planes. The average setting angle of $56.3 \pm 0.3^\circ$ observed for the PPP oligomers agrees very well with that derived for the polymer. The intersection angle ϕ remains relatively stable at approximately $72 \pm 0.3^\circ$ and does not appear to approach 90° defined for PPP. The intersection angle, ω , however, fluctuates with oligomer chain length. With p-sexiphenyl being the exception, ω decreases with oligomer chain length approaching a value of zero defined for PPP. At this time it is not

clear as to why PSP does not fit the data trend. Perhaps PSP exists as a polymorph and changing the conditions of crystallization will influence the crystal structure. *p*-Sexiphenyl has been suggested⁴⁴ to be good model compound for PPP due to highly similar X-ray Photoelectron Spectroscopy (XPS) spectra. We report that, structurally speaking, *p*-sexiphenyl, possessing the maximum ω of 26° , is a poor model for the polymer.

PQP, PSP, and PSeptiP all possess a center of symmetry making one half of the molecule identical to the other. Observations of edge-on drawings of the oligomers (see Figure 14) confirmed by a calculation of the angles between the atoms making up the molecular axis (see Table XI) revealed that the oligomers are straight. Interestingly enough, the largest deviation is again with *p*-sexiphenyl with a 3.6° kink between phenyl rings 3 and 4 (at the asymmetric point) and a 3.3° kink between phenyl rings 2 and 3 setting the terminal phenyl ring as 1.

The C-C bond distances within and between the phenyl rings of PQP, PSP, and PSeptiP all agree quite well with expected values. The endocyclic bond angles of the chain axis carbon atoms are less than the expected 120° , which is consistent with the lower oligomer structures³⁸⁻⁴⁰. This narrowing of the benzene ring would make the overall oligomer or polymer slightly longer than expected from calculation making direct alignment with the long crystallographic axis difficult. *p*-Sexiphenyl, once again, has the widest range of these endocyclic bond angles varying from 114.0° to 120.3° . The other bond angles agree well with the expected values. In summary, out of the three structural anomalies predicted to occur, anomalies (i) and (iii) are the largest and probably the most important factors in accounting for the discrepancy between the the calculated and observed unit cell parameters.

Fitting all of the carbon atoms to a least-squares plane reveals that for the room temperature structure of the oligomer all of the phenyl rings lie in the same plane (see Figure 14). This planar structure is thought to be the averaged structure of all the rotational degrees of freedom belonging to the phenyl units of PPP oligomers. Measurements of librational tensors for the lower oligomers⁴¹ reveal that the rings do have a high degree of torsional motion. The largest deviation from the oligomer plane was 0.05 \AA for C9 of PSeptiP. Measurement of inter-ring torsion angles confirmed this averaged planarity in PQP, PSP, and PSeptiP. PPP conformations simulated in the absence of crystal packing forces¹⁵ have the rings perpendicular to each other and calculations on a trimer⁴⁵ indicate inter-ring torsion angles of approximately 50° . This suggests that constraints within the unit cell are strong enough to overcome the ortho hydrogen repulsion. A double well potential⁴⁶ exists as a result of the competition of these two forces.

The oligomers in this study pack in a herringbone (non-parallel) structure⁴⁷ also observed in the lower oligomers and calculated to occur in the polymer. No close

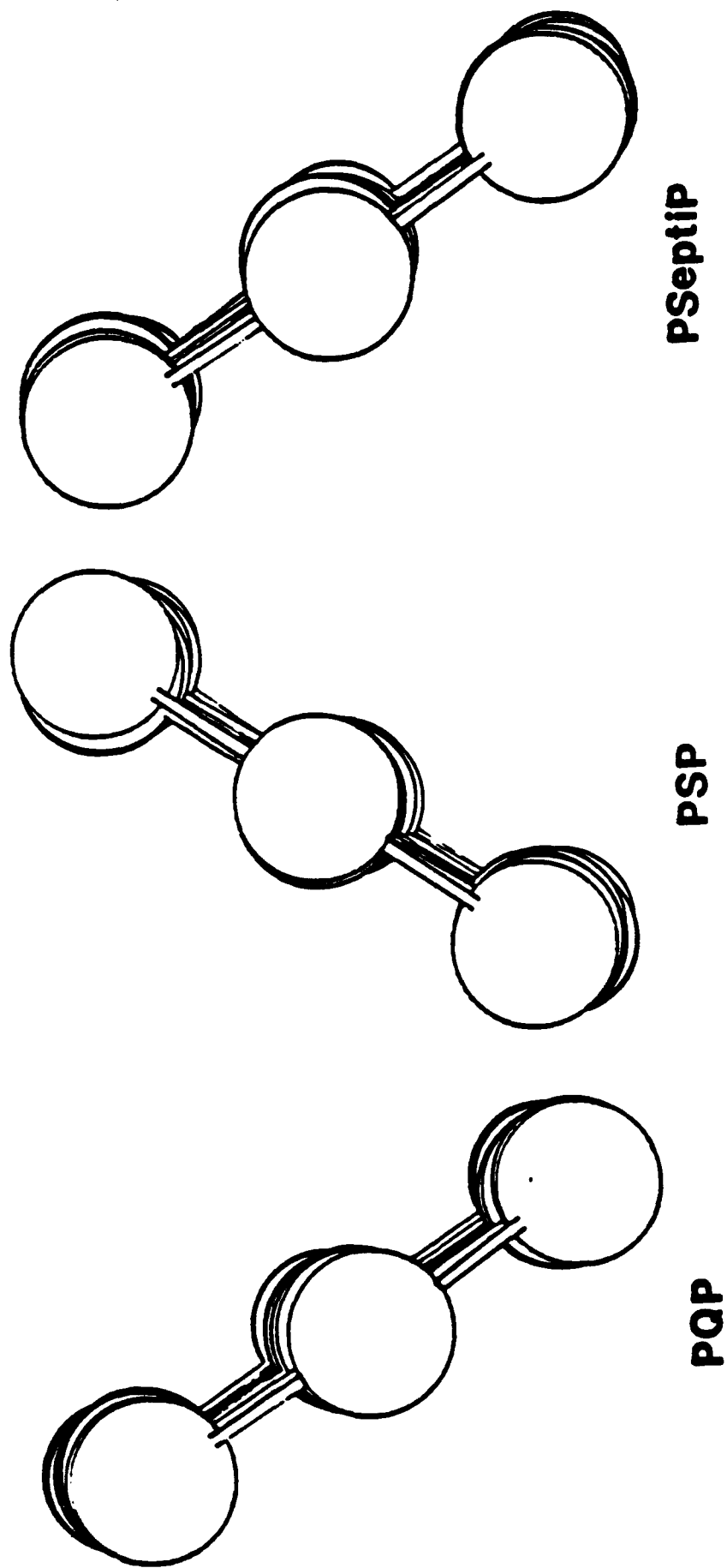
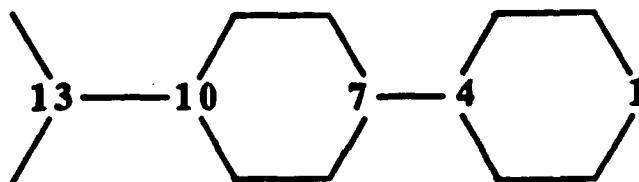


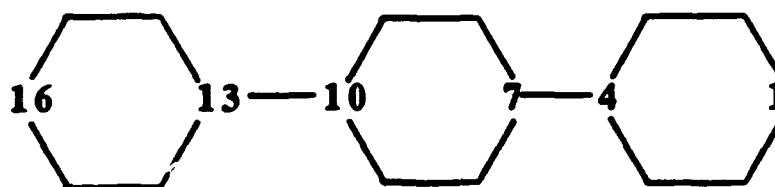
Figure 14. Edge-on PLUTO drawings of PQP, PSP, and PSeptIP showing molecular linearity and planarity.

Table XI
Angles (°) Between Molecular Axis Carbon Atoms

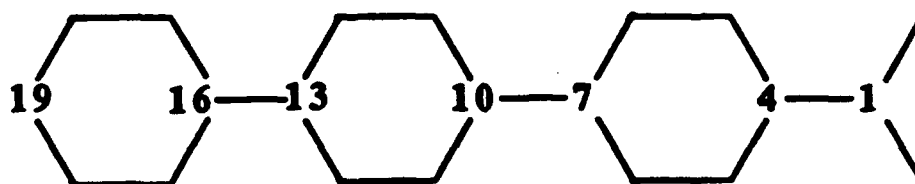
	Tables	Angles
PQP	C1-C4-C7	179.5
	C4-C7-C10	178.5
	C7-C10-C13	179.5
	C10-C13-C13'	178.7
PSP	C1'-C1-C4	176.4
	C1-C4-C7	178.2
	C4-C7-C10	177.6
	C7-C10-C13	178.3
	C10-C13-C16	178.0
PSeptiP	C1'-C1-C4	179.6
	C1-C4-C7	179.8
	C4-C7-C10	178.2
	C7-C10-C13	178.0
	C10-C13-C16	179.2
	C13-C16-C19	178.1



PQP Asymmetric Unit



PSP Asymmetric Unit



PSeptiP Asymmetric Unit

molecular interactions of any significance are found, the closest one being (C2)-C1-H6 at 2.9 Å and 90° (the C1-H6 distance is 2.6 Å) occurring in p-sexiphenyl.

Low temperature (110 K) structure determinations for PQP, PSP, and PSeptiP are currently underway. Research done on the lower polyphenyls⁴⁸⁻⁵⁰ have discovered that a structural transition occurs such that the "averaged" planar structure observed at room temperature changes to a nonplanar configuration at lower temperature. The low temperature unit cell is a superstructure of the room temperature unit cell with the parameters *b* and *c* approximately doubled to account for the greater displacement of the nonplanar molecule. The temperatures of these transitions are presented in Table III and are plotted in Figure 15 along with the melting points of the PPP oligomers up to *p*-octiphenyl.

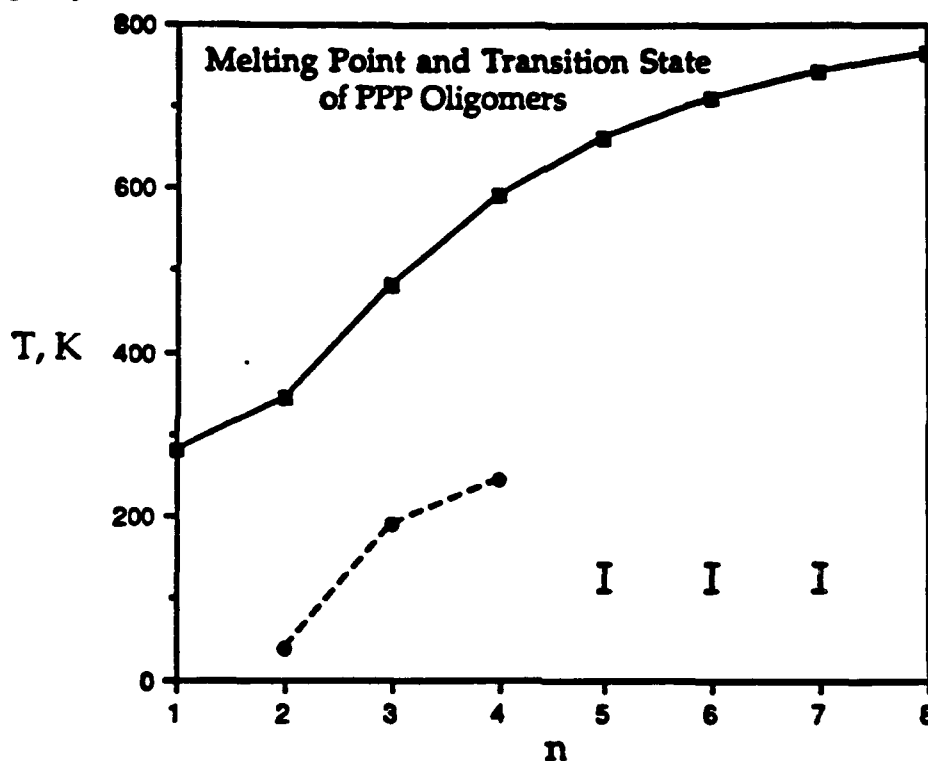


Figure 15. Plot of transition (---●---) and melting point (—■—) vs. oligomer length (*n*). Error bars at *n* = 5 - 7 indicate temperature range for observed transition.

Preliminary experiments on PQP, PSP, and PSeptiP have produced very interesting results which we are in the process of confirming. Information from Figure 15 suggests that the transition temperatures for PQP, PSP, and PSeptiP to be above room temperature, but the room temperature structures are planar and DSC measurements indicate that no transitions occur until the vicinity of the melting point is reached. Upon cooling to 110 K, both PQP and PSP single crystals index to unit cells slightly larger than the room temperature unit cells. After approximately one day, a structural transition occurs to a

monoclinic unit cell where *b* and *c* are approximately doubled from the original unit cell. PSeptiP transformed to an orthorhombic unit cell with *b* and *c* approximately doubled from the original unit cell within the time it took the software to find 25 strong reflections and index them - approximately 1 to 2 hours. Unfortunately, it has not been possible yet to resolve the low temperature reflection data to a structure or space group verification.

We believe these oligomers to have a time dependent phase transition. DSC measurements taken on polycrystalline samples cooled to -140°C at a rate of $10^{\circ}\text{C}/\text{min}$. show no transition. Low temperature X-ray photographs cooling as low as -130°C and holding the sample there for as long as five days shows no transition taking place. We conclude that the transition temperature must exist between these two temperatures (between 143 and 110 K) as indicated in Figure 15 by the error bars and is time dependent. This transition temperature, being much lower than the other polyphenyls and to have a time dependency, could be explained by a non-first order phase transition such that is observed for biphenyl^{48,51} for which a soft mode exists below its transition temperature.

DSC measurements on PQP, PSP, PSeptiP, and p-octiphenyl (POP), shown in Figure 16a-d, respectively, indicate that the samples undergo transitions around the melting point which have been attributed to liquid crystal transitions. PQP (Figure 16a) shows a small peak at 418°C probably indicating the nematic \rightarrow isotropic transition after the melting point at 388°C in total agreement with previous reports.^{34,36} PSP (Figure 16b) likewise shows good agreement with previous research^{34,52} with peaks at 410° , 440° , and 474°C probably indicating a high temperature crystal \rightarrow crystal transition, crystal \rightarrow smectic phase transition, and a smectic \rightarrow nematic phase transition. We observe a higher temperature for the crystal \rightarrow crystal transition than that reported by Wunderlich, et al.¹⁷ Unfortunately decomposition of the sample did not permit the observation of the nematic \rightarrow isotropic phase transition.^{34,52} The DSC of PSeptiP (Figure 16c) shows three peaks at 420° , 473° , and 486°C probably indicating a crystal \rightarrow crystal transition, crystal \rightarrow smectic phase transition, and a smectic \rightarrow nematic phase transition in the same manner as PSP. Wunderlich, et al.⁵³ reports a smectic \rightarrow nematic transition at 534°C which is approximately 50° higher than what we observe. This discrepancy can not be explained at this time. POP (Figure 16d) shows two peaks probably indicating a smectic \rightarrow nematic transition at 510°C after the melting point (sharp peak at 489°C). Sample decomposition did not permit going to higher temperatures for PSeptiP and POP. Single crystals of POP are attempting to be grown in order to perform a structure determination completing this series.

Our findings are plotted next to published values^{34,53} in Figure 17.

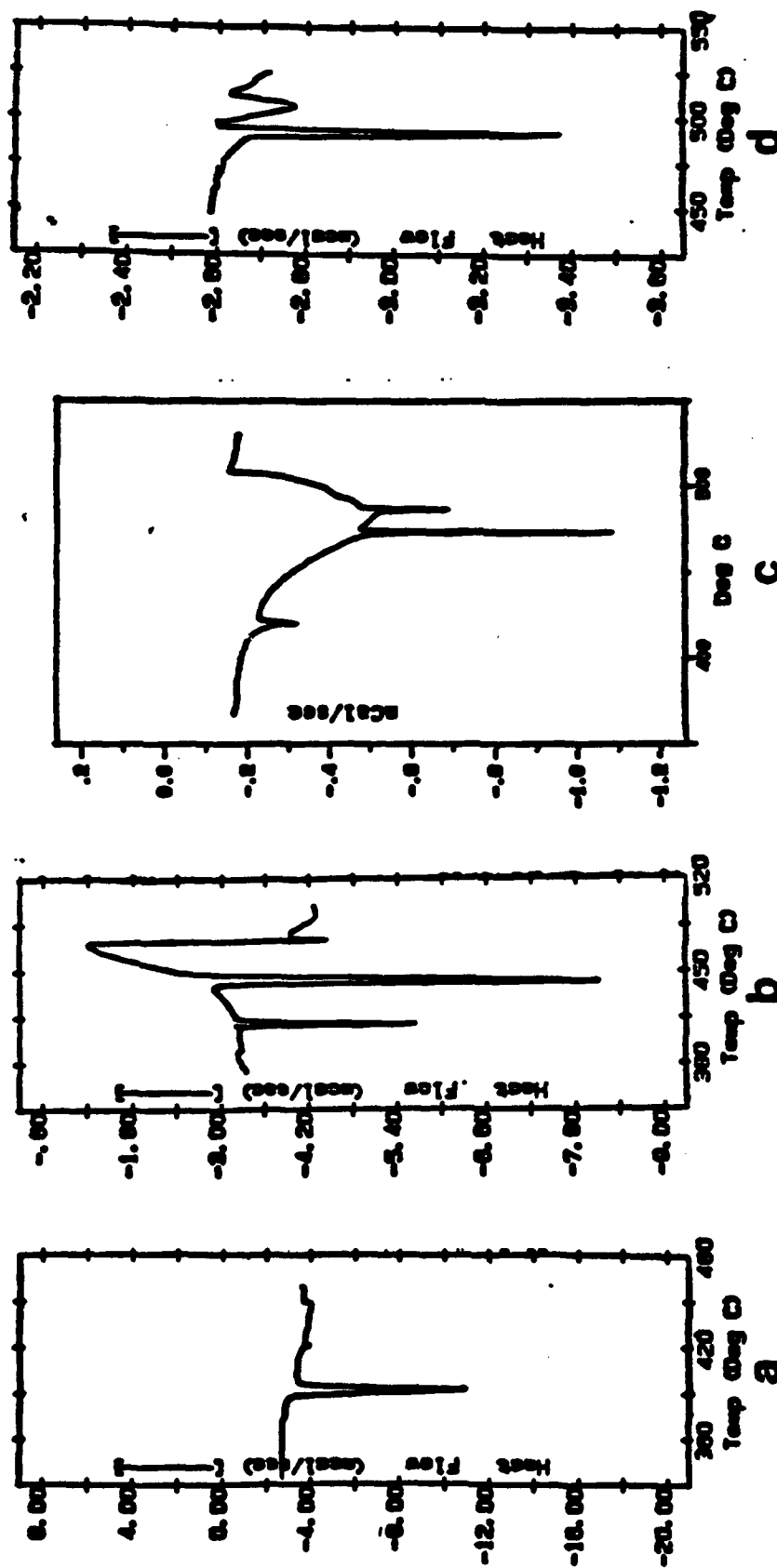


Figure 16. DSC measurements of PQP (a), PSexiP (b), PSeptiP (c), and POctiP (d). Scan rate was 10°C/min.

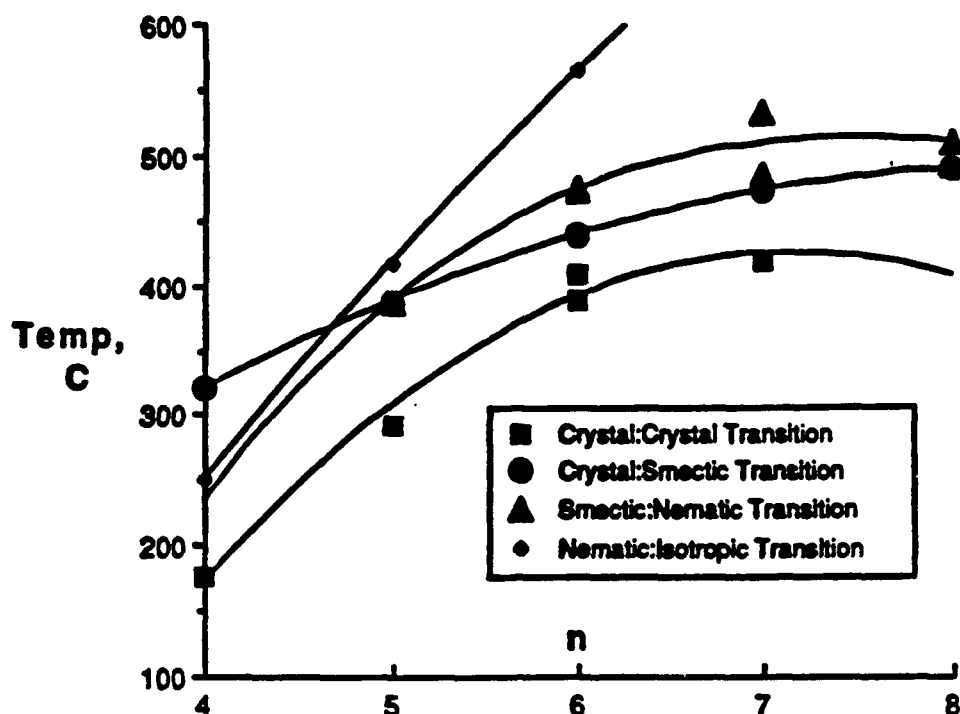


Figure 17. Plot of high temperature liquid crystal phase transitions for PPP oligomers $n = 4 - 8$.

If PSeptiP and POP follow the examples of the lower polyphenyls, the nematic \rightarrow isotropic transitions could be as high as 700° and 800°C for PSeptiP and POP, respectively. These temperatures are much higher than thermal decomposition⁵⁴ will allow stability to the polymer and any practical use of the mesophase region will require special containments such as high-pressure, inert atmosphere cells.

Also the plot indicates that a high temperature phase transition exists between the crystal \rightarrow crystal transition and the melting point. In addition is the low temperature phase transition mentioned earlier (see Figure 15). Nuclear magnetic resonance (NMR) studies^{55,56} in this temperature range indicate that the phenyl rings undergo 180° flips along the molecular axis for the amorphous phase. The rate of flipping is rapid at room temperature and increases dramatically as the temperature rises. At low temperature the rate of ring flips⁵² decreases to about $20 - 30^\circ$ and the low temperature cell and structure predominates.

Slow scan rates ($10^\circ\text{C}/\text{min.}$) were used primarily to obtain accurate melting point data. Decomposition, which is so common with the polyphenyls, may be preventing the observation of many liquid crystal transitions. Additional DSC experiments using a faster scan rate and pressurized containers are suggested in hopes of fully studying the phase transitions of the higher polyphenyls.

CONCLUSIONS

The higher oligomers of PPP follow the same pattern as the lower oligomers previously studied. The unit cell parameters are very similar with the exception of crystallographic axis a increasing with oligomer length to accommodate the growing chain. All the oligomers have similar space groups, bond distances and bond angles. Linear, planar molecular structures are observed in all but the herringbone crystal structures are very different. The longer even numbered oligomers are shewed in the unit cell much more than the longer odd numbered oligomers. The setting angle for the oligomers match that of PPP polymer.

Low temperature transitions for PQP, PSP, and PSeptiP exist between 110 K and 140 K and are time dependent, but detailed molecular structures could not be resolved nor could a transition temperature be pinpointed. Liquid crystal transition states were observed but due to sample decomposition at temperatures above 500°C need to be studied further.

REFERENCES

1. Noren, G.K. and Stille, J.K. *J. Polym. Sci. Macromol. Rev.* 1971, 5, 385.
2. Speight, J.G., Kovacic, P., and Koch, F.W. *J. Macromol. Sci. Rev. Macromol. Chem.* 1971, 5, 295.
3. Kovacic, P. and Jones, M. B. *Chem. Rev.* 1987, 87, 357.
4. Kovacic, P. and Kyriakis, A. *J. Am. Chem. Soc.* 1963, 85, 454.
5. Yamamoto, T., Hayashi, Y., and Yamamoto, A. *Bull. Chem. Soc. Jpn.* 1978, 51, 2091.
6. Unroe, M.R. and Reinhardt, B.A. *Polymer* 1987, 11, 981.
7. Martinek, T. W., Haines, R. M., Weichman, R.L., and Trainor, W. J. U.S. Patent 3476687, 1969; *Chem. Abstr.* 1969, 72, 14472d.
8. McMahon, M. A., Jr., Chafez, H., and Coppoc, W. J. U.S. Patent 3384588, 1968; *Chem. Abstr.* 1968, 69, 20938q.
9. McCarthy, P. R. and Tempalski, C. S. U.S. Patent 3291733, 1966; *Chem. Abstr.* 1966, 66, 57627b.
10. Agnew, R. J. and Dille, K. L. U.S. Patent 3278429, 1966; *Chem. Abstr.* 1966, 66, 12765d.
11. Accountis, O. E. U.S. Patent 3443899, 1969; *Chem. Abstr.* 1969, 71, 22829v.
12. Sato, M., Yamazaki, H. and Yamaguchi, S. Japan Patent 63/102982, 1988; *Chem. Abstr.* 1988, 109, 160647p.
13. Gale, D. M. *J. Appl. Polym. Sci.* 1978, 22, 1955.
14. Ostrum, G. K., Lawson, D. D., and Ingham, J. D. *Polym. Prepr., Am. Chem. Soc., Div. Polym.* 1966, 7, 895.
15. Wierschke, S.G. in The Materials Science and Engineering of Rigid-Rod Polymers, edited by W. W. Adams, R. K. Eby, and D. E. McLemore (Mater. Res. Soc. Proc. 134, Boston, MA 1988) p 313; AFWAL-TR-88-4201 (October 1988).
16. Gale, D. M. *J. Polym. Sci., Polym. Lett. Ed.* 1977, 15, 439.
17. Ivory, D. M., Miller, G. G., Sowa, J. M., Shacklette, L. W., Chance, R. R., and Baughman, R. H. *J. Chem. Phys.* 1979, 71, 1506.
18. Pradere, P. and Boudet, A. *J. Mater. Sci. Lett.* 1988, 7, 10.
19. Baughman, R. H., Shacklette, L. W., Murthy, N. S., Miller, G. G., and Elsebaumer, R. L. *Mol. Cryst. Liq. Cryst.* 1985, 118, 253.
20. Baughman, R. H., Bredas, J. L., Chance, R. R., Elsebaumer, R. L., and Shacklette, L. W. *Chem. Rev.* 1982, 82, 209.
21. Patil, A. O., Heeger, A. J., and Wudl, F. *Chem. Rev.* 1988, 88, 183.

22. Bredas, J. L., Dory, M., Themans, B., Delhalle, J. and Andre, J. M. *Synthetic Metals* 1989, 28, D553.
23. Dory, M., Bodart, V. P., Delhalle, J., Andre, J. M., and Bredas, J. L. in *Nonlinear Optical Properties of Polymers*, edited by A. J. Heeger, J. Orenstein, and D. R. Ulrich (Mater. Res. Soc. Proc. 109, Pittsburg, PA, 1988) p 239.
24. Bredas, J. L., Chance, R. R., and Baughman, R. H. *J. Chem. Phys.* 1982, 76, 3673.
25. Leising, G., Leitner, O., Aldrian, F., and Kahlert, H. *Synthetic Metals* 1987, 17, 635.
26. Bredas, J. L. *J. Chem. Phys.* 1985, 83, 3208.
27. Bredas, J. L., Themans, B., Tripiat, J. G., Andre, J. M., and Chance, R. R. *Phys. Rev. B: Condens. Matter* 1984, 29, 6761.
28. Yi, X., Xiaoming, L. and Duanming, Z. *J. Mol. Sci.* 1987, 5, 229.
29. Pelous, Y., Froyer, G., Herold, C. and Lefrant, S. *Synthetic Metals* 1989, 29, E17.
30. Kispert, L. D., Joseph, J., Miller, J. J., and Baughman, R. H. *J. Chem. Phys.* 1984, 81, 2119.
31. Irvine, P. A., Wu, D. C., and Flory, P. J. *J. Chem. Soc., Faraday Trans. 1*, 1984, 80, 1795.
32. Flory, P. J. and Ronca, G. *Mol. Cryst. Liq. Cryst.* 1979, 54, 311.
33. Smith, G. W. *Mol. Cryst. Liq. Cryst. Lett.* 1979, 49, 207.
34. Frenz, B.A. and Associates, Inc. (1985), College Station, Texas, 77840 and Enraf-Nonius, Delft, The Netherlands.
35. Main, P. (1982), editor, MULTAN 11/82, A System of Computer Programs for the Automatic Solution of Crystal Structures from X-ray Diffraction Data, Department of Physics, University of York, York, England.
36. Sheldrick, G. M. in *Crystallographic Computing 3*, Eds. G. M. Sheldrick, C. Fruger, and R. Goddard, (Oxford University Press, 1985), pp. 175-89.
37. Starkweather, H.W. *Macromolecules* 1986, 19, 1131.
38. Gardner, K. (Private Communication).
39. Flory, P.J. *Principles of Polymer Chemistry* (Cornell University Press, Ithaca, New York, 1953) p. 570.
40. Charbonneau, G.-P. and Delugeard, Y. *Acta Cryst.* 1977, B33, 1586.
41. Baudour, J. L., Delugeard, Y., and Sanquer, M. *Acta Cryst.* 1974, B30, 691.
42. Delugeard, Y., Desuche, J. and Baudour, J. L. *Acta Cryst.* 1976, B32, 702.

43. Kawaguchi, A. and Petermann, J. *Mol. Cryst. Liq. Cryst.* 1986, 133, 189.
44. Seki, K., Kailsson, U. O., Engelhardt, R., Koch, E.-E. and Schmidt, W. *Chem. Phys.* 1984, 91, 459.
45. Farmer, B.J., Personal Communication.
46. Cailleau, H., Baudour, J.L., Meinel, J., Dworkin, A., Moussa, F., and Zeyen, C.M.E. *Faraday Discussions Chem. Soc.* 1980, 69, 7.
47. Desiraju, G. R. and Gavezzotti, A. *Acta Cryst.* 1989, B45, 473.
48. Cailleau, H., Baudour, J.L. and Zeyen, C.M.E. *Acta Cryst.* 1979, B35, 426.
49. Cailleau, H. and Dworkin, A. *Mol. Cryst. Liq. Cryst.* 1979, 50, 217.
50. Baudour, J. L., Delugeard, Y., and Rivet, P. *Acta Cryst.* 1978, B34, 625.
51. Bree, A. and Edelson, M. *Chem. Phys. Lett.* 1977, 46 (3), 500.
52. Lewis, I.C. and Barr, J. B. *Mol. Cryst. Liq. Cryst. Lett.* 1981, 72, 65.
53. Wunderlich, B., Moller, M., Grebowicz, J. and Baur, H. *Advances in Polymer Science*, 87. (Springer-Verlag Berlin, Heidelberg 1988).
54. Windle, A. *MRS Bulletin* 1987, 12, 18.
55. Toudic, B., Gullieu, J., Rivet, P., and Delugeard, Y. *Chem. Phys.* 1985, 99, 275.
56. Dumais, J. J., Jelinski, L. W., Galvin, M. E., Dybowski, C., Brown, C. E., and Kovacic, P. *Macromolecules* 1989, 22, 612.

Appendix A

General Displacement Parameter Expressions, U's, for P-Quinquephenyl

Name	U(1,1)	U(2,2)	U(3,3)	U(1,2)	U(1,3)	U(2,3)
C1	0.036(2)	0.062(3)	0.058(2)	0.008(3)	0.011(2)	0.003(3)
C2	0.048(2)	0.054(3)	0.074(3)	-0.007(3)	0.008(2)	-0.013(3)
C3	0.037(2)	0.059(3)	0.063(3)	0.001(3)	0.015(2)	-0.013(3)
C4	0.028(2)	0.041(2)	0.031(2)	0.008(2)	0.004(1)	0.004(2)
C5	0.046(2)	0.053(3)	0.060(2)	-0.015(3)	0.011(2)	-0.014(2)
C6	0.039(2)	0.061(3)	0.069(3)	-0.012(3)	0.013(2)	-0.005(3)
C7	0.036(2)	0.032(2)	0.033(2)	-0.010(2)	-0.001(2)	0.002(2)
C8	0.035(2)	0.060(3)	0.105(3)	0.005(2)	0.036(2)	-0.033(3)
C9	0.053(2)	0.050(2)	0.082(3)	-0.010(3)	0.014(2)	-0.044(2)
C10	0.045(2)	0.026(2)	0.028(2)	-0.014(2)	0.001(2)	-0.002(2)
C11	0.034(2)	0.058(3)	0.096(3)	0.002(3)	0.027(2)	-0.032(3)
C12	0.051(2)	0.054(2)	0.086(3)	-0.012(3)	0.018(2)	-0.044(2)
C13	0.028(2)	0.042(2)	0.029(1)	0.015(2)	0.006(1)	0.003(2)
C14	0.056(2)	0.048(2)	0.069(3)	-0.022(3)	0.007(2)	-0.034(2)
C15	0.024(2)	0.055(2)	0.087(3)	-0.016(2)	0.019(2)	-0.021(3)

The form of the anisotropic displacement parameter is:

$$\exp[-2\pi^2\{h^2a^2U_{1,1} + k^2b^2U_{2,2} + l^2c^2U_{3,3} + 2hkabU_{1,2} + 2hlacU_{1,3} + 2klbcU_{2,3}\}] \text{ where } a, b, \text{ and } c \text{ are reciprocal lattice constants.}$$

Appendix A

General Displacement Parameter Expressions, U's, for p-Sexiphenyl

Name	U(1,1)	U(2,2)	U(3,3)	U(1,2)	U(1,3)	U(2,3)
C1	0.017(3)	0.049(3)	0.030(3)	-0.001(3)	0.010(3)	-0.000(3)
C2	0.041(4)	0.060(4)	0.064(5)	-0.020(4)	-0.014(4)	-0.027(4)
C3	0.058(4)	0.044(4)	0.064(4)	0.029(4)	-0.007(4)	-0.028(4)
C4	0.015(3)	0.012(3)	0.036(3)	0.001(2)	0.017(2)	0.000(3)
C5	0.032(3)	0.027(3)	0.086(5)	0.014(3)	0.001(4)	-0.032(4)
C6	0.048(5)	0.079(5)	0.083(6)	-0.009(5)	-0.009(4)	-0.042(5)
C7	0.059(4)	0.048(4)	0.026(3)	-0.008(4)	-0.005(3)	-0.001(4)
C8	0.043(4)	0.076(5)	0.085(5)	0.007(4)	0.003(4)	-0.037(5)
C9	0.029(4)	0.053(4)	0.081(5)	0.007(4)	0.002(4)	-0.031(4)
C10	0.032(4)	0.051(4)	0.031(3)	-0.011(4)	-0.007(3)	0.006(4)
C11	0.046(4)	0.074(4)	0.076(5)	0.027(4)	-0.013(4)	-0.045(4)
C12	0.029(4)	0.055(4)	0.085(5)	0.002(4)	-0.011(4)	-0.018(5)
C13	0.045(4)	0.025(3)	0.032(3)	0.005(3)	0.010(3)	0.009(3)
C14	0.051(4)	0.049(4)	0.053(4)	0.029(4)	-0.009(4)	-0.005(4)
C15	0.038(4)	0.065(4)	0.070(5)	0.014(4)	-0.008(4)	-0.010(5)
C16	0.074(5)	0.070(5)	0.053(4)	0.014(5)	-0.007(4)	0.008(5)
C17	0.049(4)	0.071(5)	0.060(5)	-0.004(5)	-0.013(4)	-0.006(5)
C18	0.026(3)	0.047(4)	0.054(4)	0.010(3)	0.004(3)	-0.014(4)

The form of the anisotropic displacement parameter is:

$$\exp[-2\pi^2(h^2a^2U_{1,1} + k^2b^2U_{2,2} + l^2c^2U_{3,3} + 2hkabU_{1,2} + 2hlacU_{1,3} + 2klbcU_{2,3})] \text{ where } a, b, \text{ and } c \text{ are reciprocal lattice constants.}$$

Appendix A

General Displacement Parameter Expressions, U's, for P-Septiphenyl

Name	U(1,1)	U(2,2)	U(3,3)	U(1,2)	U(1,3)	U(2,3)
C1	0	0	0	0	0	0
C2	0	0	0	0	0	0
C3	0	0	0	0	0	0
C4	0	0	0	0	0	0
C5	0	0	0	0	0	0
C6	0	0	0	0	0	0
C7	0	0	0	0	0	0
C8	0	0	0	0	0	0
C9	0	0	0	0	0	0
C10	0.029(5)	0.062(7)	0.014(4)	0.003(6)	-0.001(4)	0.003(6)
C11	0	0	0	0	0	0
C12	0	0	0	0	0	0
C13	0.024(4)	0.047(6)	0.019(4)	-0.006(5)	0.002(4)	0.006(5)
C14	0	0	0	0	0	0
C15	0	0	0	0	0	0
C16	0.036(5)	0.019(5)	0.037(5)	-0.002(5)	0.006(4)	-0.009(5)
C17	0.037(5)	0.055(7)	0.064(6)	0.007(6)	0.025(4)	0.013(7)
C18	0.059(7)	0.081(9)	0.054(6)	0.014(7)	0.014(5)	0.020(7)
C19	0.020(4)	0.070(7)	0.052(5)	0.005(6)	0.020(4)	-0.004(7)
C20	0.052(6)	0.072(8)	0.056(7)	-0.002(7)	0.016(5)	0.014(7)
C21	0.030(5)	0.060(7)	0.077(7)	-0.019(6)	0.024(4)	0.011(7)

The form of the anisotropic displacement parameter is:

$$\exp[-2\pi^2\{h^2a^2U_{1,1} + k^2b^2U_{2,2} + l^2c^2U_{3,3} + 2hkabU_{1,2} + 2hlacU_{1,3} + 2klbcU_{2,3}\}] \text{ where } a, b, \text{ and } c \text{ are reciprocal lattice constants.}$$

(C)-H...O INTERACTIONS IN NITROANILINE DERIVATIVES

Kenneth N. Baker and Albert V. Fratini
Department of Chemistry, University of Dayton, 300 College Park, Dayton,
OH 45469-2357

W. Wade Adams
Materials Laboratory, Wright Research and Development Center, WPAFB, OH
45433-6533.

David A. Grossie
Department of Chemistry, Wright State University, Dayton OH, 45435

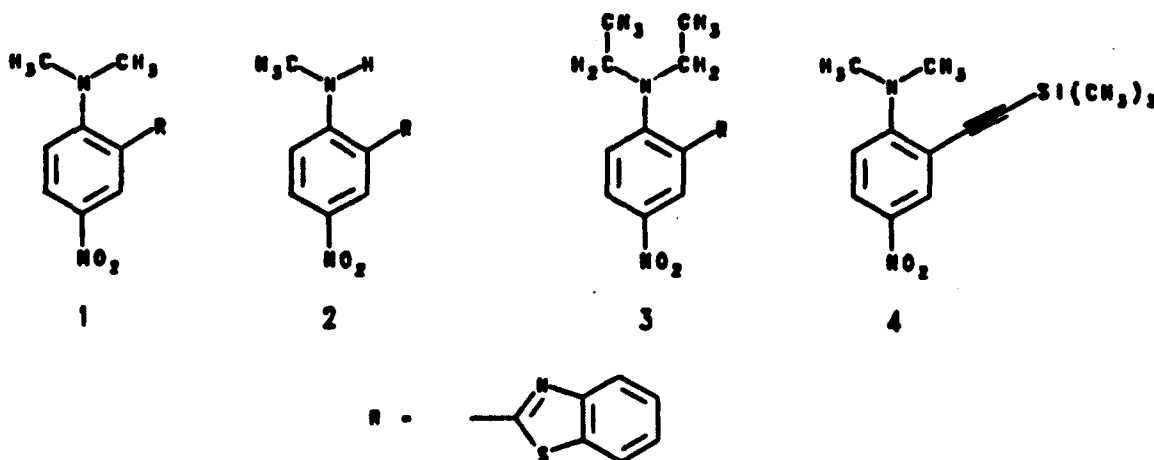
ABSTRACT

The design of organic second order nonlinear optical (NLO) materials depends on factors such as the nature and position of substituents on the aromatic ring and the hydrogen bonding patterns of donor and acceptor groups. In order to investigate the effect of alkyl substitution on the amino group and placement of bulky groups on the aromatic ring of nitroaniline derivatives, the crystal structures and unit cell packing of 2-[2-(N-methylamino)-5-nitrophenyl]benzothiazole, 2-[2-(N,N-dimethylamino)-5-nitrophenyl]-benzothiazole, 2-[2-(N,N-diethylamino)-5-nitrophenyl]benzothiazole, and 2-(trimethylsilylethynyl)-4-nitro-N,N-dimethylaniline have been determined. In all four compounds, alkyl groups attached to the amino nitrogen atom prevent the formation of intermolecular hydrogen bonds between amino and nitro groups. Instead, the molecules exhibit (C)-H...O intermolecular interactions between the nitro group and the hydrogen atoms on the aromatic ring and alkyl groups. Two distinct types of packing - herringbone patterns and planar stacks - are observed, with the closest interactions associated with the planar stacks. The dialkylamino substituents extend above and below the molecular plane, which is comprised of essentially coplanar ring systems.

INTRODUCTION

The current emphasis in designing second order nonlinear optical materials is to combine electron conjugation, polarizability, and acentricity into a molecular solid. Polymers are very good candidates for the first requirement because of their extensive π electron conjugation. Nitroaniline derivatives (2-methylnitroaniline¹ and 2-methylnitromethylaniline², for example), having conjugation and polarizability, are known to exhibit strong $\chi^{(2)}$ optical nonlinearities. Quite often compounds that have the former factors crystallize in a morphology that includes a center of symmetry, negating the effects of conjugation and polarizability and nullifying the $\chi^{(2)}$ response. In order to increase our knowledge of the factors that influence the $\chi^{(2)}$ susceptibility of an organic material, a series of compounds were synthesized and subjected to x-ray crystallographic analysis. This series includes: 2-[2-(N,N-dimethylamino)-5-nitrophenyl]-benzothiazole, 1; 2-[2-(N-methyl-amino)-5-nitrophenyl]-benzothiazole, 2; 2-[2-(N,N-diethyl-amino)-5-nitrophenyl]-benzothiazole, 3; and 2-(trimethylsilylethynyl)-4-nitro-N,N-dimethylaniline, 4.

Each of the four compounds crystallizes in a centric lattice which eliminates a second order NLO response. In spite of their similarities, the compounds exhibit two types of packing motifs and have some interesting close contacts that are different from those normally found in nitroanilines.^{3,4}



EXPERIMENTAL

The compounds were synthesized by Bruce Reinhardt, Materials Laboratory, WPAFB. Suitable crystals were selected from bulk crystalline samples and observed under crossed polarizing filters to determine extinction boundaries. Single crystals were mounted using cyanoacrylate adhesive onto glass fibers attached to long Huber pins and inserted into arcless goniometer heads. The crystals were centered on a Enraf-Nonius CAD4 diffractometer for data collection and rotation photographs taken to judge how well each crystal diffracts. Reflection data were transferred to a VAX 11/730 computer for further analysis using SDP/VAX⁵. Space group identification was accomplished with the aid of the computer program LOOK⁶ which confirmed the systematic absences found in the reflection files. Structure solutions were found using SHELXS⁷ or MULTAN⁸ and refined using full-matrix least-squares. Hydrogen atoms were placed in idealized locations calculated from geometric considerations and assigned a fixed C-H bond distance of 0.95Å. Subsequent isotropic refinement of hydrogen atoms did not significantly improve the structure due to the reduced data-to-parameter ratio. Crystal data and data collection parameters are tabulated in Table I.

RESULTS

The molecular structures of 1, 2, 3, and 4 are shown in Figures 1, 3, 5, and 7, respectively, with the non-hydrogen atoms labeled and the hydrogen atoms omitted, except for H1 in 2 which forms an intramolecular hydrogen bond with the nitrogen atom of the benzothiazole ring. Tables II, IV, VI, and VIII summarize the respective atomic coordinates. Bond distances and angles are listed in Tables III, V, VII, IX. Stereoviews of the molecular packing in the unit cell are shown in Figures 2, 4, 6, and 8. The close interactions in the forementioned compounds are summarized in Table X.

DISCUSSION

All four compounds reported here crystallize in centric space groups, thus eliminating the possibility of $\chi^{(2)}$ activity. Two different types of unit cell packing are observed. Both of the dialkyl benzothiazole derivatives, 1 and 3, pack in the herringbone or non-parallel motif. This is the simplest type of packing for polyaromatic compounds.¹⁰ Compound 1 (see Figure 2) displays a more complex herringbone diagram than 3 (see Figure 6). This is probably due to more restricted room in the unit cell than is ideal to accommodate the bulky benzothiazole group which prefers to orient along the *b* axis. If the C1-C7 bond (the bond connecting the benzothiazole group to the nitroaniline root) is extended through the molecule, the molecules within the unit cell intersect at $\approx 115^\circ$ and $\approx 146^\circ$ for 1 and 3, respectively. This makes the nitroaniline plane of 3 to lie closer to a crystallographic face than that of 1. However, the nitroaniline *plane* is not as important as the nitroaniline *axis*, also called the polar axis. The polar axis of 2 is just 2.5° off from being in the *ac* (010) plane, whereas the polar axis of 3 is 22° out of plane with the (010) plane. Moreover, the polar axes for both 1 and 3 are directed along the *c* axis making the *c* axis the mode of charge carrier motion.

Compounds 2 and 4 pack in a layered motif as shown in Figures 4 and 8, respectively. Compound 2 is the only one of the four studied that did not crystallize in a monoclinic space group. In addition, 2 is also the only compound out of the four studied that does not have its nitroaniline plane or polar axis directly related to a crystallographic plane or axis. The molecules of 4 are stacked along the *c* axis. The polar axis of compound 4 is only 7° from being parallel to the *b* axis and is 19° from occupying the *ab* (001) plane making the *b* axis the mode of charge carrier motion in this case.

Compound 2 does not order well in the unit cell. The molecule stacks parallel to the *a* axis, with the molecules being tilted 25° from being perfectly perpendicular to the *a* axis. The nitroaniline plane is 23° from occupying the (101) plane within the unit cell (see Figure 4). The polar axis of the nitroaniline moiety does not correspond well to any crystallographic axes.

In describing the molecular structure, two categories clearly emerge - the benzothiazole derivatives of nitroaniline and the silyl derivative of nitroaniline. The aromatic rings are essentially coplanar in the benzothiazole derivatives, with the dihedral angle between the nitroaniline and the benzothiazole rings systems of 5.1 , 0.4 , and 5.6° , for 1, 2, and 3, respectively. More noticeable deviations are found when examining the amino and nitro groups.

The dialkylamino groups turn relative to the nitroaniline plane so that amino carbon atoms extend out of the nitroaniline plane in order to maximize the distance between them and the sulfur atom of the benzothiazole ring. The angles about the dialkylamino nitrogen atoms in compound 1 and 3 are all within 7.4° of the 109.5° expected in an ideal sp^3 hybridized atom. However, in the methylamino function of compound 2, the methyl group is coplanar with the aromatic ring system, and the angles around the nitrogen atom are within 4° of 120° . This indicates that, while the dimethyl- and diethylamino groups of 1 and 3 are tetrahedral, the methylamino group of 2 is trigonal planar. This change in the configuration of the nitrogen atom may be traced to two discrete factors: (1) the steric interaction of an alkyl group with the benzothiazole sulfur atom if the nitrogen is planar, and (2) the conjugation of the amino nitrogen atom to the aromatic ring. This latter factor is realized with the observed shortening of the C2-N3 bond distance in 2 vs. 1 and 3 (1.353, 1.421, and 1.426 Å, respectively).

In the dialkyl benzothiazole derivatives, compounds 1 and 3, the sulfur atom is *cis* to the amino group, but is *trans* in 2, the monoalkyl derivative, via the C1-C7 bond. The *trans* geometry observed in 2 is probably due to an intramolecular hydrogen bond forming with the amino hydrogen atom, H1, and the benzothiazole nitrogen atom, N1 (see Figure 3). The hydrogen bond is observed with a N-N contact of 2.7 Å. In this case of compound 2, the orientation in which a hydrogen bond can form would be preferred. The *cis* orientation found in the dialkyl benzothiazole derivatives is due to a lesser level of steric repulsion between the amino nitrogen atom and the benzothiazole sulfur atom when compared to the repulsion between adjacent nitrogen atoms if a near planar ring conformation is adopted. Molecular modelling calculations using PCMODEL of the two possible planar configurations for the dimethyl derivative indicate that the *cis* arrangement is more stable.

In the silyl derivative of nitroaniline, the silyl group intersects the benzene ring with an angle of about 11° . The carbon-carbon triple bond deviates slightly ($\sim 5^\circ$) from linearity making the group slightly bent. The rather large thermal ellipsoids of the three carbon atoms attached to the silicon atom indicate that the C22-Si bond is rotating rapidly. The dimethylamine group is slightly twisted ($\sim 17^\circ$) from coplanarity with the benzene ring.

The nitro groups in all four compounds are virtually identical, only differing in the degree of coplanarity with the benzene ring, 8.29° , 2.45° , 8.49° , and 2.50° in 1, 2, 3, and 4, respectively. The greater deviation for the dialkylamino compounds, 1 and 3, may result from the uneven

intermolecular contact between the nitro oxygen atoms and a neighboring molecule.

ORTEP diagrams of the close interactions most resembling hydrogen bonds of 1, 2, 3, and 4 are shown in Figures 9 through 12, respectively. The close interaction distances and angles are also presented in Table X. Although these interactions are not close enough to be considered hydrogen bonds¹¹, they do influence the centricity and close packing relationships discussed above.

Two types of (C)-H...O interactions are observed involving 1) hydrogen atoms from the aromatic benzothiazole ring system and 2) hydrogen atoms from the alkylamino group. The shortest distances in all four compounds are associated with the hydrogen atoms of the benzothiazole ring and of these, the most interesting occur with the layered structures 2 and 4. These compounds appear to maintain the network structure needed to propagate a charge over large distances. All of the benzothiazole ring hydrogen atoms appear to favor this interaction while the majority of the alkylamino hydrogen atoms appear to favor crosslinking two parallel layers. This crosslinking is probably due to the close proximity of the molecules caused by the screw axis of the monoclinic space group. α -Glycine¹² also contains this type of crosslinking. The C3-H3...O2 interaction seen in 4 is the shortest observed and the observed angle of 154.2° is very close to 152.7° which is the average of 59 (C)-H...O hydrogen bond containing structures¹³ found in the Cambridge Structural Database¹⁴.

Once again 2 is unique in this study to have an amino hydrogen atom available (N)-H...O interactions. Interactions of this type hold a great deal of interest in this study^{3,4} with the desire to produce acentric materials through hydrogen bonding. Unfortunately a search for nearest neighbors revealed no oxygen atoms within 3.6Å of the amino hydrogen atom. Indeed, the amino hydrogen atom forms a good intramolecular hydrogen bond with the nitrogen atom of the benzothiazole ring system and with nothing else.

CONCLUSIONS

The frequency of (C)-H...O contacts in substituted nitroaniline derivatives suggests that they play a significant role in determining the packing arrangement and thus the observed centricity of these structures. Bulky substituents, such as benzothiazole and trimethylsilyl, in addition to being electron donors to the nitroaniline ring, may disrupt the (N)-H...O interaction, but no definite effect on centricity is observed. The (C)-H...O angle does not correlate with the values expected for a typical hydrogen bond when the H...O contact is beyond 2.8Å. A network of (C)-H...O contacts is favored over isolated (C)-H...O interactions. Compounds 2 and 4 pack in a layered motif presumably favored by the extensive network of (C)-H...O interactions and the shortest contacts are associated with this layered motif.

REFERENCES

1. Lipscomb, G. F.; Garito, A. F.; and Narang, R. S. (1981) *J. Chem. Phys.*, **75**, 1509-1516.
2. Sutter, K.; Bosshard, C.; Ehrensperger, M.; Gunter, P.; and Twieg, R. J. (1988) *IEEE J. Quantum Electron.*, **24**, 2362-2366.
3. Vinson, L. K. and Dannenberg, J. (1989) *J. Am. Chem. Soc.*, **111**, 2777-2781.
4. Panunto, T. W. ; Urbanczyk-Lipkowska, Z.; Johnson, R.; Etter, M. C. (1987) *J. Am. Chem. Soc.*, **109**, 7786-7797 and references therein.
5. Frenz, B.A. (1978) "The Enraf-Nonius CAD-4/SDP--A Real-Time System for Concurrent X-Ray Data Collection and Crystal Structure Determination," *Computing in Crystallography*, H. Schenk, R. Olthof-Hazelkamp, H. van Koningsveld, and G. C. Bassi, Eds., Delft University Press, Delft, Holland, pp. 64-71.
6. Chapius, G. (1984) "LOOK. A FORTRAN Program for Generating Simulated Precession Photographs from Diffraction Data," University of Lausanne, Switzerland.
7. Sheldrick, G. M. (1986) "SHELXS-86. A FORTRAN-77 Program for the Solution of Crystal Structures from Diffraction Data," in *Crystallographic Computing 3*, Eds. G. M. Sheldrick, C. Fruger, and R. Goddard, Oxford University Press, pp. 175-89.
8. Main, P. (1982) "MULTAN 11/82. A System of Computer Programs for the Automatic Solution of Crystal Structures from X-ray Diffraction Data," Department of Physics, University of York, York, England.
9. Solutions to monomethyl and diethyl were found using SHELXS and solutions to dimethyl and silyl were found using MULTAN.
10. Desiraju, G. R. and Gavezzotti, A. (1989) *Acta Crystallogr.*, **B45**, 473-482.
11. A hydrogen bond is considered to be 2.5Å taking the van der Waals radii of a hydrogen atom and an oxygen atom to be 1.00 and 1.50Å, respectively. The values used are from Bondi, A. (1964) *J. Phys. Chem.*, **68**, 441-451.
12. Berkovitch-Yellin, Z. and Leiserowitz, L. (1984) *Acta Crystallogr.*, **B40**, 159-165.
13. Taylor, R. and Kennard, O. (1982) *J. Am. Chem. Soc.*, **104**, 5063.
14. Allen, F. H.; Bellard, S.; Brice, M. D.; Cartwright, B. A.; Doubleday, A.; Higgs, H.; Hummelink, T.; Hummelink-Peters, B. G.; Kennard, O.; Moterwell, W. D. S.; Rogers, J. R.; Watson, D. G. (1979) *Acta Crystallogr.*, **B35**, 2331-2339.

Table I. Crystal Data and Data Collection Parameters

	<u>1</u>	<u>2</u>	<u>3</u>	<u>4</u>
Formula	C ₁₃ H ₁₃ N ₃ O ₂ S	C ₁₄ H ₁₁ N ₃ O ₂ S	C ₁₇ H ₁₇ N ₃ O ₂ S	C ₁₇ H ₁₈ N ₂ O ₂ Si
Color	Brown	Yellow	Yellow	Yellow
FW	299.35	283.3	327.41	262.39
F(000)	624	296	688	560
Crystal Dimensions, mm	.55 x .6 x .88	.05 x .15 x .5	.1 x .15 x .75	.3 x .5 x .6
Shape	Diamond	Rectangular	Needle	Rectangular
Radiation	MoK α	MoK α	MoK α	MoK α
Wavelength, Å	0.71073	0.71073	0.71073	0.71073
Temperature	23°	23°	23°	23°
Crystal Form	Monoclinic	Triclinic	Monoclinic	Monoclinic
Space Group	P2 ₁ /n	P $\bar{1}$	P2 ₁ /n	P2 ₁ /c
Reflections used for cell constants				
number	25	23	25	23
θ range	15 - 26	4 - 18	6 - 18	6 - 12
Cell Constants				
a, Å	9.070(1)	11.956(1)	7.466(6)	20.258(6)
b, Å	15.432(1)	4.188(1)	20.884(2)	10.444(4)
c, Å	10.147(5)	3.896(1)	10.714(2)	7.129(2)
α , °	90.0	92.20(1)	90.0	90.0
β , °	91.32(2)	90.20(1)	109.96(2)	93.05(2)
γ , °	90.0	106.18(1)	90.0	90.0
Cell Volume, Å ³	1419.9(10)	634.2(3)	1570.1(20)	1505.9(20)
Z	4	2	4	4
Calculated Density, g/cm ³	1.40	1.49	1.39	1.16
Absorption Coefficient, cm ⁻¹	2.2	2.5	2.1	1.5
Scan Type	$\omega/2\theta$	$\omega/2\theta$	$\omega/2\theta$	$\omega/2\theta$
Scan Rate, °/min.	1.0 - 5.5	0.7 - 2.8	0.3 - 5.5	0.57 - 2.79
Scan Width	0.55 + 0.34tan θ	0.8 + 0.34tan θ	0.55 + 0.34tan θ	1.2 + 0.34tan θ
Range of Data				
θ , °	0 - 41	0 - 30	0 - 30	0 - 32
h	0/16	-16/16	-10/10	-10/10
k	-28/28	0/19	0/29	0/15
l	-18/18	-5/5	-15/15	0/30
Numerical Abs.				
max. trans. coeff.	0.9911	0.9885	-	0.9606
min. trans. coeff.	0.8541	0.9446	-	0.9329
Reflections Meas.				
Total	21220	6094	9360	5592
Unique	6606	2979	4697	5266
Observed,				
$F_o^2 > 3\sigma(F_o^2)$	2540	1888	2332	1536
Averaging agreement on I	0.016	0.025	0.029	0.044

Table I. Crystal Data and Data Collection Parameters (continued)

	<u>1</u>	<u>2</u>	<u>3</u>	<u>4</u>
Parameters	231	225	276	164
R	0.048	0.074	0.042	0.085
R _w	0.055	0.070	0.062	0.108
S	1.96	0.75	1.45	2.98
(Δ/σ) _{max}	0.08	0.01	0.06	0.01
(Δ) _{max} (e/Å ³)	0.31(6)	0.27(5)	0.33(5)	0.30(5)
(Δ) _{min} (e/Å ³)	-0.39(6)	-0.23(5)	-0.25(5)	-0.27(5)

Table II. Positional Parameters and Equivalent Isotropic Thermal Factors for 2-[2-(N,N-dimethylamino)-5-nitrophenyl]-benzothiazole

Atom	x	y	z	B(Å ²) ^a
S1	0.51307(6)	0.42708(4)	0.73034(5)	4.71(1)
O1	1.0399(2)	0.6326(1)	1.2233(2)	6.52(4)
O2	0.8941(2)	0.5306(1)	1.2831(1)	6.33(4)
N2	0.9408(2)	0.5802(1)	1.2006(2)	4.60(4)
N3	0.6809(2)	0.5698(1)	0.6909(2)	4.16(4)
N1	0.5905(2)	0.3749(1)	0.9643(2)	4.01(4)
C2	0.7503(2)	0.5724(1)	0.8178(2)	3.74(4)
C1	0.7150(2)	0.5080(1)	0.9095(2)	3.23(4)
C6	0.7791(2)	0.5119(1)	1.0356(2)	3.48(4)
C5	0.8758(2)	0.5771(1)	1.0668(2)	3.69(4)
C4	0.9145(2)	0.6394(2)	0.9779(2)	4.95(5)
C3	0.8509(3)	0.6367(2)	0.8534(2)	5.36(5)
C14	0.5976(3)	0.6464(2)	0.6582(3)	10.68(9)
C15	0.7759(3)	0.5463(2)	0.5857(2)	6.68(7)
C7	0.6128(2)	0.4361(1)	0.8795(2)	3.30(4)
C9	0.4903(2)	0.3147(1)	0.9141(2)	3.91(4)
C10	0.4443(3)	0.2406(2)	0.9795(3)	5.48(6)
C11	0.3449(3)	0.1866(2)	0.9155(3)	6.27(6)
C12	0.2916(3)	0.2044(2)	0.7894(3)	5.73(6)
C13	0.3344(2)	0.2772(2)	0.7236(2)	5.09(5)
C8	0.4360(2)	0.3328(1)	0.7876(2)	4.01(4)
H6	0.759	0.470	1.091	1.57 ^{**}
H4	0.982	0.683	0.997	3.60
H3	0.866	0.679	0.796	4.20
H14a	0.523	0.632	0.587	7.41
H14b	0.546	0.665	0.739	7.50
H14c	0.663	0.694	0.627	7.50
H15a	0.718	0.535	0.508	4.14
H15b	0.821	0.599	0.571	7.98
H15c	0.832	0.493	0.613	10.58
H10	0.472	0.229	1.067	3.67
H11	0.309	0.139	0.962	4.53
H12	0.224	0.165	0.747	3.04
H13	0.291	0.294	0.636	3.41

^aAnisotropically refined atoms are given in the form of the isotropic equivalent displacement parameter defined as: $(4/3)[a^2B_{11} + b^2B_{22} + c^2B_{33} + ab(\cos \gamma)B_{12} + ac(\cos \beta)B_{13} + bc(\cos \alpha)B_{23}]$

^{**}Hydrogen atoms were refined isotropically.

Table III. Bond Distances (Å) and Bond Angles (°) for 2-[2-(N,N-dimethylamino)-5-nitrophenyl]-benzothiazole

Atom 1	Atom 2	Distance	Atom 1	Atom 2	Distance	Atom 1	Atom 2	Distance
S1	C7	1.751(2)	C1	C6	1.394(2)	C6	H6	0.873(3)
S1	C8	1.721(2)	C1	C7	1.474(3)	C4	H4	0.928(3)
O1	N2	1.228(2)	C6	C5	1.367(3)	C3	H3	0.884(3)
O2	N2	1.217(2)	C5	C4	1.369(4)	C14	H14a	1.000(2)
N2	C5	1.469(2)	C4	C3	1.378(3)	C14	H14b	1.001(2)
N3	C2	1.421(2)	C9	C10	1.391(3)	C14	H14c	0.999(3)
N3	C14	1.438(4)	C9	C8	1.393(3)	C15	H15a	0.951(3)
N3	C15	1.433(4)	C10	C11	1.378(4)	C15	H15b	0.927(2)
N1	C7	1.298(2)	C11	C12	1.386(4)	C15	H15c	1.002(4)
N1	C9	1.388(3)	C12	C13	1.367(3)	C10	H10	0.934(3)
C2	C1	1.403(3)	C13	C8	1.406(4)	C11	H11	0.935(2)
C2	C3	1.389(3)	C12	H12	0.956(3)	C13	H13	1.018(4)

Atom 1	Atom 2	Atom 3	Angle	Atom 1	Atom 2	Atom 3	Angle
C7	S1	C8	88.94(9)	C6	C5	C4	122.5(2)
O1	N2	O2	123.4(2)	C5	C4	C3	118.3(3)
O1	N2	C5	118.1(2)	C2	C3	C4	121.2(3)
O2	N2	C5	118.5(2)	S1	C7	N1	115.5(1)
C2	N3	C14	113.9(2)	S1	C7	C1	123.3(1)
C2	N3	C15	115.0(2)	N1	C7	C1	121.2(2)
C14	N3	C15	110.9(2)	N1	C9	C10	125.1(2)
C7	N1	C9	110.7(2)	N1	C9	C8	114.8(2)
N3	C2	C1	118.5(2)	C10	C9	C8	120.1(2)
N3	C2	C3	122.0(2)	C9	C10	C11	118.1(2)
C1	C2	C3	119.4(2)	C10	C11	C12	121.8(2)
C2	C1	C6	118.9(2)	C11	C12	C13	121.2(2)
C2	C1	C7	123.3(2)	C12	C13	C8	117.8(3)
C6	C1	C7	117.9(2)	S1	C8	C9	110.1(1)
C1	C6	C5	119.7(2)	S1	C8	C13	128.8(2)
N2	C5	C6	118.7(2)	C9	C8	C13	121.2(2)
N2	C5	C4	118.9(2)	C1	C6	H6	117.9(2)
C5	C6	H6	122.3(2)	C5	C4	H4	123.3(2)
C3	C4	H4	118.4(2)	C2	C3	H3	117.8(2)
C4	C3	H3	120.7(2)	N3	C14	H14a	108.8(2)
N3	C14	H14b	108.0(2)	N3	C14	H14c	111.6(2)
H14a	C14	H14b	109.5(2)	H14a	C14	H14c	109.5(2)
H14b	C14	H14c	109.5(2)	N3	C15	H15a	109.2(2)
N3	C15	H15b	100.0(2)	N3	C15	H15c	107.9(2)
H15a	C15	H15b	105.3(2)	H15a	C15	H15c	110.8(2)
H15b	C15	H15c	122.7(2)	C9	C10	H10	122.2(2)
C11	C10	H10	119.5(2)	C10	C11	H11	117.7(2)
C12	C11	H11	120.4(2)	C11	C12	H12	119.9(2)
C13	C12	H12	119.0(2)	C12	C13	H13	122.7(2)
C8	C13	H13	119.4(2)				

Table IV. Positional Parameters and Equivalent Isotropic Thermal Factors for 2-[2-(N-methylamino)-5-nitrophenyl]benzothiazole

Atom	x	y	z	B(Å ²) ^a
S1	0.50543(5)	0.11315(4)	0.3093(2)	2.89(1)
O1	1.0363(2)	0.3242(2)	-0.0363(7)	6.00(6)
O2	0.9035(2)	0.1869(2)	-0.0970(7)	5.83(6)
N2	0.9365(2)	0.2725(2)	0.0025(7)	3.88(5)
N3	0.6206(2)	0.4451(1)	0.6434(6)	3.18(5)
N1	0.4600(2)	0.2672(1)	0.5849(6)	2.79(4)
C2	0.6963(2)	0.4022(2)	0.4899(6)	2.46(5)
C1	0.6615(2)	0.3004(2)	0.3845(6)	2.39(5)
C6	0.7423(2)	0.2599(2)	0.2262(7)	2.71(5)
C5	0.8546(2)	0.3167(2)	0.1723(7)	2.76(5)
C4	0.8895(2)	0.4150(2)	0.2717(7)	3.10(5)
C3	0.8117(2)	0.4571(2)	0.4274(7)	3.02(5)
C14	0.6527(2)	0.5463(2)	0.7726(8)	3.61(6)
C7	0.5430(2)	0.2376(2)	0.4399(6)	2.40(5)
C9	0.3579(2)	0.1902(2)	0.5993(7)	2.64(5)
C10	0.2526(2)	0.1975(2)	0.7348(8)	3.46(6)
C11	0.1592(2)	0.1148(2)	0.7315(8)	3.80(6)
C12	0.1688(2)	0.0259(2)	0.5935(9)	3.89(6)
C13	0.2718(2)	0.0168(2)	0.4560(8)	3.30(6)
C8	0.3666(2)	0.1003(2)	0.4612(7)	2.63(5)
H6	0.722(2)	0.193(2)	0.151(6)	0.7(5)**
H4	0.969(2)	0.450(2)	0.230(7)	1.5(6)
H3	0.837(2)	0.526(2)	0.501(7)	0.7(5)
H1	0.550(2)	0.406(2)	0.674(7)	1.0(6)
H14c	0.712(3)	0.558(2)	0.959(8)	2.7(7)
H14a	0.591(3)	0.559(2)	0.879(8)	3.5(8)
H14b	0.680(2)	0.590(2)	0.595(8)	2.3(7)
H10	0.248(2)	0.256(2)	0.841(7)	1.0(5)
H11	0.086(2)	0.117(2)	0.828(8)	1.9(6)
H12	0.101(2)	-0.030(2)	0.588(8)	1.9(6)
H13	0.277(2)	-0.044(2)	0.347(7)	1.8(6)

^aAnisotropically refined atoms are given in the form of the isotropic equivalent displacement parameter defined as: $(4/3)[a^2B_{11} + b^2B_{22} + c^2B_{33} + ab(\cos \gamma)B_{12} + ac(\cos \beta)B_{13} + bc(\cos \alpha)B_{23}]$

**Hydrogen atoms were refined isotropically.

Table V. Bond Distances (Å) and Bond Angles (°) for 2-[2-(N-methylamino)-5-nitrophenyl]-benzothiazole

Atom 1	Atom 2	Distance	Atom 1	Atom 2	Distance	Atom 1	Atom 2	Distance
S1	C7	1.752(2)	C4	C3	1.369(4)	C5	C4	1.380(3)
S1	C8	1.728(2)	C4	H4	0.96(2)	C13	H13	0.96(3)
O1	N2	1.227(3)	C3	H3	0.97(2)	C6	H6	0.95(2)
O2	N2	1.215(4)	C14	H14c	0.99(3)	C13	C8	1.393(3)
N2	C5	1.450(4)	C14	H14a	0.90(3)	C6	C5	1.382(4)
N3	C2	1.353(3)	C14	H14b	0.95(3)	C12	H12	0.96(2)
N3	C14	1.449(3)	C9	C10	1.395(4)	C1	C7	1.470(3)
N3	H1	0.89(2)	C9	C8	1.397(4)	C12	C13	1.382(5)
N1	C7	1.303(3)	C10	C11	1.376(3)	C1	C6	1.390(4)
N1	C9	1.396(3)	C10	H10	0.93(3)	C11	H11	0.96(3)
C2	C1	1.430(4)	C11	C12	1.388(4)	C2	C3	1.410(3)

Atom 1	Atom 2	Atom 3	Angle	Atom 1	Atom 2	Atom 3	Angle
C7	S1	C8	89.3(1)	C5	C4	H4	118(2)
O1	N2	O2	123.1(3)	C3	C4	H4	123(2)
O1	N2	C5	118.0(2)	C2	C3	C4	121.5(2)
O2	N2	C5	119.0(3)	C2	C3	H3	120(1)
C2	N3	C14	123.5(2)	C4	C3	H3	119(1)
C2	N3	H1	116(2)	N3	C14	H14c	112(2)
C14	N3	H1	121(2)	N3	C14	H14a	109(2)
C7	N1	C9	111.0(2)	N3	C14	H14b	111(2)
N3	C2	C1	121.2(2)	H14c	C14	H14a	103(3)
N3	C2	C3	120.7(3)	H14c	C14	H14b	110(2)
C1	C2	C3	118.2(2)	H14a	C14	H14b	111(3)
C2	C1	C6	119.0(2)	S1	C7	N1	115.2(1)
C2	C1	C7	121.9(2)	S1	C7	C1	120.0(2)
C6	C1	C7	119.2(2)	N1	C7	C1	124.9(2)
C1	C6	C5	120.7(2)	N1	C9	C10	125.5(2)
C1	C6	H6	121(1)	N1	C9	C8	114.6(2)
C5	C6	H6	119(1)	C10	C9	C8	119.9(2)
N2	C5	C6	119.4(2)	C9	C10	C11	118.9(3)
N2	C5	C4	119.5(2)	C9	C10	H10	120(1)
C6	C5	C4	121.1(2)	C11	C10	H10	121(1)
C5	C4	C3	119.5(2)	C10	C11	C12	120.8(3)
C10	C11	H11	121(2)	C12	C13	H13	122(2)
C12	C11	H11	118(2)	C8	C13	H13	121(2)
C11	C12	C13	121.6(2)	S1	C8	C9	109.9(2)
C11	C12	H12	119(2)	S1	C8	C13	128.8(2)
C13	C12	H12	119(2)	C9	C8	C13	121.2(2)
C12	C13	C8	117.7(2)				

Table VI. Positional Parameters and Equivalent Isotropic Thermal Factors for 2-[2-(N,N-diethylamino)-5-nitrophenyl]benzothiazole

Atom	x	y	z	B(Å ²) ^a
S1	0.8974(1)	0.05716(3)	0.74746(5)	3.37(1)
O1	0.4498(3)	-0.2005(1)	0.2461(2)	5.69(6)
O2	0.5576(3)	-0.1149(1)	0.1852(2)	5.47(5)
N1	0.8086(3)	0.05875(9)	0.4919(2)	3.02(4)
N2	0.5325(3)	-0.1488(1)	0.2700(2)	3.81(5)
N3	0.8410(3)	-0.06865(9)	0.8046(2)	2.93(4)
C1	0.7522(3)	-0.0457(1)	0.5682(2)	2.63(4)
C2	0.7556(3)	-0.0888(1)	0.6700(2)	2.66(4)
C3	0.6767(4)	-0.1499(1)	0.6375(2)	3.68(5)
C4	0.5996(4)	-0.1694(1)	0.5068(2)	3.73(6)
C5	0.6062(3)	-0.1275(1)	0.4085(2)	3.11(5)
C6	0.6801(3)	-0.0670(1)	0.4362(2)	2.94(5)
C7	0.8152(3)	0.0212(1)	0.5905(2)	2.58(4)
C8	0.9268(3)	0.1283(1)	0.6734(2)	2.95(5)
C9	0.8707(3)	0.1199(1)	0.5360(2)	2.88(5)
C10	0.8808(4)	0.1712(1)	0.4556(2)	3.75(6)
C11	0.9480(4)	0.2292(1)	0.5139(3)	4.23(6)
C12	1.0082(4)	0.2367(1)	0.6513(3)	4.13(6)
C13	0.9967(4)	0.1869(1)	0.7322(3)	4.00(6)
C14	1.0506(4)	-0.0797(1)	0.8601(3)	3.74(6)
C15	1.1108(4)	-0.1479(2)	0.9058(3)	5.08(8)
C16	0.7420(4)	-0.0859(1)	0.8963(2)	3.68(5)
C17	0.5441(4)	-0.0558(2)	0.8563(3)	5.36(8)
H3	0.677	-0.178	0.707	5.3 ^{**}
H4	0.543	-0.210	0.485	5.3
H6	0.681	-0.039	0.366	4.2
H10	0.843	0.166	0.362	5.1
H11	0.955	0.265	0.460	5.7
H12	1.053	0.277	0.689	5.5
H13	1.039	0.192	0.826	5.5
H14a	1.083	-0.069	0.808	4.0
H14b	1.126	-0.051	0.945	4.0
H15a	1.044	-0.168	0.862	4.0
H15b	1.169	-0.134	0.918	4.0
H15c	1.044	-0.167	0.972	4.0
H16a	0.834	-0.068	0.999	4.0
H16b	0.709	-0.134	0.890	4.0
H17a	0.584	-0.034	0.861	4.0
H17b	0.462	-0.081	0.780	4.0
H17c	0.501	-0.066	0.944	4.0

^aAnisotropically refined atoms are given in the form of the isotropic equivalent displacement parameter defined as: $(4/3)[a^2B_{11} + b^2B_{22} + c^2B_{33} + ab(\cos \gamma)B_{12} + ac(\cos \beta)B_{13} + bc(\cos \alpha)B_{23}]$

^{**}Hydrogen atoms were refined isotropically.

Table VII. Bond Distances (Å) and Bond Angles (°) for 2-[2-(N,N-diethylamino)-5-nitrophenyl]benzothiazole

Atom 1	Atom 2	Distance	Atom 1	Atom 2	Distance	Atom 1	Atom 2	Distance
S1	C7	1.751(3)	C3	C4	1.381(3)	C12	H12	0.951(3)
S1	C8	1.733(2)	C3	H3	0.951(3)	C13	H13	0.951(3)
O1	N2	1.226(3)	C4	C5	1.382(4)	C14	C15	1.525(4)
O2	N2	1.216(3)	C4	H4	0.950(3)	C14	H14a	0.721(4)
N1	C7	1.304(3)	C5	C6	1.371(3)	C14	H14b	1.069(2)
N1	C9	1.387(3)	C6	H6	0.950(2)	C15	H15a	0.694(3)
N2	C5	1.466(3)	C8	C9	1.397(4)	C15	H15b	0.494(4)
N3	C2	1.426(3)	C8	C13	1.395(3)	C15	H15c	1.075(3)
N3	C14	1.490(3)	C9	C10	1.392(4)	C16	C17	1.526(5)
N3	C16	1.462(4)	C10	C11	1.379(4)	C16	H16a	1.140(2)
C1	C2	1.408(3)	C10	H10	0.950(2)	C16	H16b	1.031(3)
C1	C6	1.403(3)	C11	C12	1.393(4)	C17	H17a	0.544(3)
C1	C7	1.466(3)	C11	H11	0.950(3)	C17	H17b	0.994(3)
C2	C3	1.400(3)	C12	C13	1.375(5)	C17	H17c	1.115(3)

Atom 1	Atom 2	Atom 3	Angle	Atom 1	Atom 2	Atom 3	Angle
C7	S1	C8	89.2(2)	C1	C6	H6	120.1(2)
N3	C14	H14a	103.1(2)	N3	C14	H14b	115.4(2)
C7	N1	C9	111.2(2)	C5	C6	H6	120.0(3)
O1	N2	O2	123.5(2)	S1	C7	N1	115.1(2)
C15	C14	H14a	113.8(3)	C15	C14	H14b	103.6(2)
O1	N2	C5	117.8(2)	S1	C7	C1	123.7(2)
O2	N2	C5	118.7(2)	N1	C7	C1	121.3(2)
H14a	C14	H14b	105.8(3)	C14	C15	H15a	105.9(3)
C2	N3	C14	113.9(3)	S1	C8	C9	109.6(2)
C2	N3	C16	116.9(2)	S1	C8	C13	129.2(2)
C14	C15	H15b	72.0(4)	C14	C15	H15c	114.3(3)
C14	N3	C16	113.3(2)	C9	C8	C13	121.1(2)
C2	C1	C6	118.6(3)	N1	C9	C8	114.8(3)
H15a	C15	H15b	152.2(7)	H15a	C15	H15c	80.7(4)
C2	C1	C7	124.2(2)	N1	C9	C10	125.4(3)
C6	C1	C7	117.3(2)	C8	C9	C10	119.7(2)
H15b	C15	H15c	126.1(4)	N3	C16	C17	111.9(2)
N3	C2	C1	118.6(2)	C9	C10	C11	119.0(2)
N3	C2	C3	121.7(3)	C9	C10	H10	120.2(2)
N3	C16	H16a	106.8(2)	N3	C16	H16b	111.2(2)
C1	C2	C3	119.7(2)	C11	C10	H10	120.8(3)
C2	C3	C4	121.1(2)	C10	C11	C12	120.9(3)
C17	C16	H16a	109.9(2)	C17	C16	H16b	101.3(2)
C2	C3	H3	119.0(2)	C10	C11	H11	119.5(3)
C4	C3	H3	120.0(3)	C12	C11	H11	119.6(3)
H16a	C16	H16b	115.7(2)	C16	C17	H17a	83.1(3)
C3	C4	C5	118.3(2)	C11	C12	C13	120.9(2)

Table VII (continued)

<u>Atom 1</u>	<u>Atom 2</u>	<u>Atom 3</u>	<u>Angle</u>	<u>Atom 1</u>	<u>Atom 2</u>	<u>Atom 3</u>	<u>Angle</u>
C3	C4	H4	121.1(3)	C11	C12	H12	119.4(3)
C16	C17	H17b	106.1(3)	C16	C17	H17c	102.3(2)
C5	C4	H4	120.7(2)	C13	C12	H12	119.7(3)
N2	C5	C4	118.9(2)	C8	C13	C12	118.3(2)
H17a	C17	H17b	134.3(4)	H17a	C17	H17c	113.0(4)
N2	C5	C6	118.9(2)	C8	C13	H13	120.5(3)
C4	C5	C6	122.3(3)	C12	C13	H13	121.2(3)
H17b	C17	H17c	108.6(3)	N3	C14	C15	115.3(2)
C1	C6	C5	119.9(2)				

Table VIII. Positional Parameters and Equivalent Isotropic Thermal Factors for 2-(Trimethylsilyl-ethynyl)-4-nitro-N,N-dimethylaniline

Atom	x	y	z	B(Å ²) ^a
Si	0.87838(9)	0.0253(2)	0.3013(3)	6.47(4)
O1	0.6651(2)	0.5391(4)	-0.0576(6)	7.2(1)
O2	0.5645(2)	0.5119(4)	-0.1628(7)	7.6(1)
N1	0.6519(2)	-0.0613(4)	-0.0821(6)	4.9(1)
N4	0.6180(2)	0.4706(4)	-0.1064(6)	5.4(1)
C1	0.6450(2)	0.0688(5)	-0.0848(7)	3.9(1)
C2	0.6973(2)	0.1524(5)	-0.0226(6)	3.6(1)
C3	0.6872(2)	0.2834(5)	-0.0340(6)	3.8(1)
C4	0.6277(2)	0.3328(5)	-0.1008(7)	4.1(1)
C5	0.5755(3)	0.2529(5)	-0.1544(7)	4.6(1)
C6	0.5844(3)	0.1230(5)	-0.1444(7)	4.5(1)
C11	0.5934(3)	-0.1428(6)	-0.1179(9)	6.5(2)
C12	0.7140(3)	-0.1266(6)	-0.105(1)	6.4(2)
C21	0.7575(3)	0.1112(5)	0.0714(7)	4.1(1)
C22	0.8074(3)	0.0842(5)	0.1594(8)	5.1(1)
C23	0.8559(5)	0.009(1)	0.546(1)	13.1(3)
C24	0.9012(5)	-0.1239(9)	0.225(2)	23.5(4)
C25	0.9428(5)	0.139(1)	0.307(2)	18.7(4)
H3	0.724	0.344	0.006	5.0 ^{**}
H5	0.532	0.290	-0.199	5.0
H6	0.547	0.065	-0.181	5.0
H11b	0.558	-0.119	-0.023	5.0
H11c	0.606	-0.239	-0.101	5.0
H11a	0.574	-0.128	-0.254	5.0
H12b	0.730	-0.172	0.019	5.0
H12c	0.749	-0.059	-0.140	5.0
H12a	0.708	-0.194	-0.212	5.0
H23c	0.817	-0.055	0.554	5.0
H23a	0.896	-0.024	0.630	5.0
H23b	0.842	0.099	0.593	5.0
H24c	0.913	-0.115	0.085	5.0
H24a	0.942	-0.159	0.303	5.0
H24b	0.862	-0.187	0.234	5.0
H25c	0.967	0.137	0.182	5.0
H25b	0.922	0.230	0.326	5.0
H25a	0.976	0.119	0.419	5.0

^aAnisotropically refined atoms are given in the form of the isotropic equivalent displacement parameter defined as: $(4/3)[a^2B_{11} + b^2B_{22} + c^2B_{33} + ab(\cos \gamma)B_{12} + ac(\cos \beta)B_{13} + bc(\cos \alpha)B_{23}]$

^{**}Hydrogen atoms were refined isotropically.

Table IX. Bond Distances (Å) and Bond Angles (°) for 2-(Trimethylsilylethynyl)-4-nitro-N,N-dimethylaniline

Atom 1	Atom 2	Distance	Atom 1	Atom 2	Distance	Atom 1	Atom 2	Distance
Si	C22	1.819(6)	N4	C4	1.455(7)	N1	C12	1.447(7)
Si	C23	1.832(8)	C1	C2	1.426(7)	C21	C22	1.195(7)
Si	C24	1.72(2)	C1	C6	1.396(8)	N1	C11	1.471(7)
Si	C25	1.77(1)	C2	C3	1.387(7)	C5	C6	1.371(8)
O1	N4	1.227(6)	C2	C21	1.425(7)	N1	C1	1.368(7)
O2	N4	1.215(6)	C3	C4	1.373(7)	C4	C5	1.385(7)
C3	H3	1.000(7)	C5	H5	0.999(6)	C6	H6	1.000(7)
C11	H11b	1.04(1)	C11	H11c	1.041(7)	C11	H11a	1.039(6)
C12	H12b	1.040(6)	C12	H12c	1.040(8)	C12	H12a	1.040(7)
C23	H23c	1.040(7)	C23	H23a	1.039(7)	C23	H23b	1.041(6)
C24	H24c	1.039(6)	C24	H24a	1.039(6)	C24	H24b	1.040(6)
C25	H25c	1.039(6)	C25	H25b	1.041(6)	C25	H25a	1.039(6)

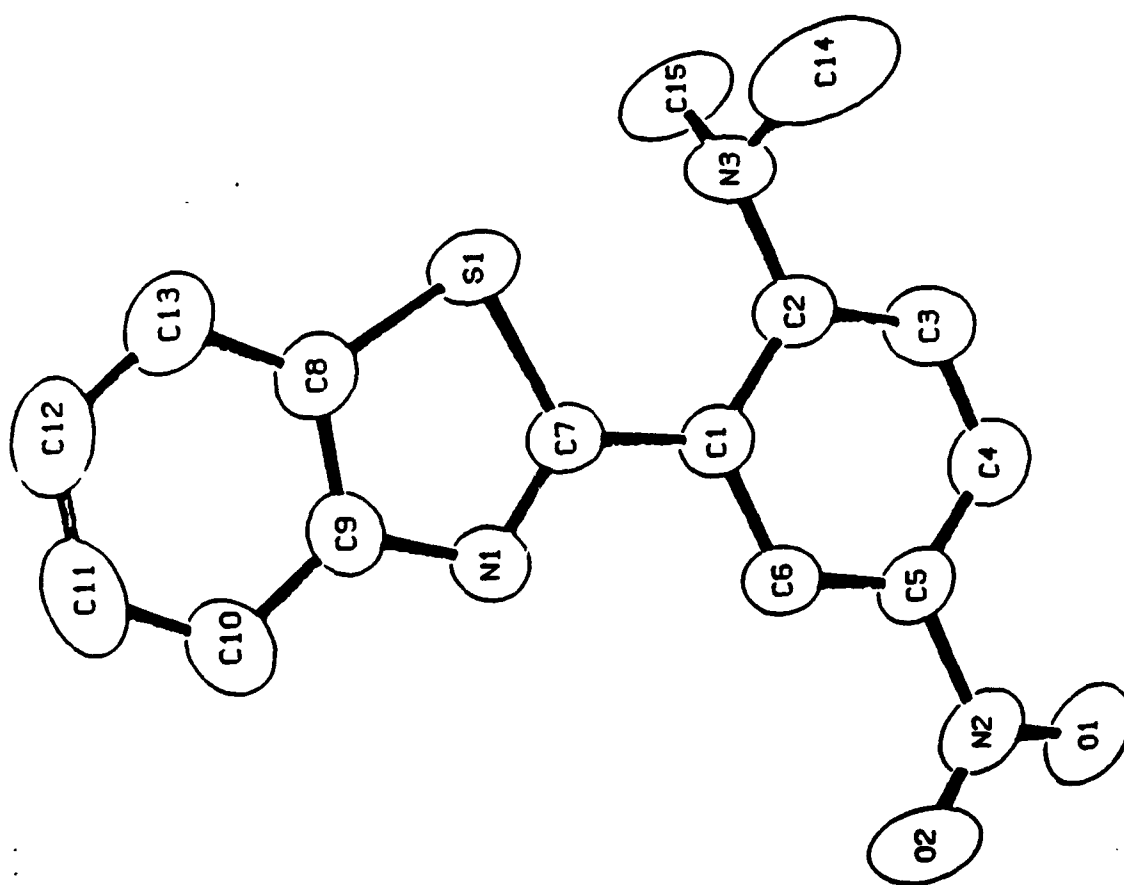
Atom 1	Atom 2	Atom 3	Angle	Atom 1	Atom 2	Atom 3	Angle
C22	Si	C23	109.4(4)	N1	C1	C6	119.7(5)
C22	Si	C24	110.4(4)	C2	C1	C6	118.1(5)
C22	Si	C25	110.1(4)	C1	C2	C3	118.9(4)
C23	Si	C24	107.5(5)	C1	C2	C21	124.2(4)
C23	Si	C25	105.2(5)	C3	C2	C21	116.5(4)
C24	Si	C25	114.1(5)	C2	C3	C4	121.0(4)
C1	N1	C11	119.6(4)	N4	C4	C3	119.7(4)
C1	N1	C12	123.8(4)	N4	C4	C5	119.4(4)
C11	N1	C12	113.8(4)	C3	C4	C5	120.8(5)
O1	N4	O2	123.4(5)	C4	C5	C6	119.1(5)
O1	N4	C4	118.0(4)	C1	C6	C5	122.0(5)
O2	N4	C4	118.6(4)	C2	C21	C22	175.0(5)
N1	C1	C2	122.1(4)	Si	C22	C21	173.0(6)
C2	C3	H3	120.0(4)	C4	C3	H3	119.0(4)
C4	C5	H5	119.7(4)	C6	C5	H5	121.2(4)
C1	C6	H6	119.0(4)	C5	C6	H6	119.1(5)
N1	C11	H11b	108.9(5)	N1	C11	H11c	110.0(4)
N1	C11	H11a	109.5(4)	H11b	C11	H11c	109.5(4)
H11b	C11	H11a	109.5(4)	H11c	C11	H11a	109.5(4)
N1	C12	H12b	110.3(5)	N1	C12	H12c	108.6(4)
N1	C12	H12a	109.5(4)	H12b	C12	H12c	109.5(5)
H12b	C12	H12a	109.3(4)	H12c	C12	H12a	109.5(4)
Si	C23	H23c	110.3(4)	Si	C23	H23a	110.6(4)
Si	C23	H23b	107.7(4)	H23c	C23	H23a	109.4(4)
H23c	C23	H23b	109.6(5)	H23a	C23	H23b	109.5(4)
Si	C24	H24c	107.6(4)	Si	C24	H24a	111.2(5)
Si	C24	H24b	109.6(4)	H24c	C24	H24a	109.5(4)
H24c	C24	H24b	109.5(5)	H24a	C24	H24b	109.4(4)
Si	C25	H25c	110.2(4)	Si	C25	H25b	108.6(4)
Si	C25	H25a	109.6(4)	H25c	C25	H25b	109.4(4)
H25c	C25	H25a	109.5(4)	H25b	C25	H25a	109.5(4)

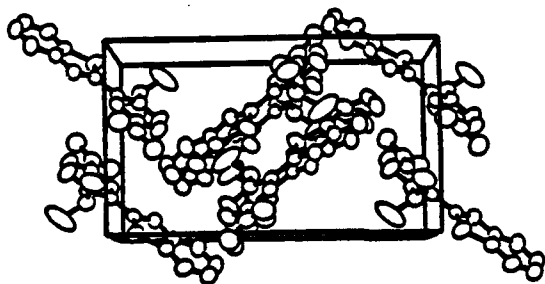
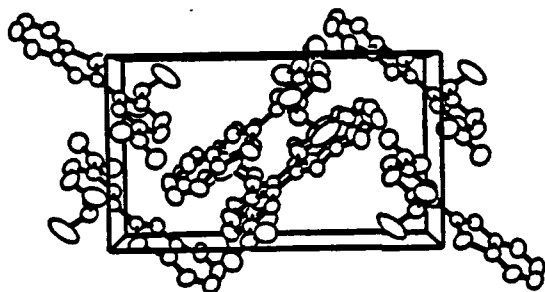
Table X. Summary of Close Interactions

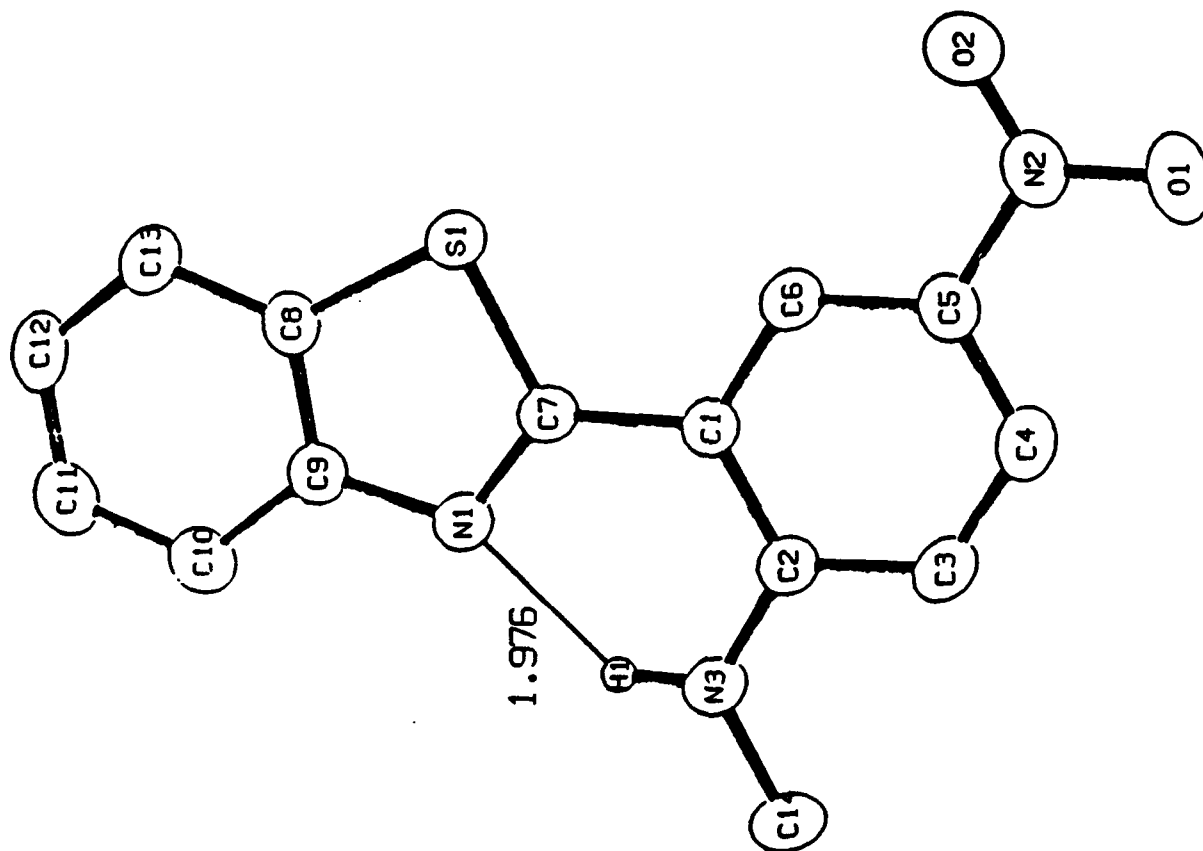
<u>Interaction</u>	<u>C...O</u>	<u>C-H...O</u>	<u>H...O</u>
<u>1</u>			
C10 - H10 ... O1	3.446 Å	150.47 °	2.601 Å
C15 - H15c ... O1	3.744 Å	160.22 °	2.785 Å
C15 - H15c ... O2	3.458 Å	133.12 °	2.694 Å
C15 - H15a ... O2	3.284 Å	111.09 °	2.818 Å
<u>2</u>			
C11 - H11 ... O2	3.542 Å	154.39 °	2.652 Å
C12 - H12 ... O2	3.419 Å	117.90 °	2.861 Å
C13 - H13 ... O2	3.316 Å	125.00 °	2.670 Å
C3 - H3 ... O1	3.535 Å	120.92 °	2.939 Å
C10 - H10 ... O1	3.633 Å	128.04 °	2.988 Å
<u>3</u>			
C11 - H11 ... O1	3.456 Å	143.48 °	2.641 Å
C15 - H15c ... O1	3.604 Å	147.61 °	2.765 Å
C17 - H17b ... O2	3.640 Å	158.55 °	2.739 Å
C15 - H15a ... O1	3.823 Å	117.90 °	3.284 Å
C15 - H15b ... O1	3.823 Å	106.03 °	3.450 Å
C17 - H17a ... O2	3.702 Å	143.51 °	2.895 Å
C15 - H15a ... O2	3.709 Å	137.40 °	2.935 Å
C11 - H11 ... O2	3.884 Å	171.38 °	2.935 Å
<u>4</u>			
C3 - H3 ... O2	3.446 Å	154.21 °	2.524 Å
C12 - H12b ... O1	3.646 Å	167.02 °	2.622 Å
C12 - H12b ... O2	3.670 Å	145.07 °	2.765 Å
C12 - H12a ... O2	3.596 Å	133.73 °	2.796 Å
C12 - H12c ... O1	3.685 Å	119.54 °	3.061 Å
C12 - H12c ... O2	4.128 Å	157.20 °	3.151 Å
C13 - H13c ... O1	3.445 Å	104.45 °	3.035 Å

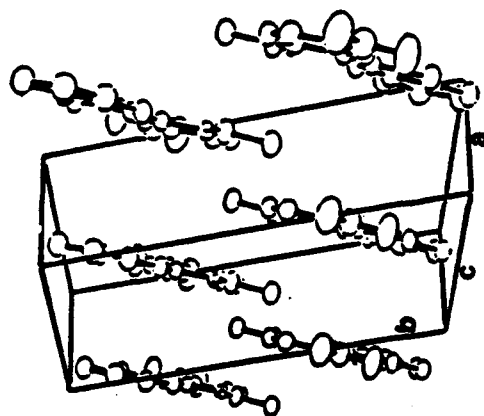
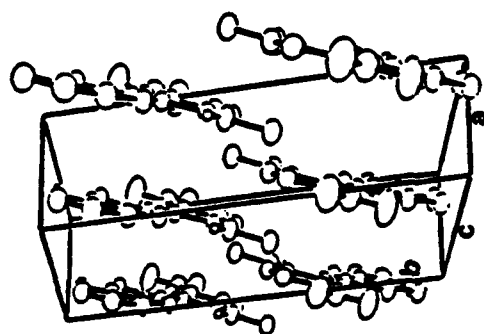
CAPTIONS FOR ILLUSTRATIONS

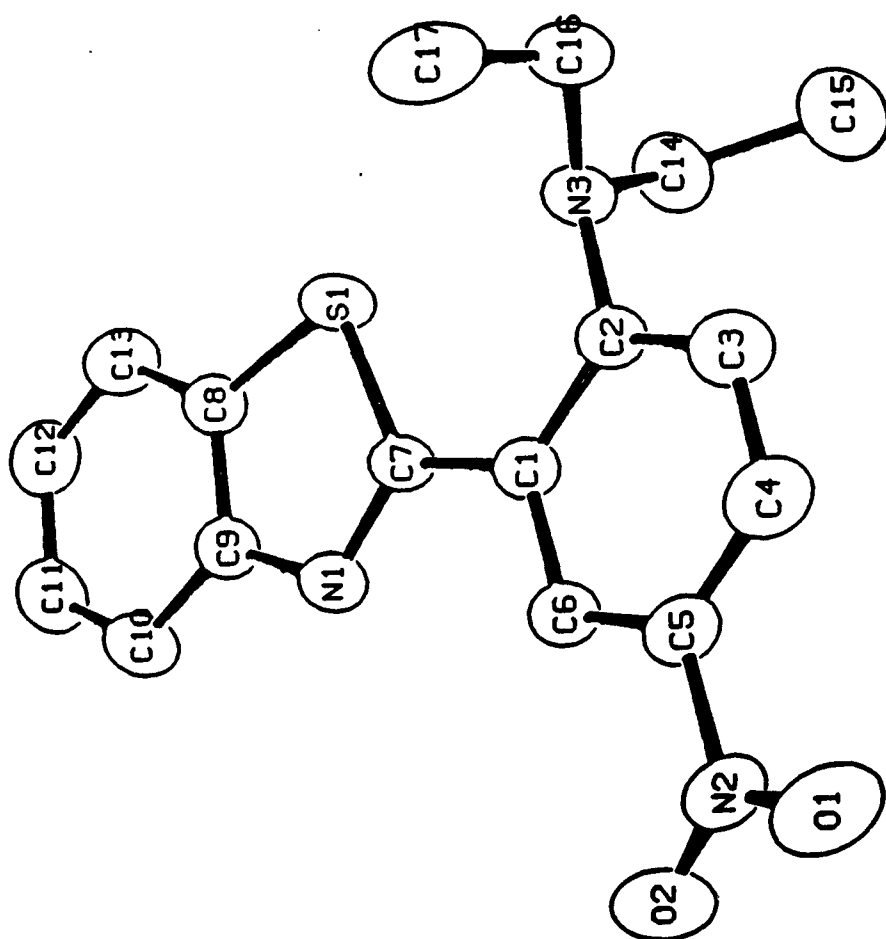
- Figure 1. Molecular structure of 2-[2-(N,N-Dimethylamino)-5-nitrophenyl]benzothiazole (1). Hydrogen atoms have been removed for clarity.
- Figure 2. Stereoview of the unit cell for 2-[2-(N,N-Dimethylamino)-5-nitrophenyl]benzothiazole (1) looking down the c axis.
- Figure 3. Molecular structure of 2-[2-(N-Methylamino)-5-nitrophenyl]benzothiazole (2). Hydrogen atoms have been omitted for clarity, except for the hydrogen atom involved in the internal hydrogen bond.
- Figure 4. Stereoview of the unit cell for 2-[2-(N-Methylamino)-5-nitrophenyl]benzothiazole (2) with the unit cell axes labeled.
- Figure 5. Molecular structure of 2-[2-(N,N-Diethylamino)-5-nitrophenyl]benzothiazole (3). Hydrogen atoms are removed for clarity.
- Figure 6. Stereoview of the unit cell for 2-[2-(N,N-Diethylamino)-5-nitrophenyl]benzothiazole (3) viewed down the c axis of the unit cell.
- Figure 7. Molecular structure of 2-(Trimethylsilylethynyl)-4-nitro-N,N-dimethylaniline (4). Hydrogen atoms are removed for clarity.
- Figure 8. Stereoview of the unit cell for 2-(Trimethylsilylethynyl)-4-nitro-N,N-dimethylaniline (4) looking down the b axis of the unit cell.
- Figure 9. Close (C)-H...O interactions for 2-[2-(N,N-Dimethylamino)-5-nitrophenyl]benzothiazole (1).
- Figure 10. Close (C)-H...O interactions for 2-[2-(N-Methylamino)-5-nitrophenyl]benzothiazole (2).
- Figure 11. Close (C)-H...O interactions for 2-[2-(N,N-Diethylamino)-5-nitrophenyl]benzothiazole (3).
- Figure 12. Close (C)-H...O interactions for 2-(Trimethylsilylethynyl)-4-nitro-N,N-dimethylaniline (4).

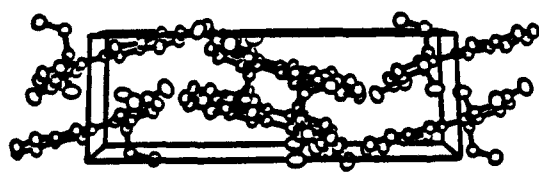
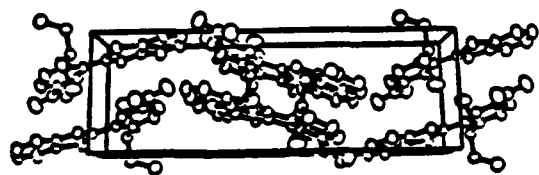


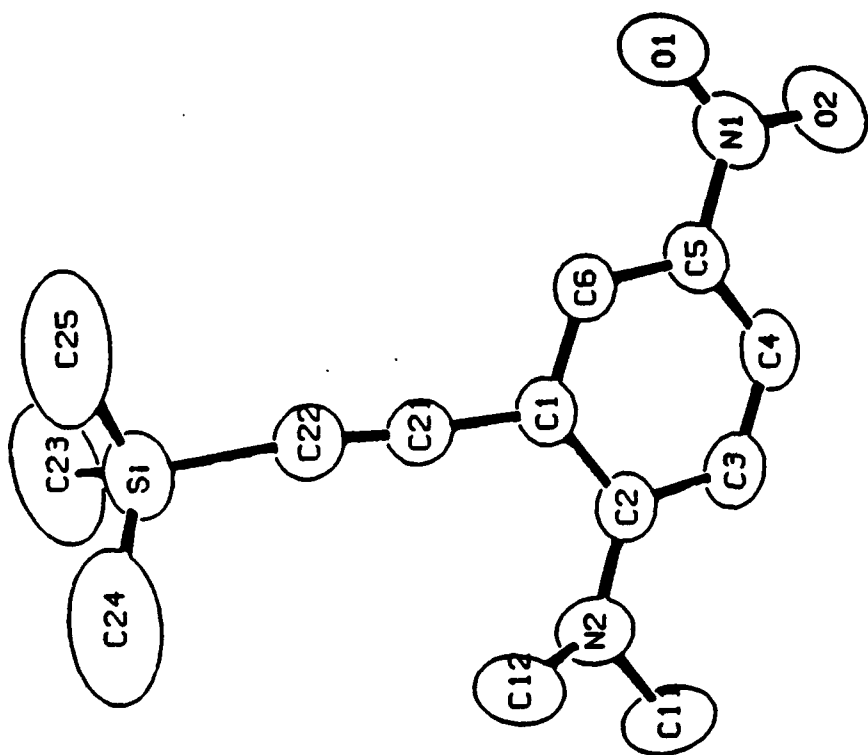


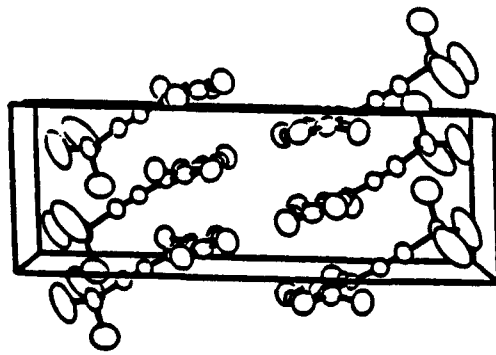
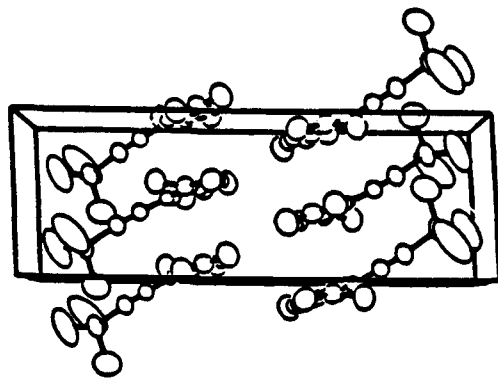


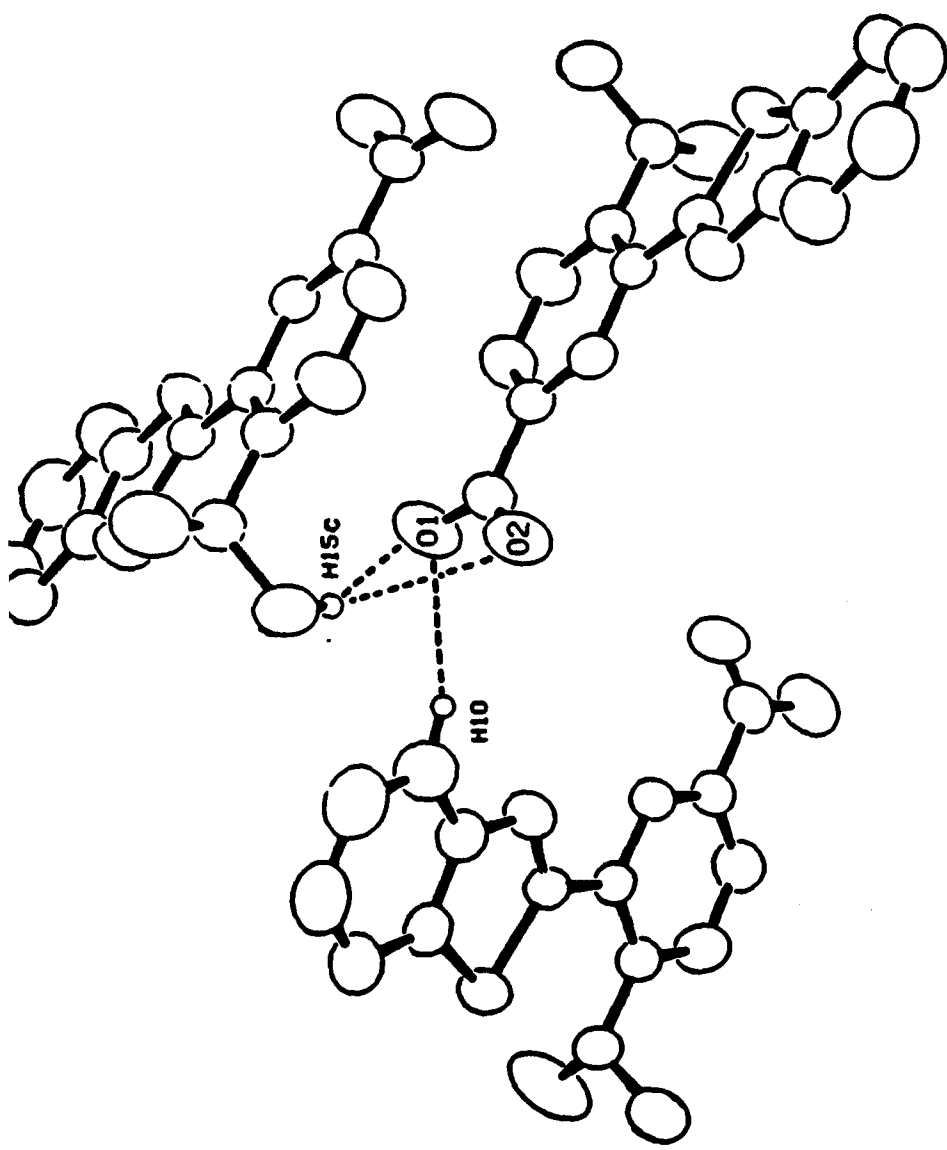








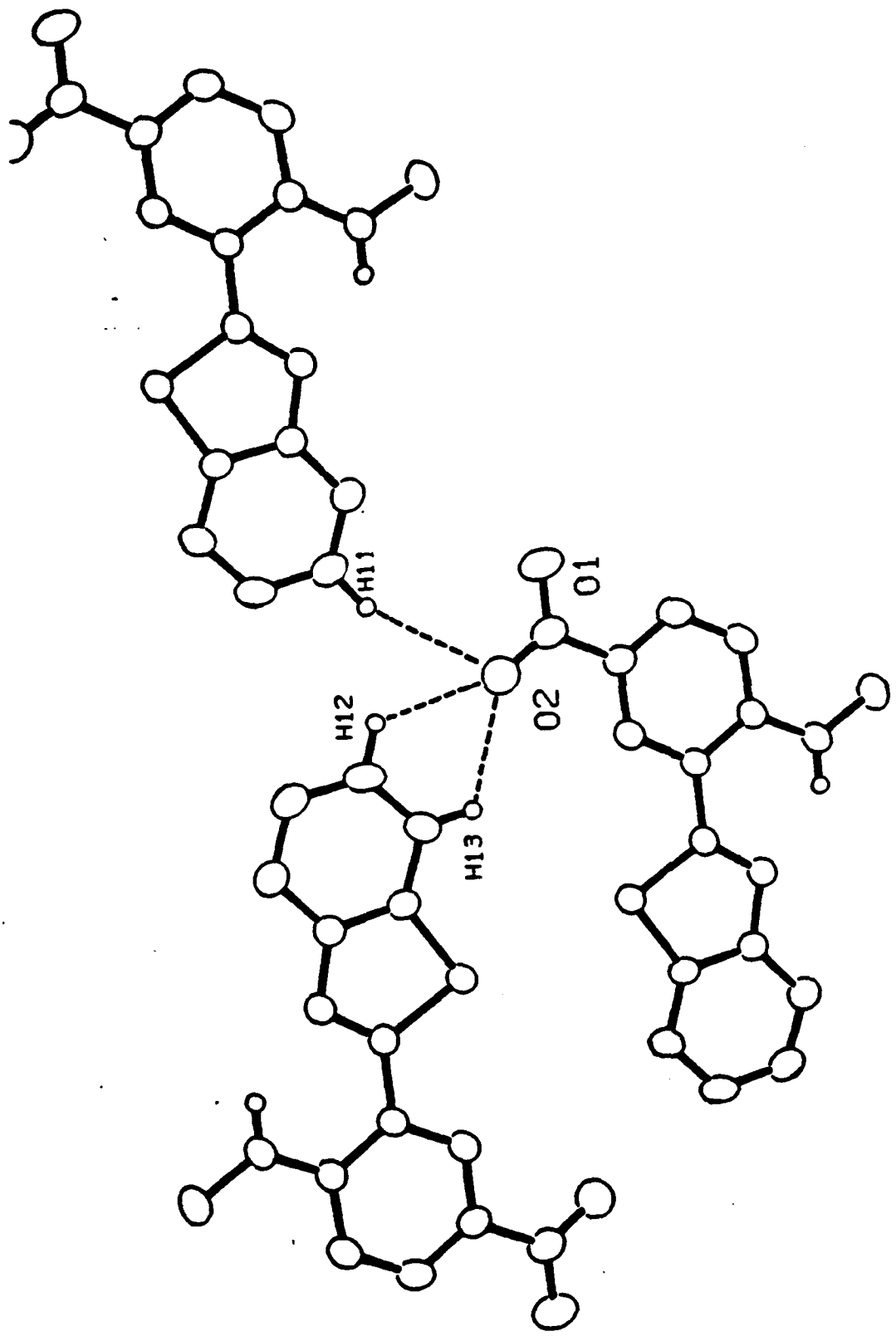




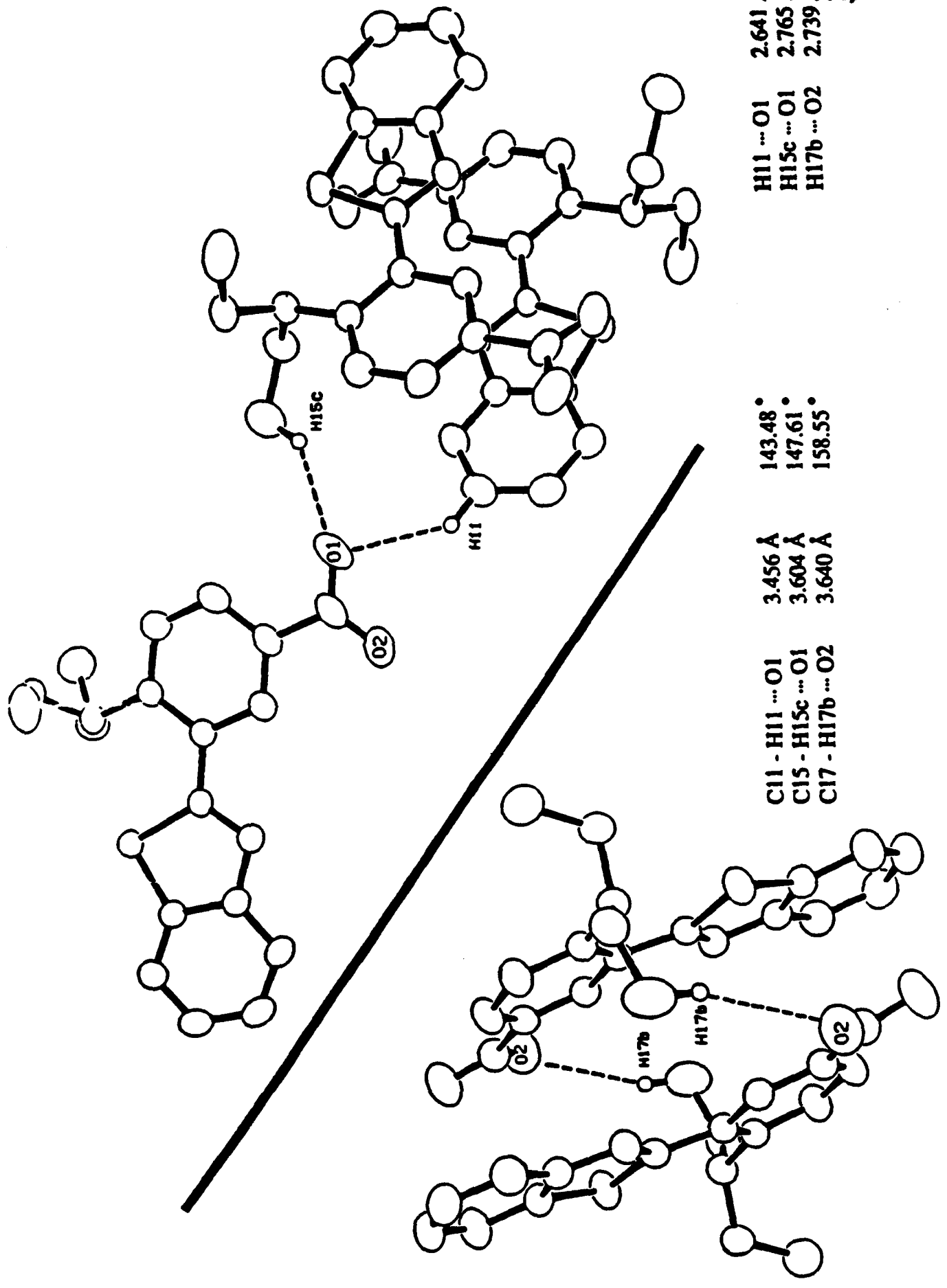
H10 ... O1 2.601 Å
 H15c ... O1 2.785 Å
 H15c ... O2 2.694 Å

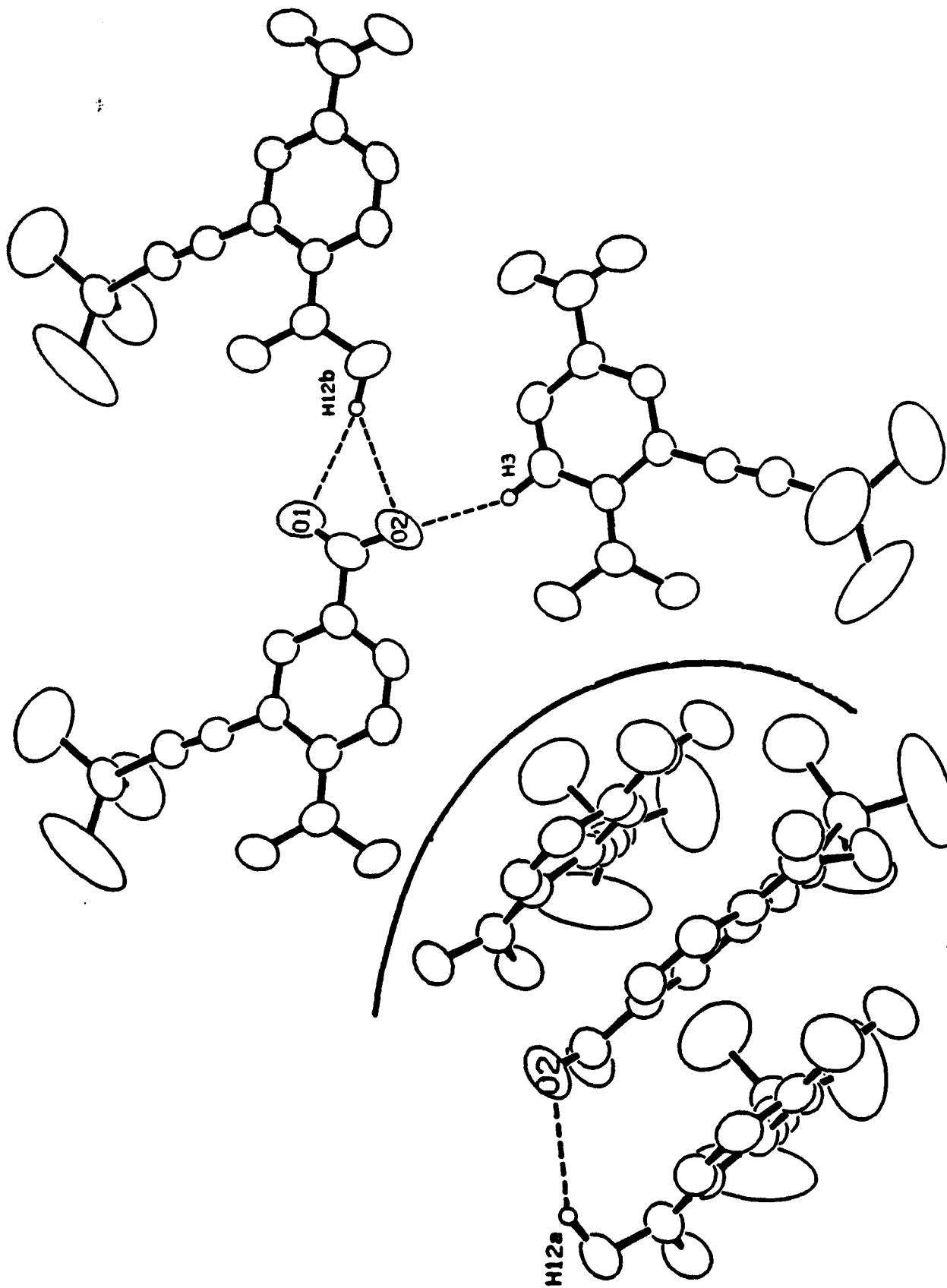
150.47°
 160.22°
 133.12°

C10 - H10 ... O1 3.446 Å
 C15 - H15c ... O1 3.744 Å
 C15 - H15c ... O2 3.458 Å



C11 - H11 ... O2	3.542 Å	154.39°	H11 ... O2	2.652 Å
C12 - H12 ... O2	3.419 Å	117.90°	H12 ... O2	2.861 Å
C13 - H13 ... O2	3.316 Å	125.00°	H13 ... O2	2.670 Å





H3 ... O2 2.524 Å
 H12b ... O1 2.622 Å
 H12b ... O2 2.765 Å
 H12a ... O2 2.796 Å

154.21°
 167.02°
 145.07°
 133.73°

3.446 Å
 3.646 Å
 3.670 Å
 3.596 Å

C3 - H3 ... O2
 C12 - H12b ... O1
 C12 - H12b ... O2
 C12 - H12a ... O2

Appendix A. General Displacement Parameter Expressions, U's, for
2-[2-(N,N-dimethylamino)-5-nitrophenyl]-benzothiazole

Name	U(1,1)	U(2,2)	U(3,3)	U(1,2)	U(1,3)	U(2,3)
S1	0.0615(3)	0.0758(4)	0.0411(2)	-0.0176(3)	-0.0079(2)	0.0061(3)
O1	0.087(1)	0.085(1)	0.074(1)	-0.0086(9)	-0.0241(8)	-0.0242(9)
O2	0.084(1)	0.112(1)	0.0440(8)	-0.004(1)	-0.0106(8)	0.0050(9)
N2	0.0543(9)	0.070(1)	0.0501(9)	0.0104(9)	-0.0072(8)	-0.0177(9)
N3	0.0526(9)	0.067(1)	0.0382(8)	-0.0045(9)	0.0000(7)	0.0099(8)
N1	0.0564(9)	0.0470(9)	0.0488(9)	0.0012(8)	-0.0068(8)	0.0043(8)
C2	0.0455(9)	0.058(1)	0.0389(9)	-0.001(1)	0.0031(8)	0.0015(9)
C1	0.0385(9)	0.046(1)	0.0377(8)	0.0041(8)	0.0032(7)	-0.0027(8)
C6	0.0454(9)	0.049(1)	0.0379(8)	0.0068(9)	0.0023(8)	0.0006(9)
C5	0.0443(9)	0.055(1)	0.0408(9)	0.0069(9)	-0.0004(8)	-0.0103(9)
C4	0.063(1)	0.065(1)	0.061(1)	-0.018(1)	-0.004(1)	-0.005(1)
C3	0.074(1)	0.076(1)	0.054(1)	-0.027(1)	-0.002(1)	0.012(1)
C14	0.137(2)	0.181(3)	0.086(2)	0.102(2)	-0.042(2)	-0.036(2)
C15	0.079(2)	0.125(2)	0.050(1)	0.022(2)	-0.007(1)	-0.019(1)
C7	0.0428(9)	0.046(1)	0.0363(8)	0.0050(9)	0.0013(7)	-0.0001(8)
C9	0.052(1)	0.042(1)	0.055(1)	0.003(1)	0.0033(9)	-0.0007(9)
C10	0.080(2)	0.053(1)	0.075(1)	-0.002(1)	-0.002(1)	0.009(1)
C11	0.081(2)	0.049(1)	0.108(2)	-0.010(1)	0.012(1)	0.003(1)
C12	0.063(1)	0.061(1)	0.094(2)	-0.009(1)	0.005(1)	-0.020(1)
C13	0.056(1)	0.072(1)	0.066(1)	-0.009(1)	0.001(1)	-0.014(1)
C8	0.046(1)	0.056(1)	0.050(1)	-0.001(1)	0.0050(9)	-0.007(1)

The form of the anisotropic displacement parameter is:

$$\exp[-2p^2\{h^2a^2U_{1,1} + k^2b^2U_{2,2} + l^2c^2U_{3,3} + 2hkabU_{1,2} + 2hlacU_{1,3} + 2klbcU_{2,3}\}]$$

where a, b, and c are reciprocal lattice constants.

Appendix B. General Displacement Parameter Expressions, U's, for
2-[2-(N-methylamino)-5-nitrophenyl]benzothiazole

Name	U(1,1)	U(2,2)	U(3,3)	U(1,2)	U(1,3)	U(2,3)
S1	0.0301(2)	0.0273(2)	0.0509(3)	0.0064(2)	0.0051(2)	-0.0048(2)
O1	0.036(1)	0.065(1)	0.119(2)	0.0032(9)	0.029(1)	-0.013(1)
O2	0.050(1)	0.049(1)	0.120(2)	0.0113(8)	0.023(1)	-0.024(1)
N2	0.034(1)	0.047(1)	0.065(2)	0.0095(9)	0.013(1)	-0.002(1)
N3	0.036(1)	0.0270(9)	0.057(1)	0.0072(7)	0.003(1)	-0.0068(9)
N1	0.0305(9)	0.0273(9)	0.047(1)	0.0069(7)	0.0052(9)	-0.0012(9)
C2	0.032(1)	0.028(1)	0.033(1)	0.0080(8)	-0.000(1)	0.001(1)
C1	0.028(1)	0.026(1)	0.036(1)	0.0057(8)	-0.000(1)	0.000(1)
C6	0.033(1)	0.027(1)	0.041(1)	0.0065(8)	0.001(1)	-0.000(1)
C5	0.029(1)	0.037(1)	0.039(1)	0.0088(9)	0.003(1)	0.001(1)
C4	0.031(1)	0.038(1)	0.044(2)	0.002(1)	0.002(1)	0.001(1)
C3	0.037(1)	0.028(1)	0.046(2)	0.0037(9)	-0.000(1)	-0.000(1)
C14	0.051(1)	0.031(1)	0.056(2)	0.014(1)	0.003(1)	-0.007(1)
C7	0.031(1)	0.0263(9)	0.033(1)	0.0080(8)	0.000(1)	-0.0000(9)
C9	0.029(1)	0.031(1)	0.040(1)	0.0080(8)	0.002(1)	0.001(1)
C10	0.036(1)	0.042(1)	0.055(2)	0.0133(9)	0.008(1)	-0.001(1)
C11	0.032(1)	0.051(1)	0.062(2)	0.012(1)	0.008(1)	0.000(1)
C12	0.028(1)	0.044(1)	0.069(2)	-0.001(1)	-0.000(1)	0.003(1)
C13	0.034(1)	0.032(1)	0.056(2)	0.002(1)	0.000(1)	-0.001(1)
C8	0.026(1)	0.033(1)	0.041(1)	0.0066(8)	0.003(1)	0.001(1)

The form of the anisotropic displacement parameter is:

$$\exp[-2p^2(h^2a^2U_{1,1} + k^2b^2U_{2,2} + l^2c^2U_{3,3} + 2hkabU_{1,2} + 2hlacU_{1,3} + 2klbcU_{2,3})]$$

where a,b, and c are reciprocal lattice constants.

Appendix C. General Displacement Parameter Expressions, U's, for
2-[2-(N,N-diethylamino)-5-nitrophenyl]benzothiazole

Name	U(1,1)	U(2,2)	U(3,3)	U(1,2)	U(1,3)	U(2,3)
S1	0.0620(3)	0.0360(3)	0.0268(2)	-0.0075(3)	0.0112(2)	-0.0007(2)
O1	0.092(1)	0.062(1)	0.055(1)	-0.019(1)	0.016(1)	-0.0273(9)
O2	0.098(1)	0.068(1)	0.0355(8)	0.003(1)	0.0153(9)	-0.0068(9)
N1	0.046(1)	0.037(1)	0.0302(7)	-0.0004(8)	0.0101(7)	0.0010(8)
N2	0.052(1)	0.049(1)	0.0384(9)	0.004(1)	0.0084(8)	-0.0147(9)
N3	0.0412(9)	0.040(1)	0.0271(7)	-0.0012(8)	0.0074(7)	0.0017(7)
C1	0.036(1)	0.034(1)	0.0293(8)	0.0006(9)	0.0093(7)	-0.0008(8)
C2	0.036(1)	0.035(1)	0.0290(8)	-0.0010(9)	0.0096(7)	-0.0015(8)
C3	0.059(1)	0.040(1)	0.042(1)	-0.009(1)	0.0182(9)	-0.003(1)
C4	0.054(1)	0.042(1)	0.046(1)	-0.012(1)	0.017(1)	-0.011(1)
C5	0.038(1)	0.043(1)	0.0323(9)	0.002(1)	0.0058(8)	-0.0096(9)
C6	0.040(1)	0.038(1)	0.0312(9)	0.0015(9)	0.0086(8)	-0.0025(8)
C7	0.035(1)	0.036(1)	0.0253(8)	0.0007(9)	0.0080(7)	0.0003(8)
C8	0.044(1)	0.034(1)	0.0345(9)	-0.0004(9)	0.0138(8)	0.0011(9)
C9	0.038(1)	0.037(1)	0.0345(9)	0.0017(9)	0.0124(8)	0.0018(9)
C10	0.058(1)	0.046(1)	0.040(1)	-0.002(1)	0.0187(9)	0.009(1)
C11	0.066(1)	0.042(1)	0.059(1)	0.000(1)	0.029(1)	0.012(1)
C12	0.064(1)	0.036(1)	0.063(1)	-0.007(1)	0.030(1)	-0.002(1)
C13	0.070(1)	0.041(1)	0.044(1)	-0.008(1)	0.023(1)	-0.004(1)
C14	0.041(1)	0.047(1)	0.045(1)	-0.000(1)	0.004(1)	0.003(1)
C15	0.063(2)	0.060(2)	0.064(2)	0.004(1)	0.014(1)	0.011(1)
C16	0.057(1)	0.051(1)	0.0314(9)	-0.003(1)	0.0140(9)	0.002(1)
C17	0.054(1)	0.104(3)	0.050(1)	-0.001(2)	0.024(1)	-0.004(2)

The form of the anisotropic displacement parameter is:

$$\exp[-2\pi^2(h^2a^2U_{1,1} + k^2b^2U_{2,2} + l^2c^2U_{3,3} + 2hkaU_{1,2} + 2hlaU_{1,3} + 2klbU_{2,3})]$$

where a, b, and c are reciprocal lattice constants.

Appendix D. General Displacement Parameter Expressions, U's, for
2-(Trimethylsilylethynyl)-4-nitro-N,N-dimethylaniline

Name	U(1,1)	U(2,2)	U(3,3)	U(1,2)	U(1,3)	U(2,3)
Si	0.0575(9)	0.084(1)	0.102(1)	0.0159(9)	-0.0179(9)	0.004(1)
O1	0.101(3)	0.057(2)	0.113(3)	0.005(2)	-0.006(3)	-0.002(2)
O2	0.094(3)	0.076(3)	0.119(3)	0.036(2)	-0.011(3)	0.009(2)
N1	0.065(3)	0.054(3)	0.066(3)	-0.007(2)	0.007(2)	-0.003(2)
N4	0.079(3)	0.064(3)	0.062(3)	0.016(2)	0.004(3)	0.004(2)
C1	0.050(3)	0.057(3)	0.040(3)	-0.003(2)	0.001(2)	0.004(2)
C2	0.043(3)	0.054(3)	0.040(3)	0.001(2)	0.004(2)	0.005(2)
C3	0.053(3)	0.052(3)	0.041(3)	-0.001(2)	0.001(2)	0.002(2)
C4	0.055(3)	0.056(3)	0.043(3)	0.009(3)	0.006(2)	0.004(2)
C5	0.051(3)	0.076(4)	0.048(3)	0.013(3)	-0.005(2)	0.002(3)
C6	0.050(3)	0.069(3)	0.051(3)	-0.004(3)	-0.005(2)	-0.001(3)
C11	0.088(4)	0.062(4)	0.096(5)	-0.024(3)	0.012(4)	-0.011(3)
C12	0.077(4)	0.055(4)	0.111(5)	0.010(3)	0.003(4)	-0.012(3)
C21	0.051(3)	0.050(3)	0.055(3)	-0.002(2)	0.000(2)	-0.002(2)
C22	0.055(3)	0.065(3)	0.071(4)	0.005(3)	-0.005(3)	-0.007(3)
C23	0.161(8)	0.22(1)	0.119(7)	0.064(7)	-0.008(6)	0.045(6)
C24	0.285(8)	0.289(9)	0.30(1)	0.220(6)	-0.182(7)	-0.163(8)
C25	0.136(8)	0.26(1)	0.30(1)	-0.059(8)	-0.111(7)	0.128(9)

The form of the anisotropic displacement parameter is:

$$\exp[-2p^2\{h^2a^2U_{1,1} + k^2b^2U_{2,2} + l^2c^2U_{3,3} + 2hkabU_{1,2} + 2hlacU_{1,3} + 2klbcU_{2,3}\}]$$

where a,b, and c are reciprocal lattice constants.

Hyperpolarizabilities of Polythiophene and Poly-p-phenylene Oligomers

Henry A. Kurtz,

**Department of Chemistry
Memphis State University
Memphis, TN 38152**

Jorge A. Medrano,

**Department of Chemistry
University of Dayton
Dayton, OH 45469**

and Douglas Dudis

**AFWAL/MLBP
Wright-Patterson Air Force Base
Ohio 45433**

ABSTRACT

Semiempirical AM1 calculations are presented for the second hyperpolarizabilities, γ , of poly-p-phenylene and polythiophene oligomers. Calculated results are compared with experimental degenerate four wave mixing results and static field estimates from these experimental results. The relative calculated values are shown to agree quite well with the experimental values when the latter are corrected for dispersion effects.

Introduction

Many recent studies of non-linear optical properties have shown that systems with electrons capable of delocalization over a large distance, such as polyacetylenes and polyphenylenes, exhibit large second hyperpolarizabilities (γ) (also referred to as third-order hyperpolarizabilities or third-order microscopic optical nonlinearities).¹ The question arises as to what is the dependence of γ on chain length, or the number of repeat units, in an oligomeric series. The purpose of this paper is to compare experimental and calculated results for poly-*p*-phenylene and all trans polythiophene oligomers of various lengths. This comparison is usually complicated by the fact that most measurements are made at laser frequencies (i.e. dynamic or time-dependent fields), while calculations using the finite field (FF) approximation can only predict static (time independent) hyperpolarizabilities. If this fact is allowed for however, the applicability of semiempirical based FF calculations in providing fast, accurate estimates of static hyperpolarizabilities will be demonstrated.

An FF method has been implemented in the MOPAC program² and is used in this work to calculate the hyperpolarizabilities. This method is based on the following expressions for the energy and dipole moment of a molecule interacting with an electric field

$$E(F) = E(0) - \mu_i^0 F_i - (1/2!) \alpha_{ij} F_i F_j - (1/3!) \beta_{ijk} F_i F_j F_k - (1/4!) \gamma_{ijkl} F_i F_j F_k F_l - \dots \quad (1)$$

$$\mu_i = \mu_i^0 + \alpha_{ij} F_j + (1/2) \beta_{ijk} F_j F_k + (1/6) \gamma_{ijkl} F_j F_k F_l + \dots \quad (2)$$

where the Einstein convention of summed repeated indices has been used, μ^0 is the permanent dipole moment and α_{ij} , β_{ijk} , and γ_{ijkl} are tensor elements of the linear polarizability and the first and second hyperpolarizabilities, respectively, of the molecule.³ The details of the FF method and its implementation in the MOPAC program have been given elsewhere.⁴

Poly-p-phenylene Oligomers

The orientational average of the γ tensor, which is defined in terms of its components as

$$\langle \gamma \rangle = (1/5) \{ \gamma_{xxxx} + \gamma_{yyyy} + \gamma_{zzzz} + 2(\gamma_{xyxy} + \gamma_{xozz} + \gamma_{yyzz}) \}. \quad (3)$$

was calculated for the planar conformation of poly-p-phenylene oligomers, $H(C_6H_4)_nH$. The shorter oligomers might depart somewhat from planarity in the gas phase, but the present approach is considered to be adequate to compare our calculations against experimental values obtained in solution.

Table 1 shows the calculated results for $\langle \gamma \rangle$ using an AM1 hamiltonian⁵ and the experimental results by Zhao *et al.*¹ (labeled Exp). The experimental technique used was degenerate four wave mixing (DFWM), which yields $\gamma(\omega; \omega, \omega, \omega)$. It is well known that frequency dispersion effects can greatly influence the $\langle \gamma \rangle$ values, rendering it larger than the static limit. This is also complicated by the fact that different experiments have different dispersion effects. For example, the dc electric field induced second-harmonic (EFISH) generation technique gives $\gamma(-2\omega; \omega, \omega, 0)$. Zhao *et al.*¹ have estimated the effect of dispersion in DFWM, under the assumption that most of the nonlinearity of a delocalized π cloud comes from the lowest excited state, by the formula

$$\gamma(0) = [(\omega_0^2 - \omega^2)^4 / \omega_0^8] \gamma(\omega) \quad (4)$$

where $\gamma(0)$ and $\gamma(\omega)$ are the static and frequency dependent values, respectively. Also $\omega_0 = 2\pi c / \lambda_{max}$ and $\omega = 2\pi c / \lambda$ with c the velocity of light and λ the wavelength at which the DFWM experiment was performed. The experimental results were thus corrected using eq. 4 and the results are also shown in Table 1 in the column labeled Exp-corr. It can be seen that the agreement between the estimated static experimental values and the calculated AM1 values is now very reasonable, given the approximations involved. The experimental values listed for $n=5$ are

with oxydecyl groups ($\text{OC}_{10}\text{H}_{21}$) para-disubstituted to one another on the central ring. These groups are necessary for solubility but also make comparisons with this data unreliable. The values of γ could be modified by either geometrical changes in the oligomer or shifts in the absorption spectrum. The UV spectra of Zhao et al.¹ indicate that λ_{max} for $n=5$ does not fall along the curve generated by $n=1$ to 4. Both of these effects could be quite substantial.

Equation 4 probably overestimates somewhat the correction due to the dispersion effect due to the approximations involved; namely the inclusion of only one excited state in the treatment.¹ It can be seen in Figure 1 however, that there is indeed an improvement of the agreement between calculated and experimental values after including the eq. 4 correction for dispersion.

The largest discrepancy is observed for benzene itself. However, $\langle \gamma \rangle$ reported from an EFISH measurement on benzene ($\lambda = 1.05 \mu\text{m}$) is 14.04×10^{-36} esu⁶. Without any correction this result comes closer to our calculated value, indicating the difference in experimental dispersion effects mentioned above. In any case, our predicted value for benzene is undoubtedly below the experimental results from whatever source. Our calculated components of the γ tensor can be compared with those reported by Perrin et al.⁷, obtained using *ab initio* methods at both the SCF level and including correlation in the MP2 approximation. With a 4-31G basis augmented on carbon with a diffuse p and d function of exponent 0.05, the $\langle \gamma \rangle$ value is 7.68×10^{-36} esu at the SCF level and 10.25×10^{-36} esu at the MP2 level. The most important conclusion is that their γ_{zzzz} value (perpendicular to the rings) is about 89% of the γ_{xxxx} value (along the oligomer axis), while the semiempirical results give only 1.2% for the same ratio. A similar underestimation of the same γ_{zzzz} component has been observed for polyacetylene oligomers.⁸ One reason for that must lie in the lack of flexibility of the small basis set implicit in these semi-empirical calculations, causing them to strongly underestimate the component of the γ tensor associated with the direction perpendicular to the ring. However, as the length of the chain grows, γ_{xxxx} grows faster than γ_{zzzz} and eventually dominates the value of $\langle \gamma \rangle$ lessening the significance of the discrepancy.

Polythiophene Oligomers

Experimental data are also available for the thiophene oligomers.¹ Here again the disagreement between calculated and experimental values increases rapidly with the number of repeat units, as was pointed out by Goldfarb *et al.*⁹ The differences here are even more pronounced than in the previous *p*-phenylene case and the values of γ are larger. There are several possible conformations for thiophene oligomers and, for reasons discussed in detail by Goldfarb *et al.*⁹, calculations in this work are restricted to the "all trans" form in which the intra-unit S-C-C-S dihedral angle is 180.0. Table 2 shows the AM1 calculated values¹⁰, the experimental DFWM results¹ and experimental-corrected values using equation 4. The experimental-corrected estimate of the static hyperpolarizability again shows a greatly improved agreement with the semiempirical results. Also the growth as a function of *n* no longer has the essentially exponential growth of the experimental $\langle \gamma(\omega) \rangle$ values, as can be clearly seen in Figure 2. The remaining discrepancy can probably be explained in a similar manner to the *p*-phenylene oligomers case, and can thus not be corrected within this approach, without increasing the basis size.

Conclusions

The results of this study indicate that the semiempirical calculation of second hyperpolarizabilities developed within the MOPAC program is indeed capable of obtaining reasonable estimates for these systems. Even more importantly, this study demonstrates the importance of accounting for frequency dependence in calculating hyperpolarizabilities. These effects are shown to be very large in some cases and are almost certainly larger than correlation errors in the calculated static values. It should be born in mind that our semiempirical calculations are about four orders of magnitude faster than *ab initio* calculations with medium-sized basis sets and incorporating correlation at the MP2 level, which is the minimum level of *ab initio* theory necessary to improve agreement with experimental results in a significant way.

A study of the energetics, structure, and hyperpolarizabilities of other conformations of small thiophene oligomers and related cyclic-diene systems is underway.

Acknowledgements

Support is acknowledged from the Air Force Office of Scientific Research through grants AFOSR-84-0044 (JAM) and AFOSR-90-0010 (HAK) as well as the Memphis State University Computer Center (HAK).

References

1. Zhao, M.-T.; Samoc, M.; Singh, B. P.; Prasad, P. N. *J. Phys. Chem.* 1989, 93, 7916.
2. Stewart, J. J. P. *QCPE Program 455*, 1983; version 3.1 (1986), version 5.0 (1989).
3. Flytzanis, C. "Theory of Nonlinear Optical Susceptibilities", in *Quantum Electronics*, Rabin, H. and Tang, C. L., Ed.; Academic Press, New York, 1975.
4. Kurtz, H. A.; Stewart, J. J. P.; Dieter, K. M. *J. Comp. Chem.* 1990, 11, 82.
5. Dewar, M. J. S.; Zoebish, E. G.; Healy, E. F.; Stewart, J. J. P. *J. Amer. Chem. Soc.* 1985, 107, 3902.
6. Levine, B. F.; Bethea, C. G. *J. Chem. Phys.* 1975, 63, 2666.
7. Perrin, E.; Prasad, P. N.; Mougnot, P.; Dupuis, M. *J. Chem. Phys.* 1989, 91, 4728.
8. J. Medrano and D. Dudis, unpublished results.
9. Goldfarb, I. J.; Reale, H. F.; Medrano, J. A. in "Theoretical Prediction of Nonlinear Optical Properties of Molecules and Polymers", 1988 MRS Fall Meeting Symposium, MRS Symposium Proceedings 1989, 134, 609.
10. The AM1 parameters used for S are from a private communication

Table 1: Second Hyperpolarizabilities $\langle \gamma \rangle$ for poly-p-phenylene oligomers.^a

Number of Subunits	AM1 $\gamma(0)$	DWFM ^{b,c} $\gamma(\omega)$	DWFM est. $\gamma(0)$
1	0.7	38.4	23.6
2	16.2	174.0	83.3
3	77.4	510.0	198.8
4	197.2		
5	367.3	1260.0 ^d	297.3
6	573.5		
7	804.6		

^aUnits are 10^{-36} esu.^bExperimental values from Ref. 1 have been multiplied by 6 to make their series expansion consistent with our eq. 1.^cThe value of N=4 was not reported in Ref. 1.^d-OC₁₀H₂₁ derivativeTable 2: Second Hyperpolarizabilities $\langle \gamma \rangle$ for polythiophene oligomers.^a

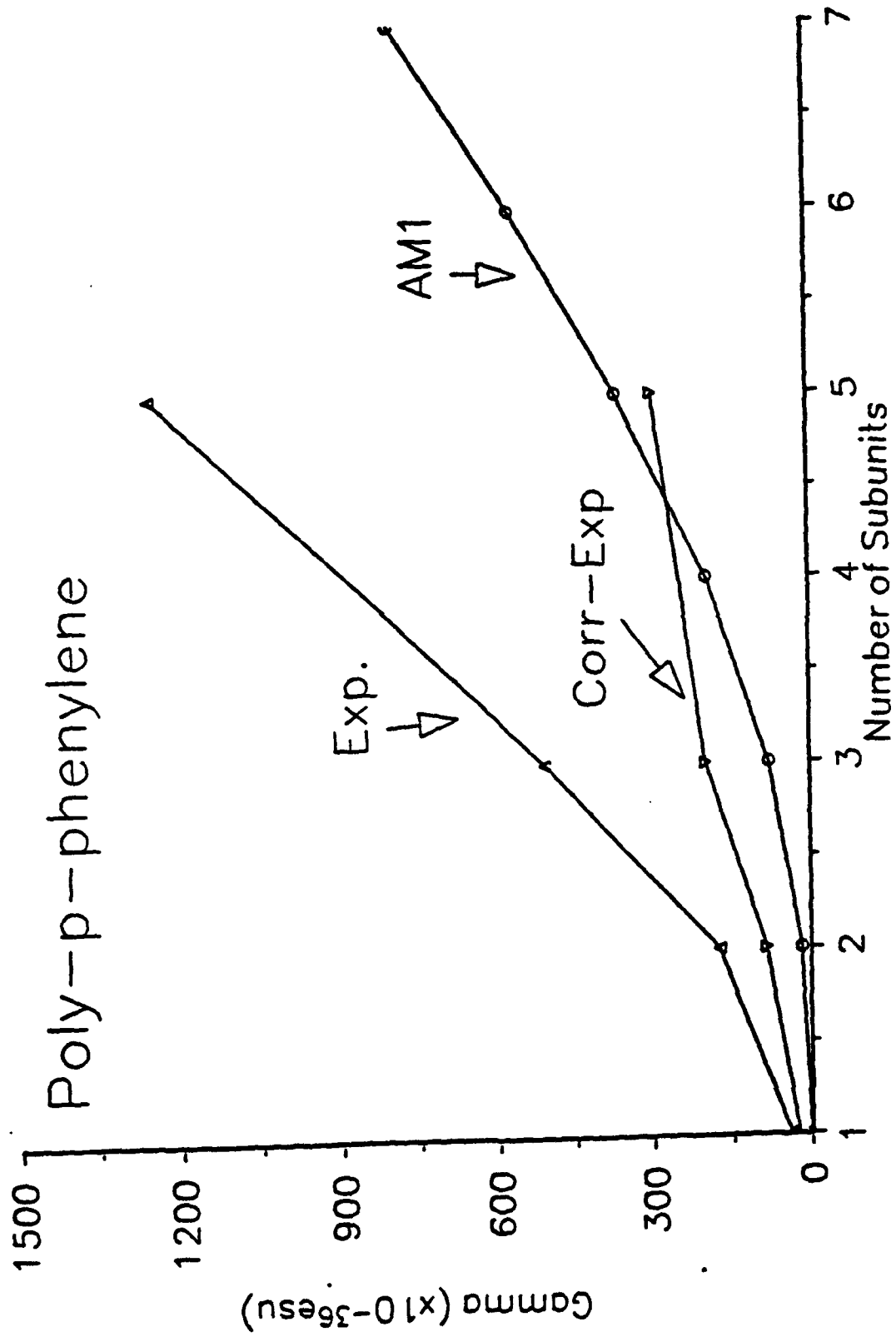
Number of Subunits	AM1 $\gamma(0)$	DWFM ^b $\gamma(\omega)$	DWFM est. $\gamma(0)$
1	1	25	13
2	22	138	43
3	103	960	184
4	284	4800	539
5	544	15600	1246
6	931		

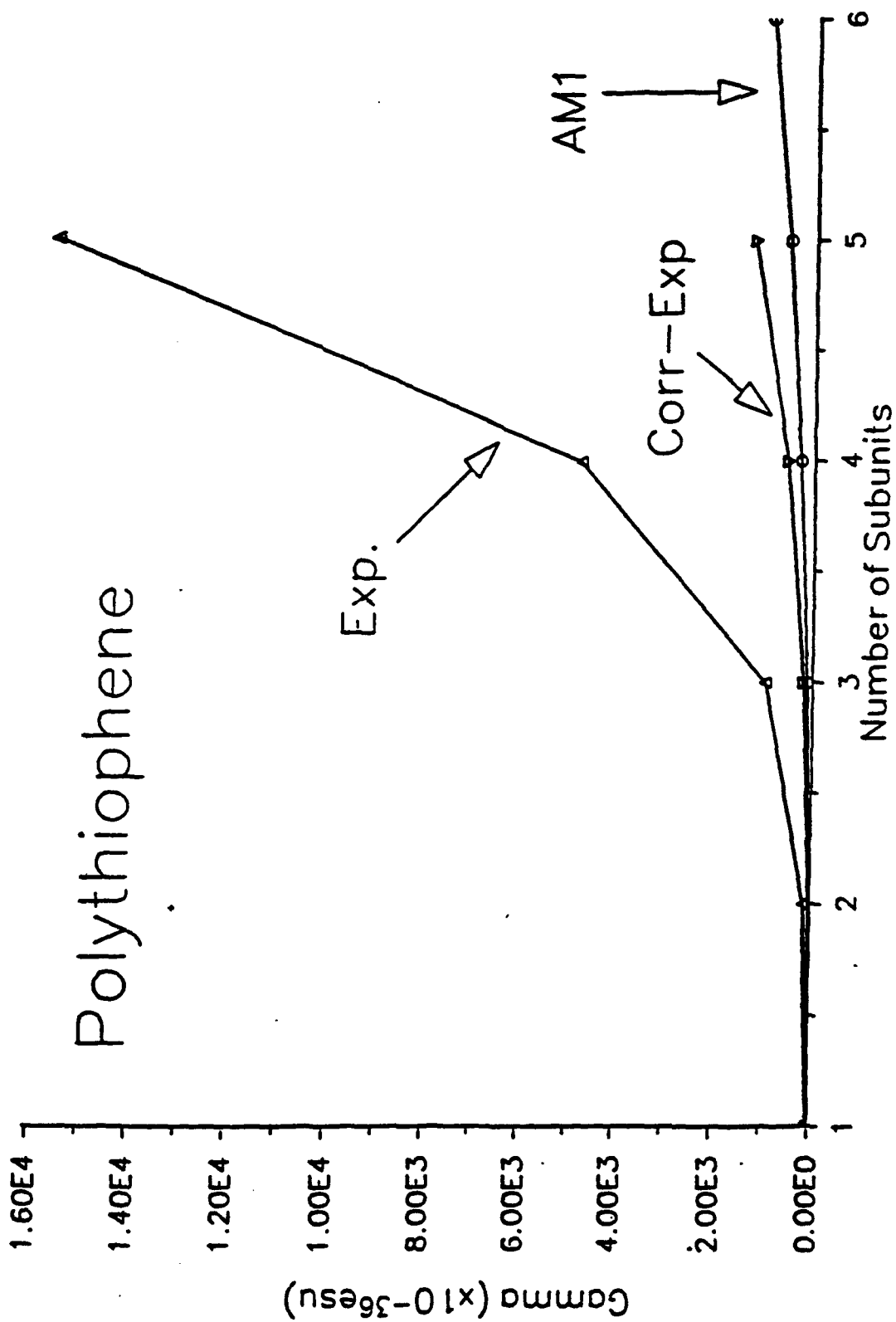
^aUnits are 10^{-36} esu.^bExperimental values from Ref. 1 have been multiplied by 6 to make their series expansion consistent with our eq. 1.

Figure Captions

Figure 1: Second Hyperpolarizability versus number of units for poly-p-phenylene oligomers. The curve labeled "Exp" is the DFWM result from ref 1 and the one label "Corr-Exp" is the same result corrected for dispersion using equation 4.

Figure 2: Second Hyperpolarizability versus number of units for polythiophene oligomers. The curve labeled "Exp" is the DFWM result from ref 1 and the one label "Corr-Exp" is the same result corrected for dispersion using equation 4.





QUASI-PARTICLES IN POLYMERIC CONDUCTORS

Jorge Medrano* and Douglas Dudis**

* University of Dayton, Chemistry Department
300 College Park
Dayton, OH 45469

**Douglas Dudis
Wright Research and Development Center
Materials Laboratory
Wright-Patterson AFB, OH 45433-6533

ABSTRACT

The studies reported here are part of an effort to understand the electronic structure and statistical properties of quasi-particles in polymeric materials. These are solitons, antisolitons, polarons, and bipolarons, and in one way or another each of them is known to play a role in the conduction of electric current in those materials. We have used pristine and doped polyacetylene as our example to study the geometrical and electronic distortions associated with quasi-particles in oligomers and infinite polymers. The computational approach has been based on the semi-empirical self-consistent LCAO-MO theory at the AM1 level of approximation for finite systems and the corresponding LCAO-CO theory in the tight binding approximation for infinite systems.

INTRODUCTION

Although conducting polymers in general and polyacetylene in particular have received much attention in recent years, there are comparatively few first-principles theoretical calculations aimed at understanding the electronic structure of quasi-particles. Most of the calculations performed have used the Su, Schrieffer, and Heeger (SSH) hamiltonian [1]. This work was indeed a very important stepping stone, mainly because it showed that the soliton model of polyacetylene could be used to explain a number of properties of this material; optical, electrical, and magnetic. No other model can claim such an accomplishment. This success prompted other work and different extensions and modifications of the SSH hamiltonian, too numerous to quote. Most notably however, H. Fukutome has very recently performed a very complete study of a Pariser-Parr-Pople (PPP) unrestricted Hartree-Fock (UHF) model of polyacetylene [2]. The SSH approach however, is still too crude for the kind of accuracy that is needed since it is basically a Huckel-type approximation with sigma bond compressibility and electron-electron Coulomb interactions are completely neglected. Moreover, the SSH model does not have an analytical solution and needs a number of empirical parameters specific to polyacetylene (or the particular polymer under study) in order to be able to make some quantitative predictions.

On the other hand, a few self-consistent LCAO-MO calculations have been performed on finite oligomers of polyacetylene, both semi-empirical [3] and ab initio [4]. The excellent agreement that we report below between one of our semi-empirical calculations and the ab initio result reported in ref. 4, convinced us that the SCF-LCAO-MO semi-empirical theory is completely adequate for the purpose of a systematic study of the electronic structure associated with quasi-particles. This methodology is still first-principles based and although there are indeed parameters incorporated into the theory, these are atomic in nature. Therefore, the same theory with the same parameters

can be used to study any molecule or infinite polymer without the need for information about the specific system.

We can mention here the only calculation of the infinite polymer of which we are aware; that of Stafstrom and Bredas [5], who used the Valence Electron Hamiltonian (VEH) method to study the band structure at various doping levels.

Many fundamental aspects of the electronic and structural properties of the conducting polymers (in particular the highly conducting ones) are not well established, and at this time theoretical understanding lags behind the rapid experimental developments. In what follows we expect to contribute information that will ultimately prove useful for a thorough understanding of the mechanisms of conductivity in polymers.

METHOD

The theoretical method used for the calculations was the semi-empirical SCF-MO theory at the AM1 level of approximation [6] as implemented in the MOPAC 5.0 program (QCPE #455). The AM1 hamiltonian has been shown to correct for some deficiencies present in the older MNDO hamiltonian. The geometries of all the systems studied were fully optimized with due allowance for the symmetry constraints in each case. Convergence of the calculation was difficult in some of the examples, especially for doublet and triplet states. In each case the optimization was very carefully performed by running a first step with the keyword PRECISE (thus increasing the criteria for terminating all optimizations, electronic and geometric by a factor of 100). In subsequent runs, the gradient was decreased even further by using the SIGMA method due to Komornicki and McIver [7] while at the same time making the criterion for self-consistent convergence even stricter (using the keyword SCFCRT = 10-10 or SCFCRT = 10-11). In this way the gradient norm was usually reduced to less than 1 (in kcal/A or kcal/degree) even when more than seventy geometrical variables were simultaneously optimized. For infinite systems we used the "cluster approximation" developed by Stewart [8] (the name is misleading because Born-von Karman cyclic boundary conditions are actually used; it is thus an approximation to a full crystal orbital (CO) calculation). This approach is known to be an excellent approximation to the full CO result when the unit cell used is large enough to ensure that atoms at one end of the repeat unit have a negligible density matrix element with atoms at the other end. Since the repeat units we used are almost 27Å long, this condition is very rigorously met even in the examples studied, where there is an extended π system. However, in at least one example (see below) the full CO calculation was performed as a check (using the MOSOL program, QCPE #495), thus verifying that the results were the same to four significant digits for the optimized geometrical variables, heats of formation and degrees of bonding. Obtaining the band structure however, requires the full solid state calculation involving sampling of the Brillouin zone using a regular mesh. The advantage of the approximation is of course that it takes 1/5 to 1/10 of the CPU time required by the full CO calculation.

We mimicked the effect of a dopant in the repeat unit by using the "sparkles" provided in the MOPAC program. These are uncharged species which immediately ionizes the polymer. They can be regarded as unpolarizable ions of diameter 1.4Å. We used an acceptor dopant in the polaron calculations; the effect of the sparkle being that a net positive charge is left in the π system.

The degrees of bonding were calculated from the density matrix using the definitions given by Medrano et al [9], for molecular and infinite polymers as well. These are known to be an accurate measure of the integrated electron density associated with a bond, and have the important advantage that the same basic formalism (based on the first-order reduced density operator) is used both for molecules and infinite polymers. In the cases we studied, the degrees of bonding give a much better description of the bond alternation (or lack of it) than the bond lengths, since the former are more directly associated with the electronic structure.

For almost all the examples, we carried out calculations both at the open-shell restricted Hartree-Fock (ROHF) and unrestricted Hartree-Fock (UHF) levels of the theory. The differences between both descriptions is discussed below.

DESCRIPTION OF THE SYSTEMS STUDIED

As already stated, it was our purpose to study the electronic structure of quasi-particles such as solitons, polarons, etc. A static neutral soliton (S) can be considered the same as a radical. The effect of the soliton on the geometrical structure is to flip the bond alternation from one to the

CHARGE and SPIN RELATIONSHIPS OF QUASI - PARTICLES

	Charge	Spin
Neutral Soliton (S)	0	1/2
Charged Soliton (S ⁺) or (S ⁻)	±1	0
Soliton - Antisoliton Pair (SS)	0	0, ±1
Polaron (P ⁺) or (P ⁻)	±1	1/2
Bipolaron (bP ⁺⁺) or (bP ⁻⁻)	±2	0

other of the two degenerate phases in the material. A soliton can be positively charged (carbenium ion) or negatively charged (carbanion). The three situations are depicted in Fig. 1. These schemes in Fig.1 should not be taken too strictly however, since they do not show the essentially delocalized nature of the quasi-particles, but are intended to allow easy electron counting. Now, solitons are known to be topological particles. Therefore, in infinite systems they are always created in pairs, called soliton-antisoliton pairs (SS^{*}) (This can also be seen as arising from stability conditions.) Any of the two members of the pair will cancel the effect of the other member next to it, so to left and right of the pair the bond alternation will be the same (cf Fig. 2).. What happens in between, and how that depends on the distance between soliton and antisoliton, can only be determined by calculation and will be discussed below. One such pair can also be regarded as a (singlet or triplet) biradical.

One electron can be removed from or added to a region of the material where a soliton-antisoliton pair has been created, giving rise to a positive or negative polaron respectively (P⁺ or P⁻). (They can also be regarded as a radical cation or radical anion respectively in the static case.) Removal or addition of two electrons results in a positive or negative bipolaron (bP⁺⁺ or bP⁻⁻) or a dication or dianion respectively. Figure 3 attempts to give a graphical representation of polarons and bipolarons, while at the same time emphasizing the delocalized nature of the particles. Again, both at right and left of a polaron or bipolaron, the bond alternation is the same; i.e. we have either phase A or phase B at both sides of the quasi-particle in a polyacetylene chain (cf. Fig 3). Once again the detailed geometrical and electronic structure can only be determined by calculation.

These particles have very unusual relations of charge-spin, in most cases at variance with elementary particles such as protons and electrons. Table 1 gives a summary of the charge and spin associated with solitons, soliton-antisoliton pairs, polarons, and bipolarons.

The actual systems we used as case studies are: (I) The polyacetylene oligomer chain C₂₁H₂₃ for studying the isolated soliton and the repeat unit C₂₂H₂₂ for studying the (SS^{*}) pair in an infinite system. We used the same repeat unit to study the polaron P⁺ created from the (SS^{*}) by including an acceptor "sparkle" in the calculation. These systems are depicted in Figure 4.

RESULTS AND DISCUSSION

1. Solitons

We fully optimized the geometry of the C₂₁H₂₃ oligomer with a neutral soliton at the central carbon atom, under C_{2v} symmetry as described above. The ground state of the system is of course a doublet, and we performed the calculation both at the UHF and ROHF level of theory. The UHF result gives no bond length alternation and no degree of bonding alternation, except close to the ends of the chain, due to the terminal effects. Close to the soliton site, all bond

Figure 1. Solitons in polyacetylene

Preprint 4



Neutral (Radical)

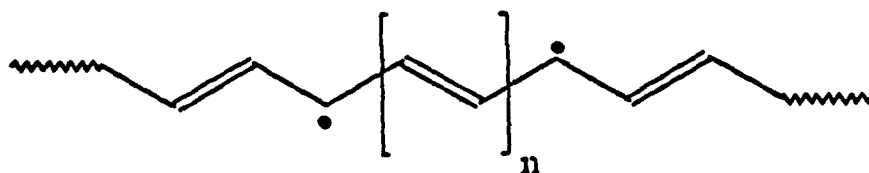


Positive (Carbenium ion)



Negative (Carbanion)

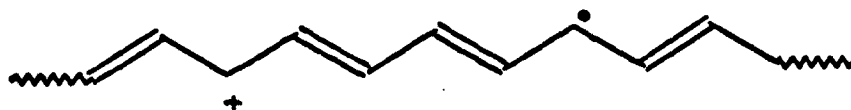
Figure 2. Soliton-antisoliton pair



Singlet or Triplet

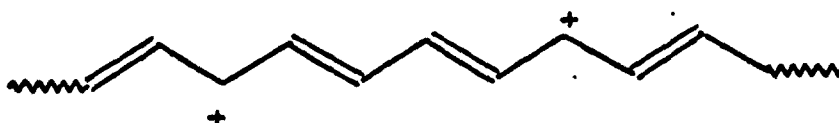
Birradical

Figure 3. Polaron and Bipolaron



Polaron (Radical cation)

LOCALIZED PICTURE



Bipolaron (Dication)



DELOCALIZED PICTURE

Figure 4. Systems used for the studies

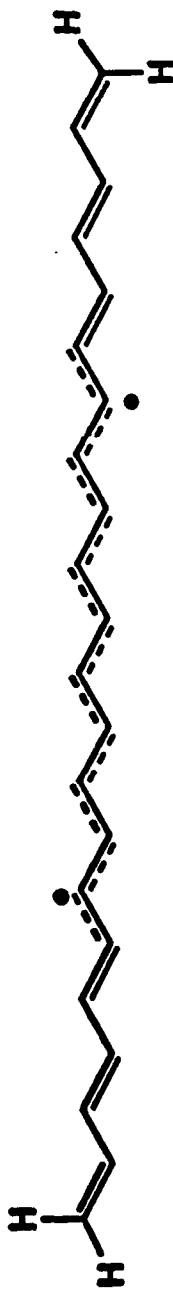
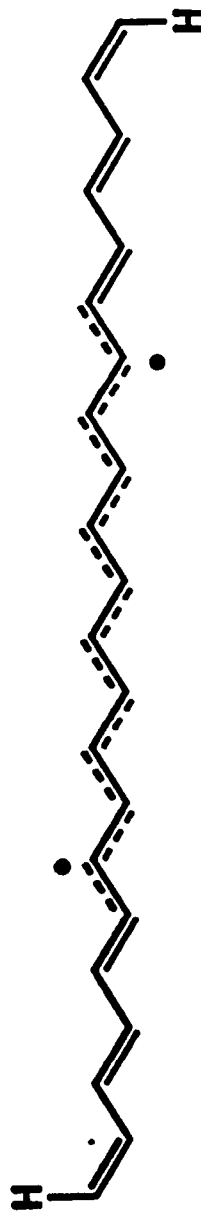
 $C_{21}H_{23}$  $C_{22}H_{24}$  $C_{22}H_{22}$ 

Figure 5
Bond length alternation in A in neutral
and positive solitons in C₂₁H₂₃ oligomer

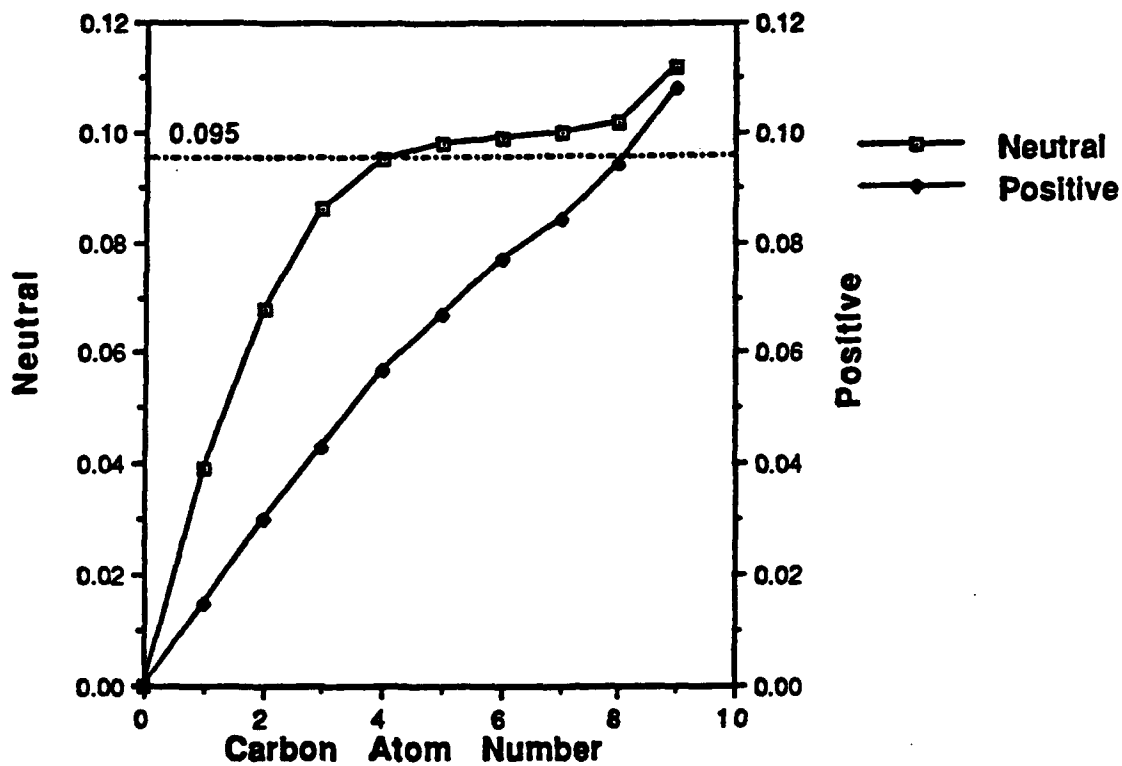
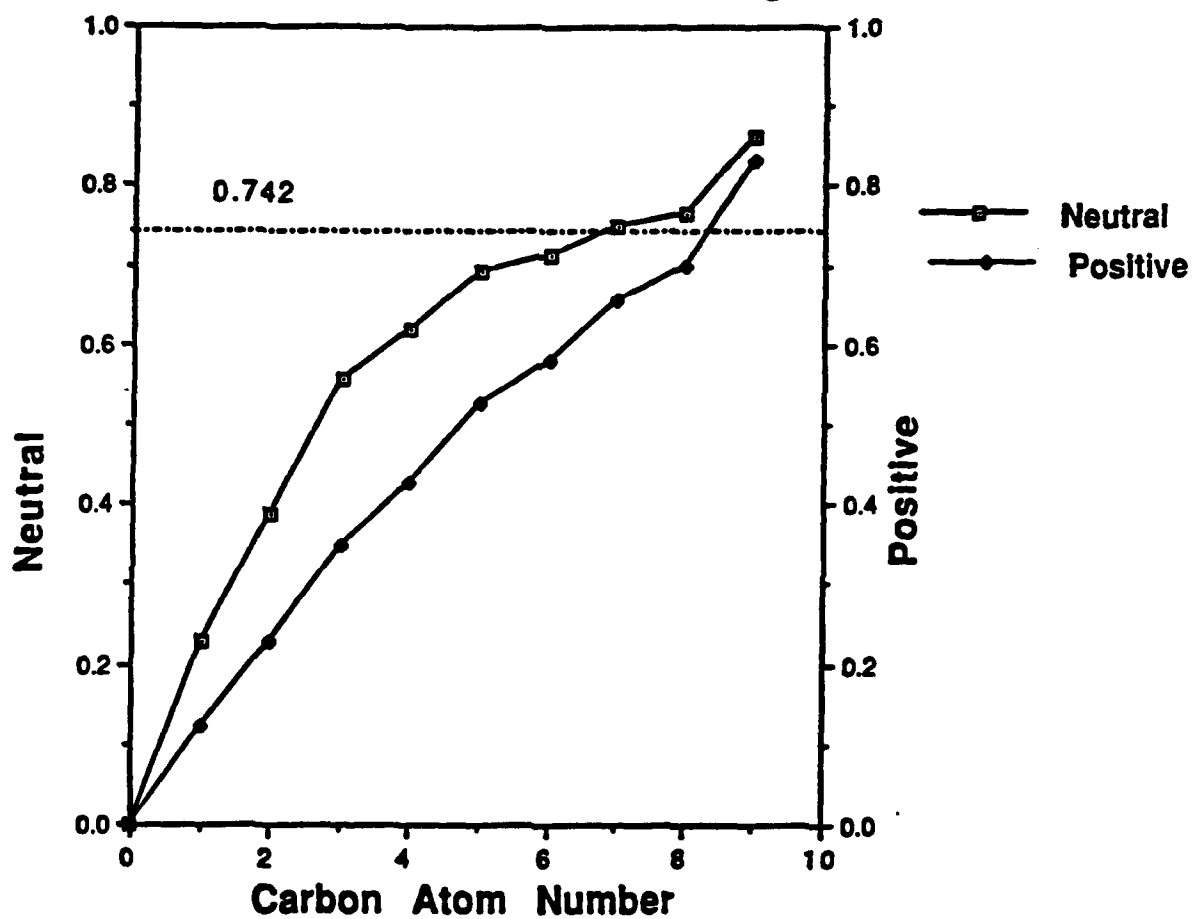


Figure 6
Degree of bonding alternation in neutral
and positive solitons in $C_{21}H_{23}$ oligomer



lengths are 1.40\AA and all degrees of bonding are 1.33. Now, the UHF wavefunction is not an eigenfunction of the operator that represents the spin squared, S^2 . The theoretical value for this case is $S^2 = 0.75$. The UHF result is $S^2 = 3.66$, i.e. there is a very large spin contamination. This is probably due to low lying excited states of higher spin multiplicity such as quartet, sextet, etc. These excited states probably have no bond length alternation. In any case this level of spin contamination indicates that the UHF wavefunction is not a sufficiently accurate representation of the doublet. It appears the UHF description exaggerates the opening of the shells due to the magnetic interactions that originates in the unpaired spin. On the other hand, because of the way it is obtained, in the ROHF wavefunction, only the singly occupied orbital contributes to the spin density wave away from the soliton, which is unrealistic. So neither type of wavefunction can give an accurate description of all the properties of interest, when the number of α and β spins is not the same. It will probably be necessary to resort to some method for incorporating correlation to improve over both the UHF and ROHF descriptions. Some preliminary calculations along that direction have already been carried away in our laboratory at the MP2 level, and they confirm, as expected, the above discussion. As regards the bond lengths and degrees of bonding alternation, the ROHF calculation gives quite accurate results. At the same time the agreement between those fragment-based approximate ab initio calculations [10] and ours, lends additional credibility to the semi-empirical approach in these situations.

Therefore, we used the ROHF/AM1 calculations hereafter, which is of course the same as closed-shell RHF/AM1 in the cases where there is the same number of α and β spins.

Figure 5 shows the difference in adjacent bond lengths Δr , plotted against carbon site distance from the soliton, for both the neutral and the positively charged quasi-particles. Only the right half of the molecule is included in the plot, since the other half can be derived by symmetry. $\Delta r = 0$ implies no bond alternation, and this happens precisely at the soliton center.

The plot in Figure 5 also shows a horizontal line drawn at the value of $\Delta r_{\infty} = 0.095\text{\AA}$ corresponding to infinite polyacetylene, as obtained through a full CO calculation with the MOSOL program. This value is in very good agreement with the experimental result of $\Delta r_{\infty} = 0.104\text{\AA}$. The end effect is clearly visible in Figure 5 in that the values of Δr for the last carbon atoms exceed the infinite polymer value.

Both curves for the neutral and positive solitons, can be approximated by a function of the form $\Delta r = \Delta r_{\infty} \tanh(n/l)$ as proposed by Su et al. in ref. 1. Taking for Δr_{∞} the value quoted above, we obtain the best fit for the neutral soliton when $l=2$. This is a measure of the extent of the quasi-particle, and is in very good agreement with the result obtained by Boudreaux et al. [3], who found $l=3$ through a calculation on $C_{41}H_{43}$ using the MNDO hamiltonian and $\Delta r_{\infty} = 0.106\text{\AA}$ (in ref. 1, the authors came up with $l=7$).

The values of Δr for the positive soliton are in excellent agreement with those obtained by Villar et al. [4] who carried out an ab initio calculation on the same oligomer $C_{21}H_{23}$ as we did, using a double-zeta 6-31G basic set. All the bond lengths we obtained by geometry optimization agree within 1% with the ab initio ones. The hyperbolic tangent that best interpolates among the calculated points, is calculated with $l=7$ if $\Delta r_{\infty} = 0.112$ is used (as in ref. 5) or with $l=6$ if $\Delta r_{\infty} = 0.095$ is used, as we did for the neutral soliton. In any case this is somewhat larger than the value $l=5$ obtained in ref. 3. The difference could be due to the fact that we used the AM1 hamiltonian and Boudreaux et al. used the MNDO one. The agreement is still very good however.

We also calculated the degrees of bonding B_{AB} between consecutive carbon atoms, and ΔB_{AB} analogously to Δr for both the neutral and positive soliton. Except for the last three points where the discrepancy is slightly larger, we again have an agreement within 1% with the ab initio values in ref. 4 for the positive soliton. This, and the agreement for the bond lengths mentioned above, gave us an assurance that the semi-empirical method we used is sufficiently reliable for this purpose. The result for ΔB_{AB} versus carbon site distance from the center, are shown in Figure 6. Once again the value for the infinite polymer is shown as a horizontal line, as calculated with the MOSOL program. Again, the end effects are visible in the last few points. It is an interesting and completely new result that a hyperbolic tangent interpolates very well among the calculated points, with $l=3$ for the neutral soliton, and $l=6$ for the positive one. This means that the relation between these curves and the solution of the solitary wave equation in ϕ^4 field theory [11] goes beyond the geometrical distribution caused by the defect, and reflects in the associated electron-density distribution.

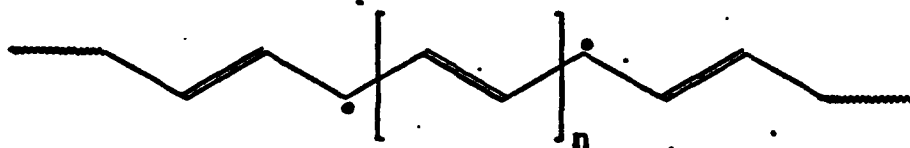
We calculated the singlet state of neutral soliton-antisoliton pairs in infinite systems using the cluster approximation described above, and $C_{22}H_{22}$ as the repeat unit. Besides, we repeated the calculation for separation of $R=1,5,9$ and 11 bonds between the soliton and antisoliton. Table 2 shows the heats of formation of the system for the different separations and the heat of formation of the $C_{22}H_{22}$ repeat unit when it is used to represent pristine polyacetylene. This comes out to be 141.65 kcal/mol or 12.87 kcal/mol per CH unit. The full CO calculation with the MOSOL program gives 12.93 kcal/mol for the same quantity, showing that the cluster approximation is providing the correct energies to within hundredths of a kcal/mol. As Table 2 shows, the calculated heats of formation are independent of the soliton-antisoliton separation, within the uncertainty of the method of a few hundredths of a kcal/mol. This result is at variance with a previous calculation by Bredas et al. [12], who used a Huckel-type method with sigma bond compressibility and cyclic polyene molecules with about 110 carbon atoms to represent the system. These authors find an attractive interaction between soliton and antisoliton in the electronic ground state of the system, i.e. the energy of the system when the soliton and antisoliton are in close proximity is about 0.9eV lower than that corresponding to a large separation. This is tantamount to stating that when they are in close proximity we have the perfectly dimerized state, and when they are separated by a distance larger than approximately twice the width of a soliton, then we have two transitions: for instance, $A \rightarrow B \rightarrow A$. (This meaning that the system is in phase A left and right of the pair and in phase B in between.) The energy would then rise rapidly when R goes to infinity, to its asymptotic value of twice the energy of one isolated soliton. The two limits $R \rightarrow 0$ and $R \rightarrow \infty$ cannot be argued of course, but the total energy should depend on the exact shape of the soliton pair at intermediate distances. Interestingly, we obtained an unexpected result regarding this point. The two bond lengths adjacent to the soliton and to the antisoliton are constrained to be equal, but in spite of that, the bond length alternation is not changed by either particle. Their alternation to the right of each soliton for example, recovers to what it was to the left two bonds past the quasi-particle. This picture is even clearer when the degree of bonding alternation is examined. It decreases somewhat together with the bond length alternation, without ever vanishing, and recovers together with the latter, too. In fact it decreases from its infinite polymer value of 0.74 to 0.65 at the center of each soliton, i.e. less than 0.1! This implies that the two bonds at each side of either soliton have the same length but very different degrees of bonding: one is a double bond, $B_{AB}=1.75$ and the other is single, $B_{AB}=1.10$. Figure 7 shows precisely that, for the case when both quasi-particles are nine bonds apart, but the same is true irrespective of the separation. In case there were an influence of a different environment left and right of each particle, we checked carefully the situation when they are eleven bonds apart. Then each of the particles has its left and right neighbor at exactly the same distance in a $C_{22}H_{22}$ repeat unit. The same picture is obtained also in this case. This is of course consistent with our finding that the energy is the same irrespective of the separation. It is also consistent with the small energy of creation of the soliton-antisoliton pair. According to the results in Table 2, this is only 5.55 kcal/mol (or 0.24 eV). Exactly at what distance, both parts of the pair start behaving as independent particles we of course do not know. Trying larger separations would entail using larger repeat units, making the system intractable at this level of the theory. The question immediately arises regarding the nature of the interaction between both particles. In other words, how does each of them know about the presence of the other when their separation is as large as eleven bonds? (It should be kept in mind that their width is two bonds or three bonds to each side of the center.) The answer to this question is not clear to us at the present time.

The description based on the more simplistic picture (based on a SSH-type of calculation) described above has already been published in a book on the subject [13] by S. Kivelson. According to their study however, the details of the shape of the pair are at the very least debatable matter. Moreover, we can conclude that due consideration of electron-electron interactions is absolutely necessary for an accurate description of the details of the electronic structure of these systems.

3. Polarons

Although the polaron calculations are still being run, the two values for the energy that we already have, one for the situation with the two parts of the system nine bonds apart and the other five bonds apart, show that there is indeed an attractive interaction in this case. The values are $E(R=9)=271.10$ kcal/mol and $E(R=5)=266.30$ kcal/mol. Their difference amounts to 4.8 kcal/mol, or 0.21 eV. In this case, we find a better agreement with Bredas et al. calculation [12] of an attractive interaction of 0.35 eV.

Table 2 Energies of the soliton-antisoliton pair for different separations



	ΔH_f (kcal/mol)	$\Delta\Delta H_f$
Normal $C_{22}H_{22}$	141.65	
n R		
0 1	147.20	5.55
2 5	147.19	5.54
4 9	147.26	5.61
5 11	147.28	5.63

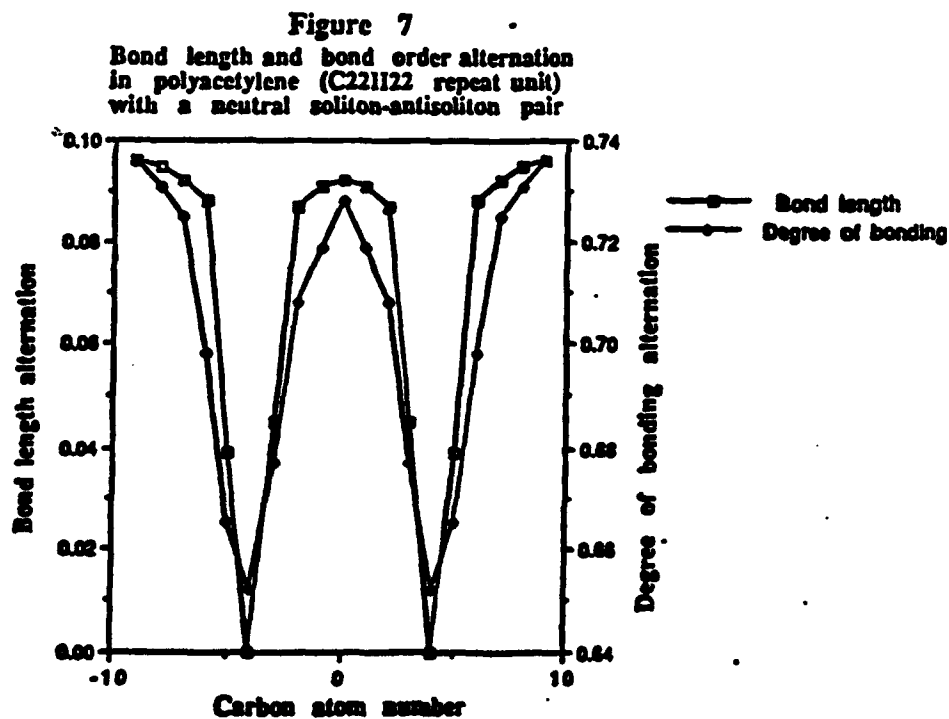
In both our calculations, we placed the dopant above the plane of the polymer, 3.5Å on top of the hydrogen bonded to the carbon atom where the center of the left soliton is. This of course destroys the C_{2h} symmetry and gives rise to a large dipole moment, of about 18 debyes.

Energetically, it takes about 121 kcal/mol (or 5.2 eV) to introduce the dopant (i.e. ionize the polymer) and create the polaron, as compared with the energy of the system with a neutral soliton-antisoliton pair. A more detailed study of the electronic structure is presently underway.

LINES OF FUTURE RESEARCH

This research can be extended to include negative polarons and positive and negative bipolarons in polyacetylene. Several issues regarding this subject need clarification.

Also, other interesting highly conducting polymers can be studied with these techniques, including $(SN)_x$ which is known to be superconducting at very low temperature.



Then, the next step would be the detailed study of the band structure associated with quasi-particles. The few publications on this subject are not in agreement with one another. For example, Fukutome's calculation [2] (see above) gives a structure of levels in the band gap very different from what is routinely accepted from the SSH-type of work. This is a challenging calculation in any case, because Hartree-Fock based methods, whether *ab initio* or semi-empirical are known to exaggerate notoriously the band gap and not give very accurate densities of states.

There are also some very important theoretical issues to explore. For instance, which is the relation (if any) between conductivity and hyperpolarizabilities. This subject can be investigated with the same tools described here.

The statistical mechanical aspects of quasi-particles, are also essentially unexplored, for instance the coupling of two fermions into a boson, as in the formation of a soliton-antisoliton pair. Can this be considered a pairon? Does it obey a strict Bose Einstein statistic? Does it bear any relation with Cooper-type pairs? These are only a few examples of unanswered questions.

Finally, it would certainly be worth exploring in more detail an interesting, very recent suggestion by Mazunder and Ramasesha [14] about a bipolaronic mechanism for superconductivity in organics to see if the same idea can be applied to polymers of other structures and compositions.

Some of these issues will be addressed in our laboratory, and the results published elsewhere.

CONCLUSIONS

We have been able in this investigation to use some new tools and ideas and have found some previously unreported aspects of the electronic structure of quasi-particles.

Ours is one of the first calculations of infinite polymers when quasi-particles are present, and the first to our knowledge in which the dopant is explicitly taken into account. This is also the first calculation (at this level of theory) of the interaction between the two parts of the system in a soliton-antisoliton pair or in a polaron.

The difference between the ROHF and UHF descriptions had not been pointed out before. The question still remains, if correlation has to be included, which is the minimum level of theory necessary for an accurate description of all the properties of the system. We intend to address this issue.

We also believe that the use of the "degree of bonding wave" (DOBW) is the most descriptive tool available to understand, in the most pictorial way, the characteristics of the electron density distribution. We have shown as well that the DOBW also can be described by a hyperbolic tangent functional dependence with the distance from the center of the soliton.

Finally, we have found some unexpected features of the electron structure associated with a soliton-antisoliton pair, that we believe are important for the detailed understanding of this, and probably other quasi-particles.

REFERENCES

1. W. P. Su, J. R. Schrieffer, and A. J. Heeger, *Phys. Rev. Lett.* **42**, 1698 (1979).
2. H. Fukutome, *J. Molec. Struct. (Theochem)*, **188**, 337 (1989).
3. D. S. Boudreaux, R. R. Chance, J. L. Bredas, and R. Silbey, *Phys. Rev. B* **28**, 6927 (1983).
4. H. O. Villar, M. Dupuis, and E. Clementi, *Phys. Rev. B* **37**, 2520 (1988).
5. S. Stafstrom and J. L. Bredas, *J. Molec. Struct.* **188**, 393 (1989).
6. M. J. S. Dewar, E. G. Zoerich, E. F. Healy, and J. J. P. Stewart, *J. Am. Chem. Soc.* **107**, 3902 (1985).
7. (a) A. Komornicki and J. W. McIver, *Chem. Phys. Lett.* **10**, 303 (1971); (b) A. Komornicki and J. W. McIver, *J. Am. Chem. Soc.* **84**, 2825 (1961).

8. J. J. P. Stewart, *New Polymeric Mat.* **1**, 53 (1987).
9. (a) M. A. Natiello, H. F. Reale, and J. A. Medrano, *J. Comp. Chem.*, **6**, 108 (1985); (b) R. C. Boicchio, H. F. Reale, and J. A. Medrano, *Phys. Rev. B* **40**, 7186 (1989).
10. G. P. Das, *Chem. Phys. Lett.* **147**, 591 (1988).
11. A. S. Davidov in "Solitons in Molecular Systems," D. Reidel Publishing Co., 1985.
12. J. L. Bredas, R. R. Chance, and R. Silbey, *Phys. Rev. B* **26**, 5846 (1982).
13. S. Kivelson, "Soliton Model of Polyacetylene," in "Solitons," page 325; V. M. Agranovich and A. A. Maradudin, editors; North Holland Publishing Co., 1986.
14. S. Mazumdar and S. Ramasesha, *Synth. Metals* **27**, A105 (1988).

APR 1989
LIBRARY
UNIVERSITY OF CALIFORNIA